

The Pennsylvania State University

The Graduate School

Department of Aerospace Engineering

**A METHOD OF SELECTING AND CONFIGURING OPTIMAL ENERGY ABSORBING  
CARGO RESTRAINT SYSTEMS TO IMPROVE CRASHWORTHINESS**

A Thesis in

Aerospace Engineering

by

William Kong

© 2010 William Kong

Submitted in Partial Fulfillment  
of the Requirements  
for the Degree of

Master of Science

December 2010

The thesis of William Kong was reviewed and approved\* by the following:

Edward C. Smith  
Professor of Aerospace Engineering  
Thesis Co-Advisor

Michael A. Yukish  
Head of Product and Process Design Department  
The Applied Research Laboratory  
Thesis Co-Advisor

Charles E. Bakis  
Distinguished Professor of Engineering Science and Mechanics

George A. Lesieutre  
Professor of Aerospace Engineering  
Head of the Department of Aerospace Engineering

\*Signatures are on file in the Graduate School

## ABSTRACT

This thesis describes the development of methods and tools to design optimal energy absorbing cargo restraint systems to improve crashworthiness, and demonstrates them in a sample design study. The energy absorbing cargo restraint systems considered have two components: load limiter and lanyard. The load limiter acts as the energy absorbing device of the restraint system. A closed-form solution does not exist due to the changing geometry of the configuration during a crash and the nonlinear behavior of the restraints. Therefore, a cargo dynamics simulation (CDS) was developed to analyze the interaction between the cabin floor, cargo, and restraint system in a crash event. The simulation solves a system of state-variable equation for six degree-of-freedom rigid body dynamics. An optimization method was developed in which the cargo dynamics simulation is coupled with Applied Research Laboratory Trade Space Visualizer (ATSV) — a multi-dimensional data exploration and visualization software — to exercise the simulation over the design space and visualize the results. A comparative study was conducted to compare restraint system components and the results from static and dynamic analysis. A parametric study was conducted to provide a rule-of-thumb for tie-down angles that would optimize the design of simple restraint configurations. Design studies are presented as exercises of the optimization method for a generic cargo handling scenario. The crash loads and parameters for the analytical studies were obtained from U.S. Department of Defense specifications as provided in the Aircraft Crash Survival Design Guide and MIL-STD-1290. The results of the comparative and optimization studies revealed the importance of lanyard characteristics in restraint system performance. The ideal lanyard was found to exhibit high stiffness, high strength, low weight, and low elongation. The allowable cargo displacement constraint proved to be the most influential factor in optimal restraint system design. Within the confined space of the aircraft, centimeters of displacement can be the difference between a survivable and fatal crash. Finally, a new set of requirements and design criteria are proposed to address normal flight

maneuvering conditions, crash conditions, and usability. The requirements were created to provide guidance to cargo handlers for using energy absorbing cargo restraint systems.

## TABLE OF CONTENTS

Chapter 1 Introduction .....	1
1.1 Motivation.....	1
1.2 Challenges.....	2
1.3 Scope and Objectives .....	3
1.4 Organization of Thesis .....	4
 Chapter 2 Literature Review .....	 6
2.1 Crashworthiness Requirements.....	6
2.2 Current Restraint Technology .....	9
2.3 Energy Absorbing Restraints .....	10
2.3.1 Load Limiter Technology.....	10
2.3.2 Lanyard Technology .....	14
2.4 Load Preparation .....	15
2.5 Design Methods and Tools for Energy Absorbing Cargo Restraint Systems .....	18
2.6 Summary .....	21
 Chapter 3 Analytical Tools and Methods .....	 23
3.1 Cargo Dynamics Simulation (CDS).....	23
3.1.1 Cargo Dynamics Simulation: Analytical Approach .....	24
3.1.2 Model Formulation.....	25
Reference Frames .....	26
Energy Absorbing Restraint Load Profile .....	28
Cargo Dynamics .....	28
Cabin Floor Dynamics.....	31
Mounting Points Locations.....	33
Collision .....	34
3.1.3 CDS Flowchart.....	35
3.1.4 Experimental Validation .....	36
3.2 Optimization Method .....	39
3.2.1 Approach .....	39
3.2.2 Background on ATSV .....	39
3.2.3 Algorithm .....	41
3.2.1 Optimization Problem Formulation.....	43
Objective Functions.....	44
3.2.2 Design Variables .....	45
3.2.3 Additional Constraints.....	47
3.3 Static Analysis Method .....	47
3.4 Summary .....	49
 Chapter 4 Results and Discussion.....	 50
4.1 Cargo Restraint Systems .....	50

4.2 Comparative Study of Steel Chain and Nylon Strap Lanyards With and Without Load Limiters in Simplified Tie-Down Configurations.....	54
4.2.1 Comparative Study Parameters .....	55
4.2.2 Comparative Study Results .....	56
4.3 Parametric Study .....	59
4.4 Optimization Study .....	63
4.4.1 ATSV Parameters.....	63
4.4.2 Design Space.....	64
4.4.3 Optimization Study #1: Steel Chain Restraints.....	65
4.4.4 Optimization Study #2: Steel Chain with Tear Webbing.....	69
Steel Chain/Tear Webbing – Design A .....	73
Steel Chain/Tear Webbing – Design B .....	74
Steel Chain/Tear Webbing – Design C .....	75
Steel Chain/Tear Webbing – Design D .....	76
4.4.5 Optimization Study #3: Nylon Straps with Tear Webbing .....	77
Nylon Strap/Tear Webbing – Design E.....	81
Nylon Strap/Tear Webbing – Design F.....	82
4.4.6 Discussion of Results .....	83
Chapter 5 Requirements and Design Criteria for Cargo Restraint Systems .....	88
5.1 Design Conditions and Requirements.....	88
5.1.1 Normal Maneuvering Flight Conditions .....	89
5.1.2 Crash Conditions.....	90
5.2 Cargo Restraint System Design Criteria .....	91
5.2.1 Lanyard .....	91
5.2.2 Load Limiter.....	92
5.2.3 Tie-Down Configuration.....	93
5.3 Restraint Tables.....	94
Chapter 6 Conclusions and Recommendations for Future Work.....	99
6.1 Summary .....	99
6.2 Analytical Studies .....	100
6.3 Design Requirements and Guidance .....	103
6.4 Recommendations for Future Work.....	104
6.4.1 Cargo Dynamics Simulation .....	105
Cargo/Cabin Floor Friction .....	105
Restraint Modeling .....	105
Beyond Unidirectional Impacts .....	106
Structural Analysis .....	106
Experimental Validation.....	107
Design Space .....	107
6.4.2 Optimization Method .....	107
6.4.3 Guidance for Cargo Handlers.....	108
References.....	109
Appendix A Restraint Table Regression Models.....	111

## LIST OF FIGURES

Figure 1-1. Comparison of force-stroke response for elastic and energy absorbing restraints.....	2
Figure 2-1. Typical aircraft floor acceleration pulse [Zimmermann et al. 1989].....	8
Figure 2-2. Wire bender load limiter with wire stored outside housing [Zimmermann et al. 1989].....	11
Figure 2-3. Photographs from a quasi-static test of SRD [Hagon 2009].....	12
Figure 2-4. Photographs from quasi-static test of tear webbing [Miller 2010].....	12
Figure 2-5. Comparison of SEA values in [J/g] of textile load limiters and existing technologies [Hagon et al. 2007].....	13
Figure 2-6. Restraint system with a tie-down configuration that is symmetric about the longitudinal axis [FM 55-450-2 1992].....	16
Figure 2-7. Supplemental restraint by wrapping around cargo [FM 55-450-2 1992].....	17
Figure 2-8. Nylon tie-down devices in series with load limiter. Based on pulse-duration-envelope design criterion and an elongation of 30 cm at 22.5 kN [Russo 1966].....	19
Figure 2-9. Force-stroke response of a load limiter.....	20
Figure 2-10. Diagram of the vehicle-level system for analyzing restraint system featuring a cargo net combined with a load limiter [Avery 1965].....	21
Figure 3-1. Diagram of the vehicle-level system used in the cargo dynamics simulation before and after a crash event.....	24
Figure 3-2. Screenshot of cargo dynamics simulation results video.....	25
Figure 3-3. Diagram of detailing the local coordinate systems for the cargo and cabin floor.....	26
Figure 3-4. Load profile of energy absorbing restraints.....	27
Figure 3-5. Shape of crash acceleration pulse.....	32
Figure 3-6. Displacement profile of cabin floor during crash event.....	33
Figure 3-7. CDS flowchart.....	35
Figure 3-8. Diagram of drop test setup [adopted from Hagon 2009].....	37

Figure 3-9. Comparison plot of CDS results and drop tests data for drop weight displacement.....	38
Figure 3-10. Comparison plot of CDS results and drop test data for transmitted forces.....	38
Figure 3-11. System architecture of ATSV's Exploration Engine [Stump et al. 2009]. .....	40
Figure 3-12. Examples of visualization tools in ATSV: (a) linked views that display the same brush settings; (b) using brushing to zoom in within the trade space [Stump et al. 2009]. .....	41
Figure 3-13. Flowchart of optimization method algorithm.....	42
Figure 3-14. Restraint configuration with 30/30 tie-down angles [FM 55-450-2 1992].....	49
Figure 4-1. Energy absorbing cargo restraint system featuring nylon strap and tear webbing [Shefrin et al. 1969]. .....	52
Figure 4-2. Load profile of steel chain/tear webbing and nylon strap/tear webbing restraints.....	54
Figure 4-3. CDS screenshot of two restraints attached to the cargo using the tie-down configuration featured in the comparative study.....	55
Figure 4-4. Sketch of the simple dynamic model for analyzing chain restraints (MB-I, MB-II).....	56
Figure 4-5. Diagram depicting the cargo, cabin floor, restraint, side tie-down angle ( $\theta$ ), and the vertical tie-down angle ( $\alpha$ ). .....	60
Figure 4-6. Plot of the number of restraints vs. side/vertical tie-down angle. Each series label provides the restraint type and the vertical tie-down angle. Series "SC/TW – 20" refers to steel chain/tear webbing restraint with vertical tie-down angle ( $\alpha$ ) of 20°. ....	62
Figure 4-7. Plot of the number of restraints vs. side/vertical tie-down angle. Each series label provides the restraint type and the vertical tie-down angle. Series "NS/TW 2 – 20" refers to nylon strap/tear webbing restraint with vertical tie-down angle ( $\alpha$ ) of 20°. ....	62
Figure 4-8. Top view of mounting points on cabin floor (blue) and cargo (red). ....	65
Figure 4-9. Plot of the results for Optimization Study #1 for MB-I and MB-II restraints.....	67
Figure 4-10. Visualization of restraint system closest to being feasible with steel chain restraints.....	68
Figure 4-11. Glyph plot of the feasible results for Optimization Study #2. The Pareto optimal designs are marked by "+" in white.....	71

Figure 4-12. Scatter plot of the feasible results for Optimization Study #2. The Pareto optimal designs are marked by “+”.....	72
Figure 4-13. Visualization of Design A restraint configuration. ....	73
Figure 4-14. Visualization for Design B restraint configuration. ....	74
Figure 4-15. Visualization for Design C restraint configuration. ....	75
Figure 4-16. Visualization for Design D restraint configuration. ....	77
Figure 4-17. Glyph plot of sample set of Optimization Study #3 results. The Pareto optimal designs are marked by “+” in white. No feasible designs.....	79
Figure 4-18. Scatter plot of Optimization Study #3 results. The Pareto optimal designs are marked by “+”. No feasible designs.....	80
Figure 4-19. Visualization for Design E restraint configuration.....	82
Figure 4-20. Visualization for Design F restraint configuration.....	83
Figure 4-21. Glyph plot results from optimization studies on steel chain/tear webbing (SC/TW) and nylon strap/tear webbing (NS/TW) restraints.....	85
Figure 4-22. Scatter plots of longitudinal cargo displacement results from optimization studies on steel chain/tear webbing (SC/TW) and nylon strap/tear webbing (NS/TW) restraints.....	85
Figure 4-23. Scatter plots of lateral cargo displacement results from optimization studies on steel chain/tear webbing (SC/TW) and nylon strap/tear webbing (NS/TW) restraints.....	86
Figure 5-1. Histogram plot of the error from “SC/TW – Longitudinal” regression model. ....	98
Figure A-1. Histogram plot for SC/TW – Longitudinal error.....	112
Figure A-2. Histogram plot for SC/TW – Lateral error.....	113
Figure A-3. Histogram plot for NS/TW – Longitudinal error. ....	113
Figure A-4. Histogram plot for NS/TW – Lateral error.....	114

## LIST OF TABLES

Table 2-1. Summary of current restraint technology.....	9
Table 3-1. Restraint configuration matrix defined by user for CDS.....	34
Table 4-1. Specifications of current restraint technology featured in comparative study.....	51
Table 4-2. Specifications of the energy absorbing restraints used in comparative study. ....	53
Table 4-3. Comparative study results comparing energy absorbing restraints and current technology.....	57
Table 4-4. Summary of results for Optimization Study #2 on steel chain/tear webbing restraints.....	70
Table 4-5. Summary of results for Optimization Study #3 on nylon strap/tear webbing restraints.....	81
Table 4-6. Summary of sample designs from Optimization Study #2 and #3.....	84
Table 5-1. Restraint table parameters and values. .....	94
Table 5-2. Sample restraint table for longitudinal impacts.....	95
Table 5-3. Summary of the details from regression analysis.....	97
Table A-1. Coefficients for regression model equations. ....	112

## **ACKNOWLEDGEMENTS**

I must first express my sincere gratitude to Prof. Edward C. Smith for his advice, guidance, and understanding throughout my time at Penn State. I will be forever in his debt for the numerous opportunities he has created for me in the past, for they will continue to open doors for me in the future. I would like to thank the Army Research Office for sponsoring my National Defense Science & Engineering fellowship without which I could not have finished my graduate studies. I would also like to extend my gratitude to Prof. Charles E. Bakis and Dr. Michael Yukish whose valuable insight, patience, and tireless efforts were indispensable to the completion of this thesis. The author also wishes to recognize Matt Hagon, Chandrashekahr Tiwari, Simon Miller, Eric Little, Gary Stump, and the NAVAIR Internal Cargo & Special Operations group for their generous efforts. I would also like to thank those who have made life bearable during times of stress: friends, family, Zeno's, Euroclub, Penn State Argentine Tango Club, open mics, Belgium, all the followers I have danced with, all the musicians I have jammed with, and my band (IPS). Finally, I would like to thank my father for his perspective, philosophy, support, compassion, sense of humor, emphasis on education, and for telling me that the more things I do, the more interesting I will become.

## Chapter 1

### Introduction

#### 1.1 Motivation

In the event of a helicopter crash or hard landing, high acceleration loads from the impact can result in the failure of the cargo restraint system and allow heavy cargo to move freely inside the cabin. The dangers of out-of-control cargo are severe and can lead to fatalities in what could otherwise be considered a survivable incident. The large payload requirements expected for future heavy-lift rotorcraft, such as that under investigation in the Joint Heavy Lift program [Tenney 2008], will further increase the risks involved for aircrew flying with heavy cargo. Simply increasing the amount or strength of cargo restraints, however, is not the most effective solution. The design of cargo restraint systems must be improved for crashworthiness without significant increases in weight or sacrificing usability for the cargo handlers. In addition to changes in restraint system design, cargo handling procedures for both future and current rotorcraft must be modified to satisfy the proper crash requirements.

The proposed idea for improving cargo restraint system design is to incorporate load limiters to create energy absorbing restraints and replace currently used elastic restraints (e.g., steel chains, nylon straps). A comparison of the force-stroke response of elastic and energy absorbing restraints is shown in Figure 1-1. Although elastic restraints have their own advantages in terms of high stiffness and low elongation, they suffer from the major shortcoming of transmitting high peak forces to the mounting points and airframe structure. The use of load limiters allow restraints to dissipate energy and reduce transmitted forces. The trade-off with using energy absorbing restraints is the inevitable displacement of the cargo due to the stroke that

is required by load limiters to arrest the cargo in a crash event. The amount of allowable cargo displacement is often limited by cabin space and seat locations of the crew.

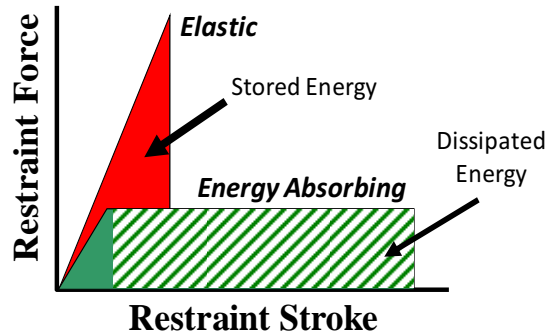


Figure 1-1. Comparison of force-stroke response for elastic and energy absorbing restraints.

## 1.2 Challenges

Incorporating load limiters can improve the crashworthiness of cargo restraint systems, but also complicate their design. To design and evaluate crashworthy energy absorbing restraint systems, simulation of a crash event is required. Closed-form analysis is not feasible due to both the changing geometry of the system and the highly nonlinear relationship between cargo displacement, velocity, and the applied restraint forces. Furthermore, designing energy absorbing restraint systems is a multi-objective optimization problem involving a trade-off between the total number of restraints, total weight of the restraint system, and cargo displacement. Constraints on the problem include the maximum force a restraint can transmit to mounting points, the requirement that the cargo does not move during normal operations, and the maximum allowable cargo displacement in a crash.

The ideal cargo restraint system would minimize all three objectives while satisfying all of the constraints, but the objectives are in conflict with each other. Therefore, selecting a configuration requires the decision maker to understand their options in trading off each of the objectives against each other.

Existing documentation regarding load preparation does not uniformly address the range of conditions experienced by cargo rotorcraft which can be categorized as normal operating conditions and crash events. The U.S. Army FM 55-450-2 field manual, for one example, provides procedures for restraining cargo but does not address energy absorbing cargo restraint systems or crash conditions. Another example is the military standard on aircraft crashworthiness (MIL-STD-1290) which does address crash conditions, but does not provide requirements for restraint systems regarding normal operating conditions. To prove sufficient crash safety, the cargo restraint system must be able to properly restrain cargo for both scenarios and the requirements must be tailored to specifically address the design of energy absorbing cargo restraint systems.

Past attempts at introducing energy absorbing cargo restraint systems were abandoned due to issues regarding usability for the cargo handlers. The characteristics of energy absorbing cargo restraint systems are very different from current restraint technology, and thus the current load preparation procedures must be modified to address a wide range of cargo handling scenarios through general guidelines and rules-of-thumb.

### **1.3 Scope and Objectives**

The focus of this thesis is to provide guidance to cargo handlers, using methods and design tools, on how to select and configure optimal energy absorbing cargo restraint systems to improve crashworthiness. The energy absorbing cargo restraint system considered in this thesis is composed of a load limiter and a lanyard. Sample exercises of the optimization method are conducted within a design space based on existing rotorcraft. To achieve crashworthiness, the restraint system is optimized to satisfy the MIL-STD-1290 crash requirements for unidirectional impacts in the forward longitudinal and lateral directions.

The overall goals are as follows:

1. Develop a cargo dynamics simulation to evaluate cargo restraint configurations
2. Investigate the influence of design variables on the performance of energy absorbing cargo restraint systems
3. Develop method and tools to configure the optimal energy absorbing restraint configuration
4. Create guidelines for cargo handlers to use in the field when using energy absorbing restraint systems
5. Create a new set of requirements for crashworthy cargo restraint systems

#### **1.4 Organization of Thesis**

This thesis begins with a literature review to document crash safety requirements for military rotorcraft, provide examples of energy absorbing restraint technology, and summarize analytical methods used in the past for cargo dynamics simulation and restraint system design. The chapter on analytical tool and methods (Chapter 3) describes the tools developed to design crashworthy cargo restraint systems. These tools include the cargo dynamics simulation and the optimization method. The chapter on results and discussion (Chapter 4) provides details on comparative, parametric, and optimization studies conducted using the tools discussed in Chapter 3. The studies were conducted to compare current restraint technology with energy absorbing cargo restraints, and as an exercise of the optimization method for a generic cargo handling scenario. The results from the analytical studies and any trends observed are discussed in Chapter 4. Recommended requirements, design criteria, as well as guidance on load preparation are

provided in Chapter 5 for energy absorbing cargo restraint systems. Finally, Chapter 6 consists of conclusions and recommendations.

## Chapter 2

### Literature Review

#### 2.1 Crashworthiness Requirements

Crashworthiness is an important topic for military rotorcraft as they often operate in treacherous conditions and hostile environments. In 1974, MIL-STD-1290 was created as the standard to establish crashworthiness criteria for the U.S. military's light fixed and rotary-wing aircraft. In the standard, aircraft crashworthiness is defined as “the ability of an airframe structure to maintain a protective shell around occupants during a crash and minimize accelerations applied to the occupiable portion of the aircraft during crash impacts [**MIL-STD-1290A(AV) 1988**.]” MIL-STD-1290 takes a systems approach to achieve crashworthiness by designing the individual components to cooperatively contribute in preventing occupant injuries and fatalities. For example, the crew seats are designed while considering the energy attenuating contributions from the airframe structure and landing gear; allowing for the system as a whole to provide the desired crash response. MIL-STD-1290 was largely based on the design criteria of the Aircraft Crash Survival Design Guide which was first published in 1980 and had its most recent revision in 1989 [**Zimmermann et al. 1989**].

The Aircraft Crash Survival Design Guide (ACSDG) is a five volume document created by Simula Inc. and prepared for the Aviation Applied Technology Directorate (AATD). Each volume of the ACSDG focuses on specific set of aircraft system components to address the five factors that influence survivability: crash resistance of aircraft structure, tie-down strength, occupant acceleration during crash impact, occupant crash impact hazards, and post-crash hazards. The ACSDG provides design engineers with the crash conditions and guidelines to

design crashworthy aircraft. The parameters which define a crash condition are the direction of impact, the magnitude, shape and duration of the pulse peak, and the impact velocity. The values of these parameters depend on the type of crash as well as the aircraft system component and the method in which they enhance survivability. Several aircraft components (e.g., crew seats, landing gear, subfloor structure) are designed to limit the acceleration applied to the occupants. For these components, the design conditions are based on human tolerance and each component dissipates energy to attenuate the peak, and the duration, of the acceleratory loads on the occupants. In addition to attenuating the impact loads on the occupants, there are other system components (e.g., engine mounts, cargo restraints) that are designed to maintain a “protective structural envelope” for the occupants [Zimmermann et al. 1989].

The third volume of the ACSDG specifically addresses cargo retention by providing crash conditions and guidelines for cargo restraints. The purpose of the cargo restraint system is to control cargo motion to protect the occupants. The crash condition used to evaluate cargo restraint systems in the forward longitudinal direction is a 16-G peak cabin floor acceleration with an impact velocity of 13 m/s. The requirement for a lateral impact is a 10 G peak with a 6.4 m/s impact velocity. There are other additional crash conditions (e.g., vertical, aft, combined), but the scope of this thesis extends only to purely forward longitudinal and lateral impacts. The crash conditions are approximated as a triangular shaped pulse as shown in Figure 2-1. The pulse duration can be calculated given the pulse peak and impact velocity.

Past research on crash data for fixed-wing cargo aircraft also considered a triangular pulse to be a reasonable approximation of the acceleration response in a crash event [Avery 1965, Russo 1966, Shefrin et al. 1969]. Avery also investigated the effects of pulse characteristics on the performance of the cargo restraint system. It was found that changes in the peak had the most influence on restraint system performance. Although changes in the shape (e.g., triangular, sinusoidal) of the pulse or pulse duration, while conserving total energy, did not have a

significant effect [Avery 1965]. Shefrin et al. points out that the current ACSDG crash loads satisfy the 80<sup>th</sup> and 90<sup>th</sup> percentile of survivability criteria for longitudinal and lateral impacts, respectively [Shefrin et al. 1969].

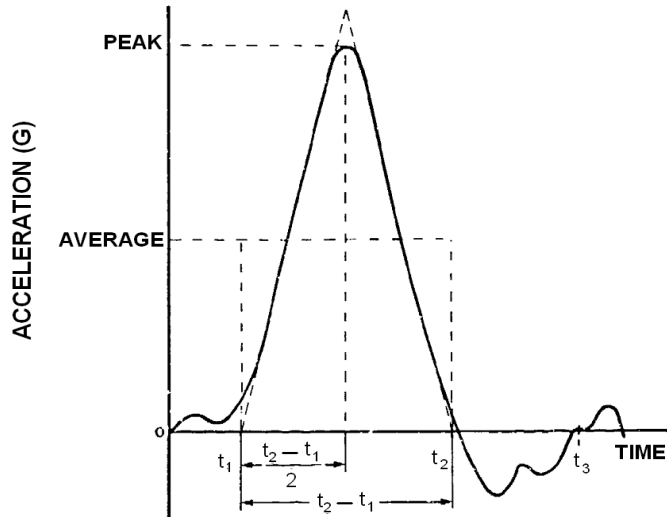


Figure 2-1. Typical aircraft floor acceleration pulse [Zimmermann et al. 1989].

Although MIL-STD-1290 is currently an active standard, cargo handlers are not restraining cargo in compliance with the specification. For Army cargo rotorcraft, cargo handlers follow the FM 55-450-2 field manual on helicopter internal load operations [FM 55-450-2 1992]. The field manual instructs cargo handlers to restrain cargo for loads experienced in normal operating conditions instead of crash conditions as defined in MIL-STD-1290 and the ACSDG. The factors which influence the normal operations restraint criteria include acceleration during takeoff, stability during flight, deceleration during landing, and the type of landing field. Furthermore, the field manual provides cargo handlers with static load factors and requires a static analysis to configure the restraint system. In the forward longitudinal direction, a 4 G static load factor is used. The lateral direction requires the cargo restraints to be designed for a 1.5 G static load factor. The current restraint criteria are severely deficient compared to MIL-STD-1290 and the ACSDG.

Table 2-1. Summary of current restraint technology.

Restraint Name	Restraint Type	Load Capacity	Performance Specifications
CGU-1/B	Nylon Strap	22.5 kN	MIL-PRF-27260
MB-I	Steel Chain	44.5 kN	MIL-DTL-6458
MB-II	Steel Chain	88.9 kN	MIL-DTL-6458
MA-2, MA-3	Nylon Net	44.5 kN	MIL-T-26780

## 2.2 Current Restraint Technology

A list of the restraints currently used on cargo aircraft is provided in Table 2-1. The restraint systems currently by cargo handlers are elastic and have no energy absorbing capabilities. The CGU-1/B restraint is composed of a nylon strap. The MB-I and MB-II restraints are composed of steel chains. The MA-2 and MA-3 restraints are cargo nets made of nylon webbing and are used to restrain loose cargo. The CGU-1/B restraint is rated for 22.5 kN and is typically used on lightweight and loose cargo [MIL-PRF-27260C 1998]. The MB-I and MB-II are used on heavy cargo and feature load capacities of 44.5 kN and 111 kN, respectively [MIL-DTL-6458F 2008]. The MB-II is typically found on fixed wing aircraft only, as the mounting point load capacities on cargo rotorcraft are too low to take advantage of the high strength MB-II restraint [FM 55-9 1993]. The MA-2 and MA-3 cargo nets are generally used to tie-down loose cargo and are rated for 44.5 kN cargo loads.

The MB-I and MB-II restraints provide a rigid system with very low elongation. Past research, however, found issue with rigid restraint systems as they are susceptible to unpredictable high frequency oscillations which may cause restraint failure [Avery 1965, Russo 1966]. The CGU-1/B restraint and MA-2/MA-3 cargo nets sit on the other end of the spectrum with low stiffness and high elongation at the working load limit. Furthermore, nylon straps suffered from dynamic overshoot when loaded at high rates [Shefrin et al. 1986, Avery 19865, Russo 1966]. The ACSDG defines dynamic overshoot response as “the amplification of

decelerative force on the cargo or personnel above the floor input decelerative force (ratio of output to input) [Zimmermann et al. 1989].” Dynamic overshoot response is often the cause of mounting point failure in a crash event when using nylon restraints. The issues with current restraint technology in dynamic environments, and being able to provide sufficient restraint in crash conditions, became the driving force behind research into incorporating energy absorbing devices in cargo restraint systems.

## 2.3 Energy Absorbing Restraints

Both the ACSDG and MIL-STD-1290 recommend the use of load limiters for load attenuation if the fuselage and floor structure are not strong enough to withstand the cargo crash loads. The energy absorbing cargo restraint system concepts discussed in the ACSDG and other papers have two main components: lanyard and load limiter.

### 2.3.1 Load Limiter Technology

A significant amount of research was conducted on load limiter technologies in the 1960s and 1970s. Shefrin et al. [1969] conducted an investigation into different methods of energy absorption including crushing, extrusion, twisting, bending, and shearing. This investigation also included possible candidates for materials including honeycomb, foams, fiber reinforced plastics, elastomers, and different types of fluids. One of the load limiter concepts included in the work by Shefrin et al. was the wire bender shown in Figure 2-2. As the steel wire is pulled through a set of rollers, the wire undergoes plastic deformation and energy is dissipated. The wire bender has been prominently featured in several of the earlier papers on crashworthy cargo restraint systems.

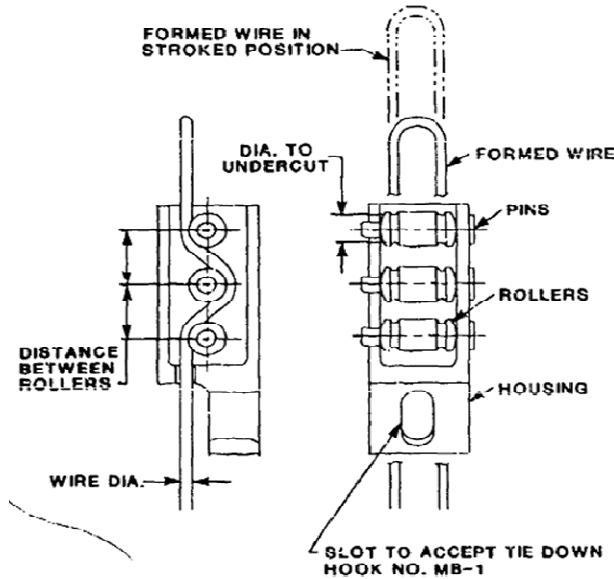


Figure 2-2. Wire bender load limiter with wire stored outside housing [Zimmermann et al. 1989].

The ACSDG [Zimmermann et al. 1989] refers to the results of an early Naval Air Development Center (NADC) sponsored report that also found the wire bender to be the optimum design for cargo retention application based on size and weight. Crash tests have shown that crashworthiness could be improved by incorporating wire benders. Furthermore, the reduction in transmitted forces from using the wire bender would permit the use of lower safety factors for mounting points and backup structure; allowing for a reduction in structural weight [Shefrin et al. 1986]. The wire bender found its way onto cargo aircraft, but was eventually abandoned due to numerous issues regarding usability. Introducing the wire bender resulted in a heavier, and bulkier, cargo restraint system; making it difficult to use for the cargo handlers and in some cases causing injury. Furthermore, guidance was not provided on how to properly account for and address cargo movement in the event of a crash as cargo handlers were typically used to using rigid cargo restraints [Anderson et al. 2010].

In addition to wire benders and other metallic load limiters, a significant amount of research has recently been conducted on textile-based load limiters. Examples of textile-based

load limiters include stitch ripping devices (SRDs) and tear webbing [Hagon 2009]. For SRDs, the energy absorbing mechanism is the breaking of stitches as shown in Figure 2-3. SRDs are constructed by folding a piece of webbing in half and stitching the halves together with thread. As the webbing is pulled apart the stitches break and energy is dissipated. Tear webbing is similar to SRDs, but two pieces of webbing are woven together with binding yarns as shown in Figure 2-4. When the webbing is pulled apart, the binding yarns break and energy is dissipated.



Figure 2-3. Photographs from a quasi-static test of SRD [Hagon 2009].

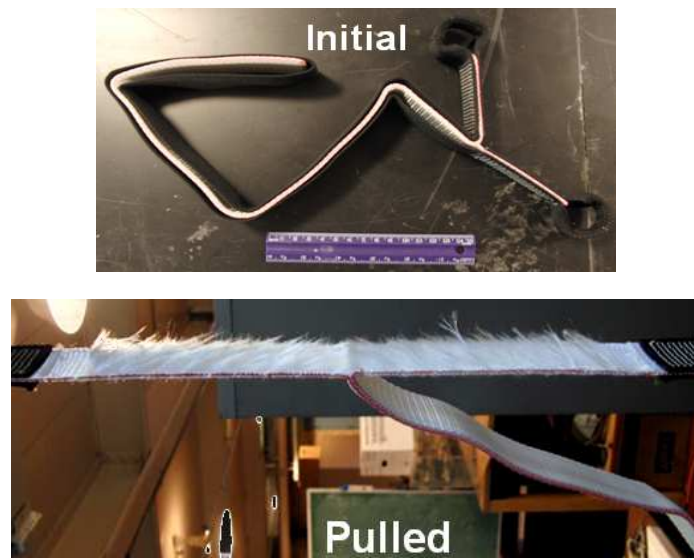


Figure 2-4. Photographs from quasi-static test of tear webbing [Miller 2010].

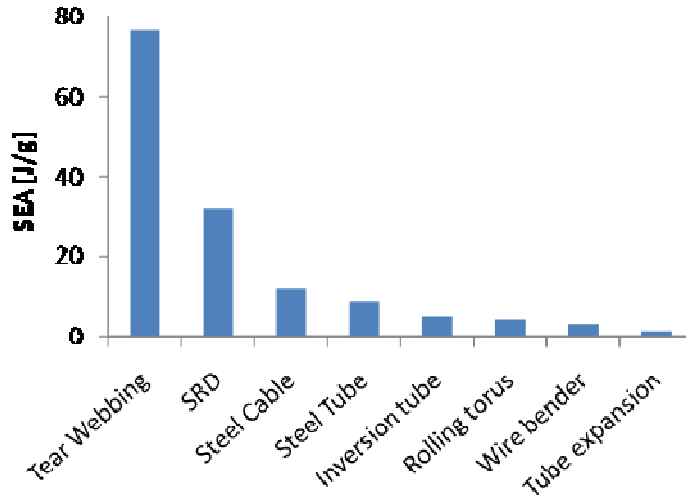


Figure 2-5. Comparison of SEA values in [J/g] of textile load limiters and existing technologies [Hagon et al. 2007].

Originally used by rock climbers, Wess investigated the possible application of SRDs to arrest the motion of fighter jets sliding across aircraft carrier decks [Wess 2004]. Scaled-up versions of the SRD are currently fielded on U.S. Navy carriers for arresting the motion of aircraft on a pitching carrier deck. The success of scaling SRDs for the aforementioned application led to further investigation into the use of textile-based load limiters in cargo restraint systems [Hagon 2009]. A chart comparing the specific energy absorption (SEA) values, which is measured in J/g, is provided in Figure 2-5. Compared to the current state-of-the-art in load limiter technology (e.g., wire bender), textile-based load limiters show a significant improvement in terms of SEA. Tear webbing in particular features the highest SEA values [Hagon et al. 2007]. The ideal load limiter will feature high SEA and a design which takes usability into consideration. The load limiter featured in the analysis presented later in this thesis is modeled after tear webbing devices.

### 2.3.2 Lanyard Technology

The ACSDG recommends using restraining lines (i.e., lanyards) with high stiffness when incorporating load limiters to achieve efficient energy absorption. The use of stiffer lanyards will reduce the amount of elongation prior to activating the energy dissipating mechanisms of the load limiter and result in less overall cargo displacement. Past research on energy absorbing cargo restraint system concepts investigated the use of fabric materials (e.g., Kevlar, Dacron, polyester, nylon) as well as metals (e.g., steel chain). Cargo restraints featuring wire benders combined with current restraint technology (e.g., CGU-1/B, MB-I) were able to provide sufficient restraint in dynamic crash tests [**Burrows et al. 1978**]. The general focus of earlier research was shifted towards finding low elongation, lightweight alternatives such as Dacron, polyester, and Kevlar. Experiments were conducted for Kevlar — similar to Air Force parachute tapes — and polyester webbing. The results show that cargo restraints that combine either Kevlar or polyester webbing with wire benders were suitable to provide crash safety, produce less cargo displacement than nylon straps, and weigh less than chains. Although Kevlar was significantly better than polyester in terms of displacement performance, it is highly susceptible to environmental conditions. The tests also showed that the energy absorbing restraint systems were statically elastic at normal maneuvering flight conditions and the resulting cargo movement was of little importance [**Shefrin et al. 1986**].

Dacron, a thermoplastic polymer, is another example of a high strength, low elongation material that was considered a candidate for the lanyard component. At a load of 22.5 kN in dynamic conditions, Dacron webbing is reported to have the least amount of elongation of 2.5% [**Russo 1966**]; while the elongation of Kevlar and polyester webbing previously mentioned is 3.5% and 7%, respectively [**Shefrin et al. 1986**]. The elongation of the currently used CGU-1/B

restraint is reportedly 18% [Anderson et al. 2010], although others have reported a 25% elongation in the nylon strap [Shefrin et al. 1986].

In addition to straps and webbing, cargo restraint concepts have also combined cargo nets with load limiters [Avery 1965]. Avery investigated the use of extensible and inextensible nets. The extensible nets were essentially cargo nets constructed with nylon webbing. Examples of inextensible nets include a steel mesh net. The investigation revealed that trade-offs exist between restraint system weight and cargo displacement. It was concluded that the combination of an inextensible net and load limiter was “the most effective for controlling cargo displacement and minimizing weight.” The key issue with using extensible nets is the large amounts of cargo displacement. Whether it is chain, webbing, or net; the desirable characteristics of a lanyard is high stiffness, high strength, and low weight.

## 2.4 Load Preparation

Cargo handlers are currently using documents such as the U.S. Army field manual FM 55-450-2 for guidance on load preparation. The field manual splits the cargo handling scenarios into two categories: restraining cargo with mounting points and without mounting points. For cargo with mounting points, the tie-down angle for all restraints should be as close to 30° sideways from the longitudinal axis and 30° from the floor as possible. This “30/30” tie-down angle is presented as a rule-of-thumb and a schematic of this configuration is shown in Figure 2-6. The rule-of-thumb was chosen to be 30/30 to provide a sufficient amount of restraint in all directions. It is important to be aware of that fact that tie-down angle can also influence the strength of the mounting points. Previously conducted studies have shown that the mounting point load capacity is prescribed for loading in the vertical direction, but the strength deteriorates significantly as the loading angle with respect to the vertical axis increases [Shefrin et al. 1986].

Neither the FM 55-450-2 nor MIL-STD-1290 address the effect of tie-down angles on mounting point load capacity.

The tie-down configuration is also required to be symmetric about the longitudinal axis as shown in Figure 2-6. The ACSDG recommends symmetrical tie-down configurations to avoid overloading individual restraints and causing failure of the restraint system.

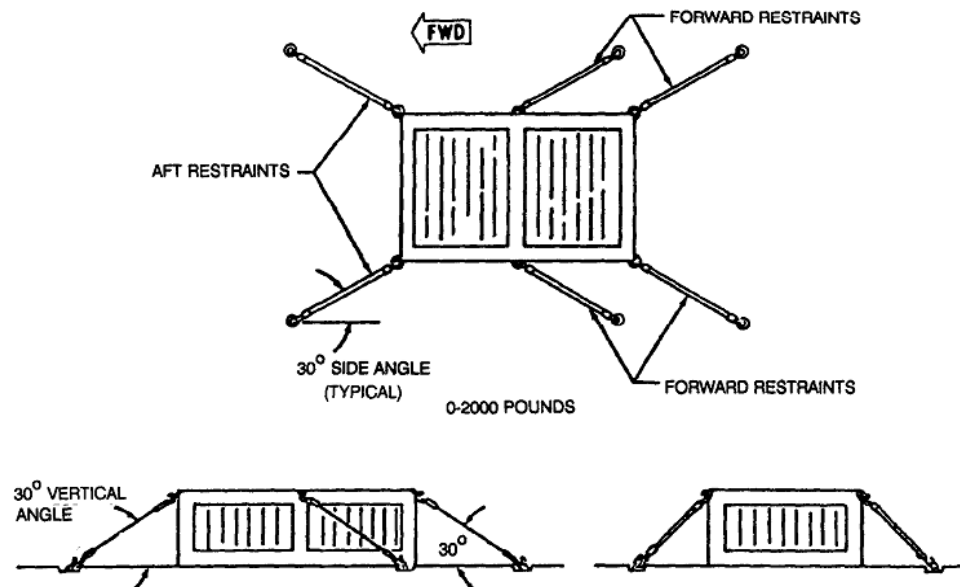


Figure 2-6. Restraint system with a tie-down configuration that is symmetric about the longitudinal axis [FM 55-450-2 1992].

The field manual also provides an overview of different methods of wrapping restraints around the cargo, as shown in Figure 2-7, instead of depending only on available mounting points. The method of wrapping around cargo is possible with nylon strap restraints (i.e., CGU-1/B), but not with steel chain. The benefits of wrapping restraints around cargo include providing supplemental restraint when no mounting points are available on the cargo and the lack of coupling for impacts in different directions.

Cargo handlers are also advised to avoid configuring restraint systems with restraints having different load-elongation characteristics in order to avoid potentially uneven restraint loads—leading to restraint system failure [Russo 1966].

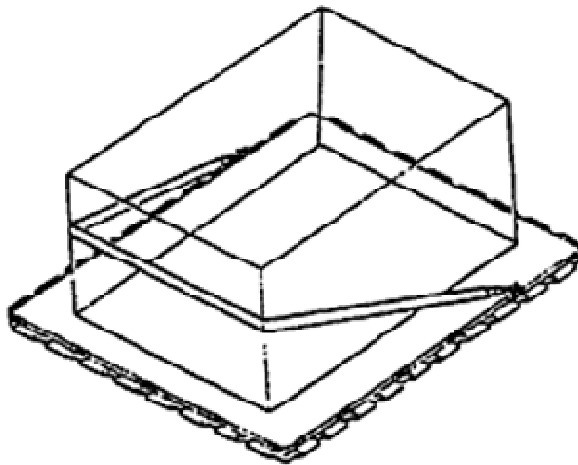


Figure 2-7. Supplemental restraint by wrapping around cargo [FM 55-450-2 1992].

Several papers on energy absorbing restraint system concepts typically focused on cargo handling scenarios where only the longitudinal impact would be of concern. For example, Avery focused on missions involving only cargo transportation, as opposed to passenger-cargo missions [Avery 1965] — the difference being that there are no occupants that sit near the cargo or even in the cabin area. Shefrin et al. [1969] noted that in actual practice, personnel are transported with all types of cargo without restriction. Although the loads in a longitudinal impact are much greater, the lateral impact may be more stringent due to the amount of allowable cargo displacement. The cabin area for existing cargo rotorcraft (e.g., CH-47) [FM 55-450-2 1992] is quite narrow and the commonly used HCU-6/E pallets [MIL-DTL-27443F 2003] are nearly flush against the walls. The papers previously mentioned did not address the issues that may arise from excessive lateral displacement. Cargo displacement should be constrained to avoid damage to the side wall structure; which is responsible for maintaining a protective structural envelope for the occupants [Anderson et al. 2010]. Shefrin et al. provided a list of the allowable displacements inside a CH-47 for common types of cargo. The lateral distance from cargo to airframe structure varied from 15 cm to 38 cm. The longitudinal dimensions were less critical, but were also

dependent on the location of the crew when seated. In general, cargo handling scenarios are unique to each mission and type of aircraft.

Energy absorbing cargo restraint systems have significantly different operating characteristics from current restraint technology, therefore one cannot assume that the current load preparation procedures and rules-of-thumb can be applied to energy absorbing cargo restraint systems. To be able to implement a new restraint system requires guidance and instructions for cargo handlers.

## 2.5 Design Methods and Tools for Energy Absorbing Cargo Restraint Systems

Several analytical methods have been used to design and evaluate cargo restraint systems. A static analysis is currently used by cargo handlers to design the cargo restraint system using chain and nylon strap restraints. Research on aircraft crash data, however, revealed that the static load factors provided in field manuals, and used by cargo handlers, are not representative of the dynamic conditions of a crash event [**Aver 1965, Russo 1966**]. The majority of the research on energy absorbing cargo restraint systems was conducted in the 1960s – 1980s. Current efforts in crash modeling are primarily focused on determining the acceleratory loads on the aircraft for impacts on different types of surfaces (e.g., soft soil, water). The early works on cargo retention did include efforts to develop models to evaluate cargo restraint systems in dynamic conditions.

Russo introduced the “equivalent static load factor” concept to simplify the analysis for evaluating cargo restraint systems in dynamic crash conditions. Although Russo’s focus was on fixed-wing aircraft, his method could be applied for rotorcraft applications with the only differencing being a crash pulse with a lower peak. From the equations of motion for the cargo and restraint system, a curve was generated to depict the relationship between restraint stroke and equivalent static load factor. The curve in Figure 2-8 was created specifically for a load limiter

connected in series with a nylon strap lanyard and depicts the restraint performance in crash conditions. The force response of the load limiter is exactly the same as the one showed in Figure 2-9. To use the curve in Figure 2-8, a value for the amount of load limiter stroke (i.e., restraint stroke) is chosen and the corresponding equivalent static load factor is multiplied by the cargo weight to determine the amount of restraint required. The amount of restraint required is then divided by the load capacity of each load limiting restraint to determine the total number of restraints required for the restraint system.

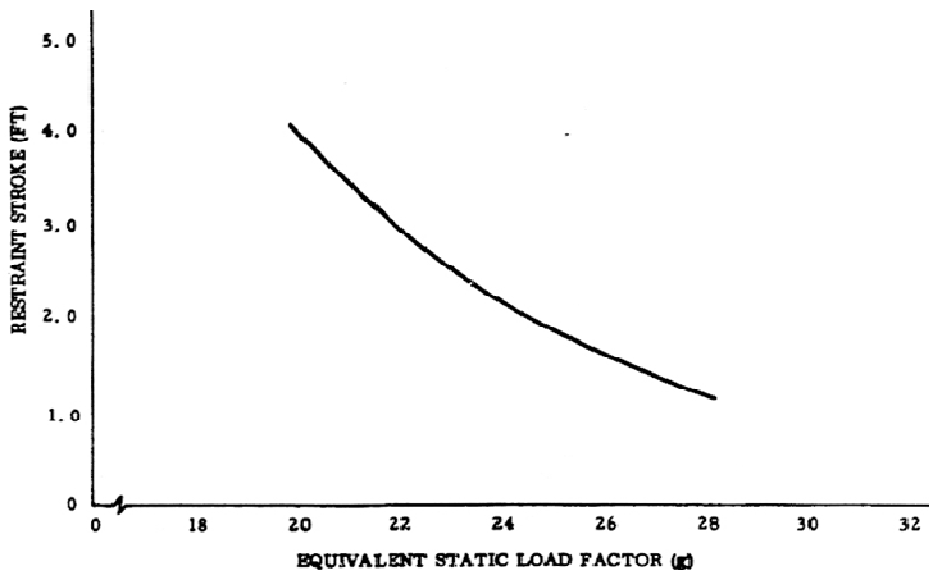


Figure 2-8. Nylon tie-down devices in series with load limiter. Based on pulse-duration-envelope design criterion and an elongation of 30 cm at 22.5 kN [Russo 1966].

This is essentially a method of conducting a static analysis while taking the dynamic crash pulse into account. There are, however, some limitations to using equivalent static load factors to design cargo restraint systems. Unless every restraint in the restraint system has the same tie-down angle and length, a separate curve must be calculated for each restraint. Russo conducted case studies of restraining several different types of cargo with energy absorbing cargo restraints and not all of the restraints had identical tie-down angles. Furthermore, the analysis does not take into the account the changing geometry of the system. As the cargo moves, the tie-

down angle will change and the amount of restraint provided in a specific direction will also change. Therefore, equivalent static load factors do not provide an accurate estimation of the amount of restraint required throughout a crash event.

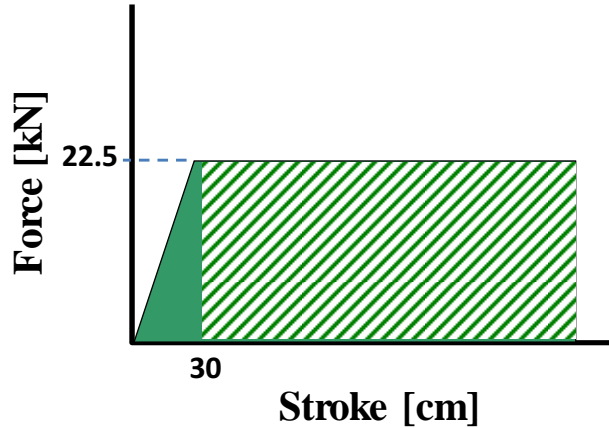


Figure 2-9. Force-stroke response of a load limiter.

Modeling work was also extended to cargo nets by Avery. The analysis was simplified for the net to provide restraint purely in the longitudinal direction as only longitudinal impacts were of concern. The cargo restraint system was composed of a cargo net connected in series with a load limiter. The force-stroke response of the load limiter is identical to the one used by Russo. The vehicle-level system modeled by Avery is shown in Figure 2-10, where  $X_F$  is the displacement of the cargo floor,  $X_L$  is the displacement of the load limiter, and  $X_C$  is the displacement of the cargo. Russo modeled the nonlinear behavior of the extensible net (i.e., nylon cargo net) as a cubic function of displacement. The only forces on the cargo were from the cargo net and load limiter. For the inextensible net (i.e., steel mesh), the cargo net was completely rigid with no deflection and the behavior of the restraint system was essentially the load profile of the load limiter. The shortcoming of Avery's model is its simplification of the design space. Although a cargo net can provide restraint in a single direction (e.g., barrier nets), the forces on the load limiters attached to the webbings of the net are dependent on the tie-down angles.

Approximating several load limiters as a single load limiting device may be convenient for a general calculation on cargo displacement, but it does not provide guidance to the cargo handlers who need to know which mounting points to use for preparing the cargo net. Analytical models require a sufficient amount of detail to be used by cargo handlers as a tool to select and configure crashworthy energy absorbing cargo restraint systems.

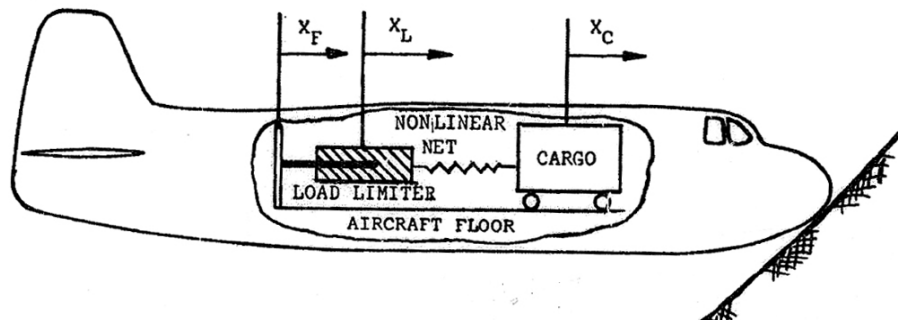


Figure 2-10. Diagram of the vehicle-level system for analyzing restraint system featuring a cargo net combined with a load limiter [Avery 1965].

## 2.6 Summary

Previous research has shown that current restraint technology cannot provide a sufficient amount of restraint to withstand a crash event as defined by MIL-STD-1290 and the ACSDG. The use of load limiting technology was shown to improve the crashworthiness of restraint systems, however, the state-of-the-art in load limiting technology at the time had issues regarding usability and therefore was abandoned. Since then, new technologies have emerged that address usability issues. The analytical methods used in past research made several simplifying assumptions due to the lack of computing resources. Furthermore, optimization methods were never introduced into the design process for cargo restraint systems.

The following chapter describes a cargo dynamics simulation (CDS) that was specifically developed to evaluate energy absorbing cargo restraint systems in a crash event. The CDS takes a

more detailed approach to solving the complex problem of simulating the nonlinear relationship between restraint forces and cargo movement. Furthermore, the simulation is capable of evaluating restraint systems with complex tie-down configurations. Finally, an optimization method is presented which is used to determine the optimal energy absorbing cargo restraint configuration.

## **Chapter 3**

### **Analytical Tools and Methods**

This chapter provides details on the analytical approach and the corresponding tools and method developed for selecting and configuring optimal energy absorbing cargo restraint systems. The cargo dynamics simulation was developed to serve as an analytical tool to evaluate cargo restraint systems in a crash event. The purpose of the simulation is to evaluate the crashworthiness of specific configurations of energy absorbing cargo restraint systems. An optimization method was created to determine the optimal cargo restraint configuration to improve crashworthiness for a given cargo handling scenario. The optimization method combines the cargo dynamics simulation with the Applied Research Laboratory Trade Space Visualizer — a multi-dimensional data exploration and visualization software — to exercise the simulation over the design space and visualize the results. Results of optimization studies conducted for this thesis, and details on the simulation and optimization parameters, are provided in the following chapter.

#### **3.1 Cargo Dynamics Simulation (CDS)**

The cargo dynamics simulation (CDS) simulates the interaction between the components of a vehicle-level system (i.e., cargo, restraint system, and cabin floor) during a crash event. Cargo restraints anchor the cargo to the cabin floor via mounting points on both the cargo and cabin floor. A diagram of the system before and after a crash is shown in Figure 3-1. In the event of a crash, the cabin floor will decelerate while the cargo continues to move until the restraints

arrest its motion. Energy absorbing restraint systems are not rigid and require stroke to absorb energy, resulting in displacement of the cargo.

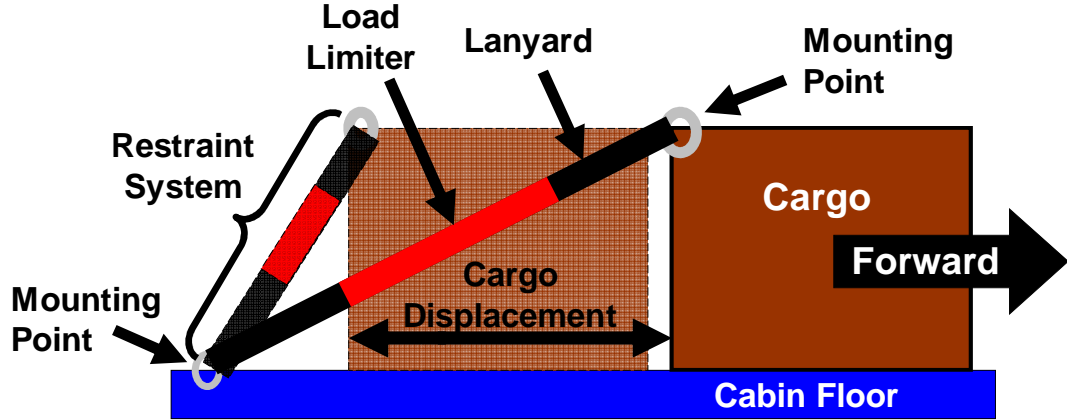


Figure 3-1. Diagram of the vehicle-level system used in the cargo dynamics simulation before and after a crash event.

The complicated dynamics and nonlinear behavior of energy absorbing restraints excludes closed form analysis. Therefore, the CDS was developed in MATLAB to run crash simulations, evaluate cargo restraint systems, and aid in the search for optimal restraint configurations.

### 3.1.1 Cargo Dynamics Simulation: Analytical Approach

The CDS is used to evaluate the crashworthiness of energy absorbing cargo restraint systems. The CDS calculates cargo movement and restraint forces throughout a crash event. The parameters of the crash pulse (i.e., shape, peak, duration) are defined by the user. The vehicle-level system model is formulated with a set of state-variable equations and is solved using MATLAB's *ode45* solver. The *ode45* solver is based on an explicit 4th and 5th order Runge-Kutta formula typically used for non-stiff problems and is a one-step solver. The cargo and cabin floor are treated as rigid bodies each with six degrees-of-freedom. Friction between the cargo and

cabin floor is not taken into account as it is not a reliable factor in arresting cargo [Romero 2004]. Orientation and rotational dynamics of the cargo and cabin floor are calculated using Euler parameters and then converted to Euler angles for the simulation output. The CDS is also capable of providing a video of the simulation for the user to visualize cargo movement during a crash event. A screenshot of a sample video result is shown in Figure 3-2.

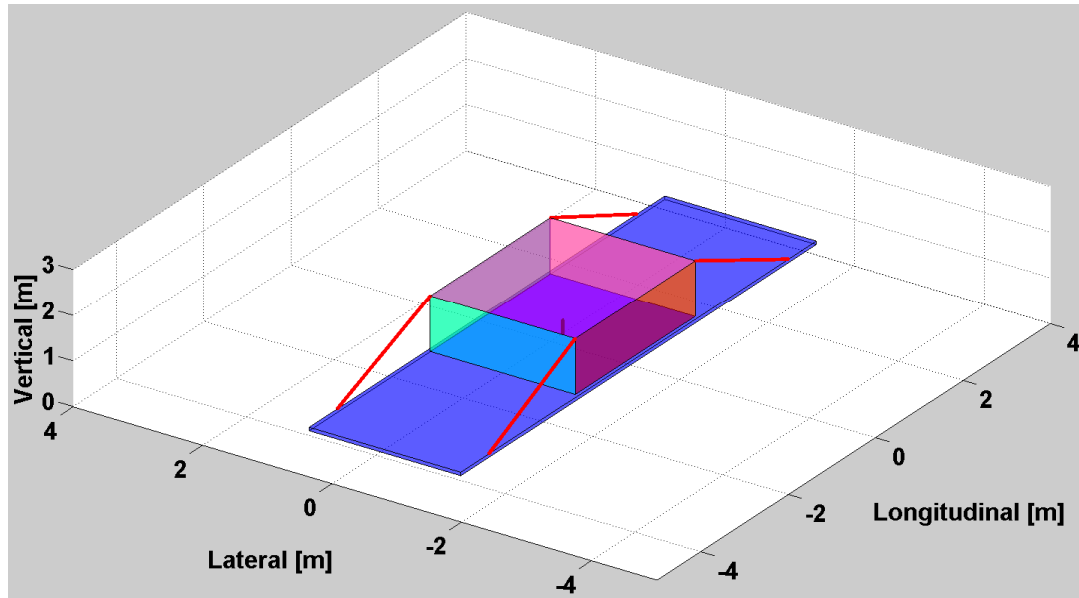


Figure 3-2. Screenshot of cargo dynamics simulation results video.

### 3.1.2 Model Formulation

The cargo is modeled as a single rigid container with mounting points for restraint attachment. To simplify the analysis, the cabin floor is used to represent the entire aircraft and contains an array of mounting points for restraint attachment. Like the cargo, the cabin floor is treated as a rigid body and is assumed not to deform. The scope of the analysis does not include an investigation into the effect of the transmitted loads on the airframe structure, however, failure of mounting points is taken into account. The locations of mounting points on both the cargo and

cabin floor depend on the cargo handling scenario (i.e., type of cargo, type of aircraft) and are inputs defined by the user. Mounting points can be located on the outside of the container like actual cargo containers. Cargo with more complicated geometry (e.g., vehicles) can be approximated as a container with mounting points located inside the container walls. The mass, geometry, and the location of the center of gravity of the cargo container and cabin floor are also specified by the user.

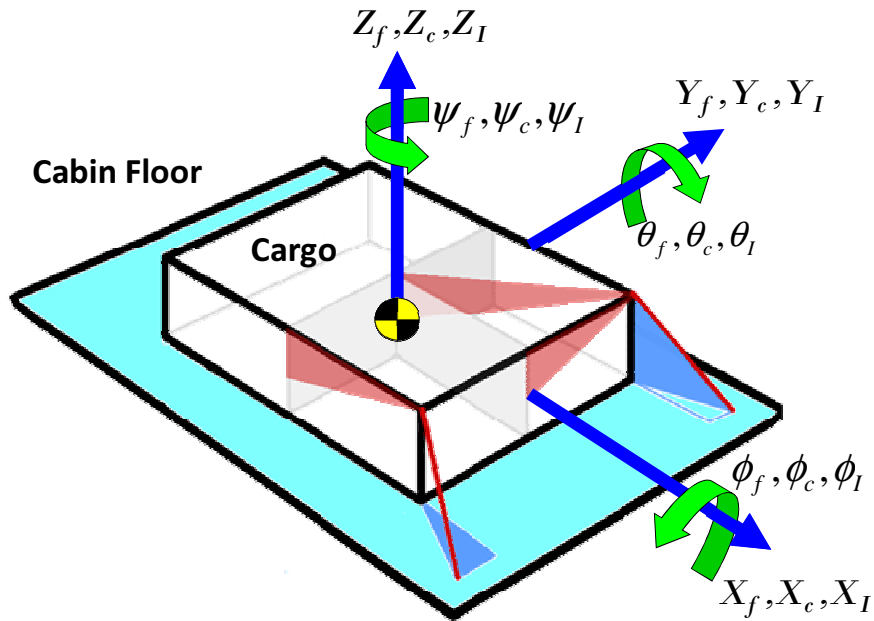


Figure 3-3. Diagram of detailing the local coordinate systems for the cargo and cabin floor.

### ***Reference Frames***

The positive directions for translation, velocity, acceleration, and restraint force components and for pitch, roll, and yaw are shown in Figure 3-3. There are three reference frames used in the CDS: the inertial reference frame and two local reference frames which are fixed to the cargo and cabin floor. Subscripts are used to differentiate the variables in the local and inertial reference frames. Variables with subscript “*f*” refer to variables in the local reference frame fixed

to the cabin floor. Variables with subscript “*c*” refer to variables in the local reference frame fixed to the cargo container. Variables with subscript “*I*” refer to variables in the inertial reference frame. For example,  $X_f$  denotes the direction of translation of the cabin floor while  $X_c$  denotes direction of translation for the cargo container. The direction of translation in the inertial reference is denoted by  $X_I$ . The origins of the local reference frames for the cargo and cabin floor are located at their respective centers of gravity (CG). Figure 3-3 shows the system at the start of the simulation where all three references frames are aligned with each other and share the same origin. In the local and inertial reference frames, the *X*, *Y*, and *Z* axes refer to the longitudinal, lateral, and vertical directions, respectively. While  $\theta$ ,  $\varphi$ , and  $\psi$  respectively refer to pitch, roll, and yaw in the local and inertial reference frame. The output of the CDS for translation, velocity, acceleration and force components are provided in the inertial reference frame. The CDS output for the orientation of the cabin floor and cargo container, however, are in the local reference frames.

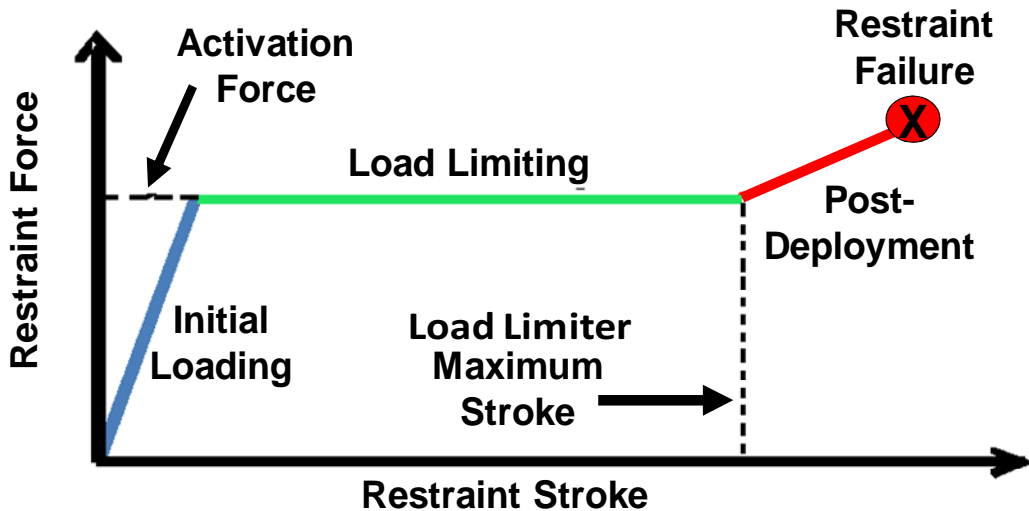


Figure 3-4. Load profile of energy absorbing restraints.

### ***Energy Absorbing Restraint Load Profile***

The load profile of energy absorbing restraints consists of three distinct phases as shown in Figure 3-4. The energy absorbing restraint exhibits linearly elastic behavior in the initial loading phase. The elongation of the lanyard is the primary contributor to the restraint stroke in this phase. The load limiting phase begins when the force in the restraint reaches the activation force. The activation force is the force required to activate the energy absorbing mechanisms of the load limiter. The transmitted restraint force is limited to the activation force throughout the load limiting phase as energy is being dissipated. The load limiter stroke contributes to the overall restraint stroke. The load limiting phase ends when the load limiter is fully deployed and is no longer able to dissipate energy. At this point, we have reached the maximum stroke of the load limiter. The final phase is post-deployment where the restraint exhibits decreased stiffness — particularly with fabric lanyards and/or textile based load limiters. The post-deployment phase continues until failure of the restraint system which can be caused by failure of the restraint itself or of the mounting points. The model does not account for recoil/rebound in the cargo restraint system.

### ***Cargo Dynamics***

For the equations presented in this chapter, subscripts are used to denote the variables which refer to the dynamics of the cabin floor and cargo. Variables with a subscript “*f*” denote variables which describe the loads and dynamics of the cabin floor in the local cabin floor reference frame. Variables with a subscript “*c*” denote variables which describe the loads and dynamics of the cargo in the local cargo reference frame. The translational dynamics of the cargo are only affected by the applied forces of the restraint system as shown in

$$\ddot{\vec{X}}_c = \frac{1}{m_c} \sum_{i=1}^N \vec{F}_c^{(i)} \quad (3-1)$$

where  $\ddot{\vec{X}}$  (i.e.,  $[\ddot{X}_c \ \ddot{Y}_c \ \ddot{Z}_c]^T$ ) is the acceleration vector of the cargo center of gravity,  $\vec{F}_c^{(i)}$  is the restraint force vector on the cargo from the  $i^{\text{th}}$  restraint,  $N$  is the number of restraints, and  $m_c$  is cargo mass. The variables describing the translational dynamics of the cargo are expressed in the inertial frame. The rotational dynamics of the cargo depend on the moments created by restraint forces as given by

$$\vec{M}_c = \sum_{i=1}^N \vec{r}_c^{(i)} \times \vec{F}_c^{(i)} \quad (3-2)$$

where  $\vec{M}_c$  (i.e.,  $[M_{c1} \ M_{c2} \ M_{c3}]$ ) is the vector for the torque applied by the restraint forces with respect to the cargo center of gravity (CG),  $\vec{r}_c^{(i)}$  is the distance vector from the cargo CG to the mounting point used by the  $i^{\text{th}}$  restraint,  $\vec{F}_c^{(i)}$  is the restraint force vector from the  $i^{\text{th}}$  restraint, and  $N$  is the total number of restraints. The variables in Eq. (3-2) are expressed in the local cargo reference frame. The components of the angular acceleration of the cargo are calculated using Euler's equations [Schaub et. al 2009] and is provided by

$$\vec{J}_c \cdot \dot{\vec{\omega}}_c + \vec{\omega}_c \times (\vec{J}_c \cdot \vec{\omega}_c) = \vec{M}_c \quad (3-3)$$

where  $\dot{\vec{\omega}}_c$  is the angular acceleration vector of the cargo,  $\vec{\omega}_c$  is the angular velocity vector of the cargo,  $\vec{J}_c$  (i.e.,  $[J_{c1} \ J_{c2} \ J_{c3}]^T$ ) is the moment of inertia tensor of the cargo,  $N$  is the total number of restraints, and  $\vec{M}_c$  is the moment vector with respect to the cargo CG. The variables in Eq. (3-3) are expressed in the local cargo reference frame. The cargo container is assumed to be a rigid body with uniformly distributed mass. The principal axes of the moment of inertia tensor are aligned with the coordinate axes of the local cargo reference frame.

The focus of the analytical studies conducted for this thesis is unidirectional impacts. The initial conditions for Eq. (3-1) are defined by the impact velocity and the direction of impact. The initial conditions for Eq. (3-2) are set to zero for unidirectional impact. An example of the initial conditions regarding cargo dynamics for a forward longitudinal impact is shown below:

$$\begin{aligned} x_{cl}(t=0) &= y_{cl}(0) = z_{cl}(0) = 0 \\ \dot{x}_{cl}(t=0) &= V_0, \dot{y}_{cl}(0) = \dot{z}_{cl}(0) = 0 \\ \vec{\omega}_{cl}(0) &= \vec{0} \\ \phi_c(0) &= \theta_c(0) = \psi_c(0) = 0 \end{aligned} \quad . \quad (3-4)$$

The only non-zero component in the set of initial conditions is the impact velocity,  $V_0$ . The location of the cargo CG is defined by the displacement variables  $x_{cl}$ ,  $y_{cl}$ , and  $z_{cl}$  which are expressed in the inertial frame.

The forces exerted by the energy absorbing restraints,  $\vec{F}_c^{(i)}$ , is a function given by

$$\vec{F}_c^{(i)} = f(\vec{r}_{MP}, K_{Total}, f_{ACT}, S_{max}), \quad i = 1, \dots, N \quad (3-5)$$

and is dependent on the distance between the cargo and cabin floor mounting points ( $\vec{r}_{MP}$ ), total restraint stiffness ( $K_{Total}$ ), activation force ( $f_{ACT}$ ) and maximum load limiter stroke ( $S_{max}$ ).

The restraint system consists of a lanyard and load limiter connected in series. Therefore, the expression for the total restraint stiffness ( $K_{Total}$ ) during initial loading and post-deployment phases can be calculated using

$$\frac{1}{K_{Total}} = \frac{1}{K_{Lanyard}} + \frac{1}{K_{LL}} \quad (3-6)$$

where  $K_{LL}$  is the load limiter stiffness and  $K_{Lanyard}$  is the lanyard stiffness. For textile-based load limiters,  $K_{LL}$  is the stiffness of the webbing of the load limiter. Prior to activation,  $K_{LL}$  is the stiffness of the piece of webbing that is not a part of the woven section. After maximum load limiter stroke is reached and the device is fully deployed, the device is now just a piece of

webbing and the value of  $K_{LL}$  will decrease. The stiffness of the lanyard can be approximated to be linear as the elongation of the lanyard at the activation force of the load limiter is of most concern. The lanyard stiffness is proportional to its effective length and load capacity. To double the load capacity of a nylon strap will result in twice the stiffness, but the amount of elongation in the lanyard will not change. The stiffness of a load limiter is also linear, but only in proportion to the activation force. A load limiter with double the activation force is twice as stiff. The value of  $K_{LL}$  is reduced in the post-deployment phase as shown in Figure 3-4, but its actual value does not play a role in the analysis. It is assumed that a mounting point fails at any load above its load capacity: rendering the restraint system incapable of providing a restraining force. Furthermore, the effect of tie-down angles on mounting point load capacity is neglected. It is assumed that the shallow tie-down angles do not cause load degradation of the mounting points [**Shefrin et al. 1986**].

At the beginning of the simulation, the restraint forces are zero because the cargo has not moved relative to the cabin floor. The effect of pretension on the restraints is approximated by increasing the stiffness of the lanyard so the load limiting phase occurs at a lower stroke value, but at the same activation force. The behavior of the lanyard and load limiter prior to activation is assumed to be linear to simplify the analysis. Although fabric lanyards (e.g., nylon straps) exhibit a non-linear force-displacement response, the final elongation of the lanyard at the activation force of the load limiter is the primary concern.

### ***Cabin Floor Dynamics***

The analysis conducted for this thesis assumes that the cargo weight is significantly less than the aircraft weight, and so the effect of restraint forces on cabin floor dynamics is neglected. The simulation begins with both the cargo and cabin floor moving at the impact velocity, when at

time,  $t = t_{impact}$ , the cabin floor is subject to the crash pulse and comes to a stop. The cargo, however, will continue to move and its motion can only be arrested by the restraint forces. The impact is treated as a boundary condition where at the time of impact the cabin floor acceleration is changed to match the crash characteristics provided by

$$\ddot{\vec{X}}_f = -\vec{a}_{crash}(t), \quad t \geq t_{impact} \quad (3-7)$$

where  $\vec{a}_{crash}(t)$  is the crash pulse vector. After impact, the dynamics of the cabin floor are fully defined by Eq. (3-7). The subscript “*f*” is used to denote variables used to describe the dynamics of the cabin floor.

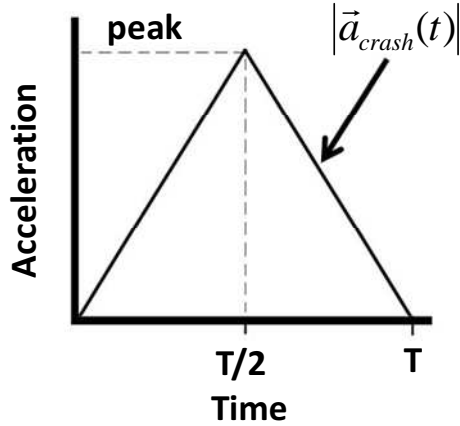


Figure 3-5. Shape of crash acceleration pulse.

The magnitude of the crash pulse vector,  $\vec{a}_{crash}(t)$ , is modeled as a triangular pulse as shown in Figure 3-5, where  $T$  is the pulse duration. The displacement of the cabin floor during the crash pulse is shown in Figure 3-6. The crash pulse vector contains a single non-zero component in unidirectional impacts. The parameters for the crash pulse include the pulse peak, pulse duration, and impact velocity. The pulse duration can be calculated given the pulse peak and impact velocity. For unidirectional impacts, the initial conditions for the cabin floor are identical to the initial conditions for the cargo shown in Eq. (3-4). The only difference is that the state-

variables are in reference to cabin floor dynamics and subscripts of all the variables are changed to “1”.

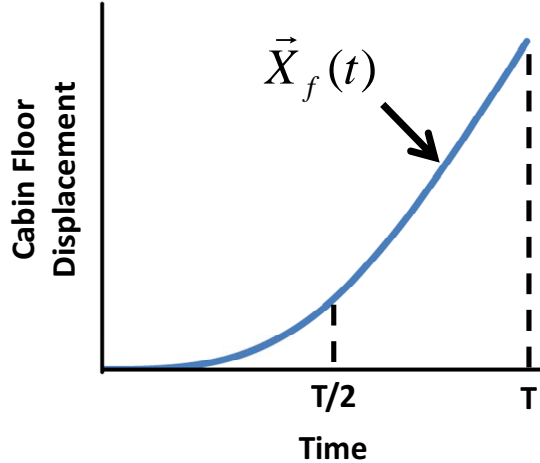


Figure 3-6. Displacement profile of cabin floor during crash event.

### ***Mounting Points Locations***

Mounting point locations are defined in the CDS by filling out an  $N \times 9$  matrix, where  $N$  is the total number of restraints used in the given restraint configuration. The matrix is shown in Table 3-1, but with the addition of the column labeled “Restraint No.” which is not a part of the actual matrix in the CDS and is only shown here only for clarification purposes. The “Cabin Floor” column of the restraint configuration matrix contain the  $x$ ,  $y$ , and  $z$  coordinates of the mounting point on the cabin floor that is used for attachment for each restraint. The “Cargo” column contains the  $x$ ,  $y$ , and  $z$  coordinates of the mounting points on the cargo container used for restraint attachment. The last three columns contain information on the load limiter activation force, total restraint stiffness, and a switch value for each restraint. The load limiter activation force also refers to the mounting point load capacities as both parameters are by definition equal to each other. The switch value is a feature that is included for use in the optimization method to vary the number of restraints used. A switch value of “1” translates to a restraint that is “turned

on” or is in use. A switch value of “0” refers to a restraint that is not in use. The coordinate values for the mounting points on the cargo and cabin floor use their respective local reference frames.

Table 3-1. Restraint configuration matrix defined by user for CDS.

Restraint No.	Cabin Floor [m]			Cargo [m]			Activation Force [N]	Stiffness [N/m]	Switch
	X	Y	Z	X	Y	Z			
1	-2.03	1.16	0	-1.37	1.11	1.21	111205	13267120	1
.	.	.	.	.	.	.	.	.	.
.	.	.	.	.	.	.	.	.	.
.	.	.	.	.	.	.	.	.	.
N	-4.06	1.16	0	0	1.11	1.21	111205	13267120	1

### *Collision*

A collision model was implemented in the CDS for simulations that include impacts with a vertical component or cargo rebound. The first attempt at a collision model featured a spring-damper system. The issue with this approach was a very stiff numerical problem resulting in long run times. The spring-damper system was replaced with a simpler rigid body collision model. The CDS tracks the location of each corner of the cargo container with respect to the cabin floor. When a corner of the cargo container comes into contact with the cabin floor, the rigid body collision model comes into effect. When the collision occurs, the CDS temporarily “stops” to switch to the collision model which uses the conservation of linear and angular momentum equations. The collision model calculates the dynamics of the cargo after the collision and “restarts” the CDS using the post-collision calculations as the initial conditions. A coefficient of restitution is also featured in the collision model for elastic collisions. The collision model was developed primarily for future work as vertical impacts and cargo rebound are beyond the scope of this thesis. Information regarding the modeling of rigid body collisions can be found in [**Baker 2010**] and [**Beer et al. 2004**].

### 3.1.3 CDS Flowchart

The CDS is used evaluate energy absorbing cargo restraint systems in a crash event. The flowchart of the CDS is shown in Figure 3-7. The user-defined inputs for the CDS are the cargo restraint configuration (e.g., mounting point locations, activation force), simulation parameters (e.g., crash pulse characteristics), and the initial conditions (e.g., impact velocity). The state variable equations are provided in Eqns. (3-1) through (3-12).

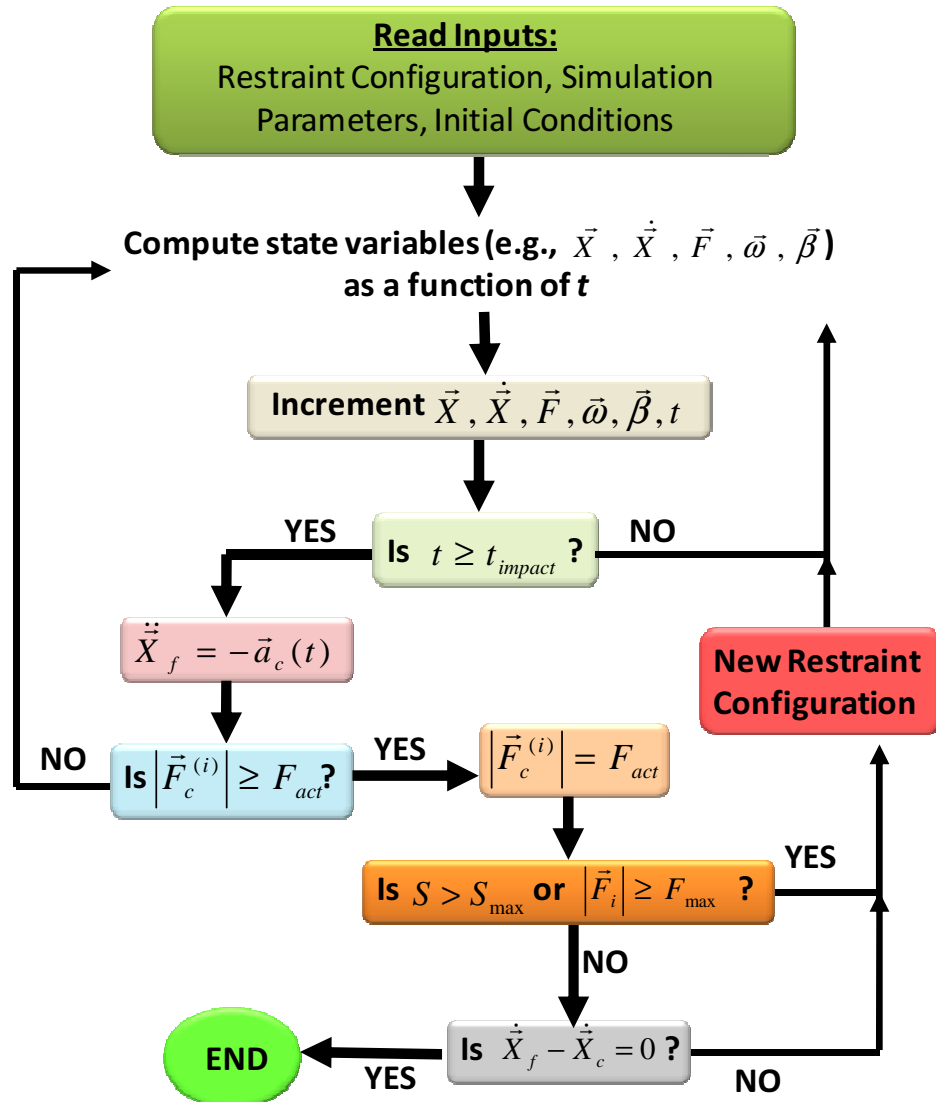


Figure 3-7. CDS flowchart.

In the beginning of the simulation, the cargo and cabin floor are moving together at the impact velocity. At the time of impact ( $t_{impact}$ ), the cabin floor dynamics are governed by the defined crash pulse provided in Eqn. (3-7). As the cabin floor decelerates, the motion of the cargo continues and the cargo restraints become engaged. The kinetic energy of the cargo is absorbed by the restraint system when the force ( $|\vec{F}_c^{(i)}|$ ) in any of the restraints reaches the activation force ( $F_{act}$ ). The restraints are capable of absorbing energy until maximum load limiter stroke ( $S_{max}$ ) is reached. After this point, the load limiter is fully deployed and can no longer absorb energy. For the analysis conducted in this thesis, a restraint has failed if it has reached the maximum load limiter stroke. The entire restraint system has failed if the cargo has not been arrested before all restraints have reached the maximum load limiter stroke. The simulation ends when either the restraint system is able to arrest the cargo or the restraint system fails. If the restraint system fails and is unable to arrest the cargo, then it that particular restraint system configuration cannot provide crash safety and must be improved.

### 3.1.4 Experimental Validation

In 2007, Hagon [2009] conducted a series of drop tests to investigate rate effects for stitch ripping devices (SRDs). Details on SRDs and their construction can be found in Chapter 2. To compare with the drop tests, the CDS was set to replicate each test by matching model parameters such as SRD parameters (e.g., activation force, maximum stroke, stiffness), drop height, and the mass of the drop weight. The SRD parameters were obtained from by analyzing the data from drop tests and quasi-static tests conducted on SRDs. The setup of the drop test is shown in Figure 3-8. A load cell is anchored to the top of the drop tower to record the forces transmitted through the SRD. The SRD is attached directly to the load cell on one end. The drop

weight is connected to the other end of the SRD via steel chain. The test is conducted by raising the drop weight to a specified height (i.e., drop height) and then released. When the chain becomes taut, an impact force is applied to the SRD. The problem modeled in the CDS was an idealized representation of the drop test as it did not account for friction between the drop weight and I-beam or stress waves through the chain. The chain was assumed to be rigid with no elongation. The CDS also modeled the SRD load profile as an idealized load limiter and did not account for the peak and valleys as shown in Figure 3-10. The results show that the CDS predictions correlate well with drop tests with the idealized load profile.

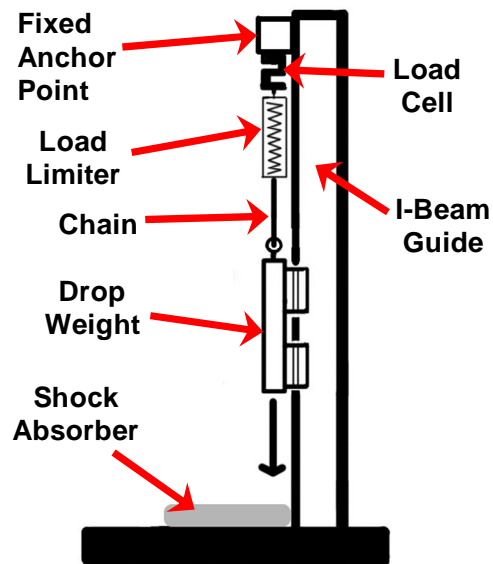


Figure 3-8. Diagram of drop test setup [adopted from Hagon 2009].

An example of the comparisons between CDS predictions and drop tests results are shown in Figure 3-9 and Figure 3-10. The test data after the drop weight had reached its maximum displacement was cropped out. The goal was to validate the modeling of the SRD behavior for the initial and load limiting phases as the CDS does not account for unloading, rebound, or recoil. The activation force of the SRD was set to 840 N and the stiffness of the SRD prior to activation was 28.4 kN/m. The drop height was 45 cm and the drop weight had a mass of

29.5 kg [Hagon 2009]. Overall, the maximum drop weight displacement (i.e., SRD stroke) from the CDS results were within 4% - 8% of the data obtained from the several drop tests conducted. Discrepancies between the CDS predictions and test data can be attributed to the approximated behavior of the SRD, stretch in the lanyard, behavior of the steel chain, drop weight friction, and the accuracy of the impact velocity measurement which was used as input for the CDS.

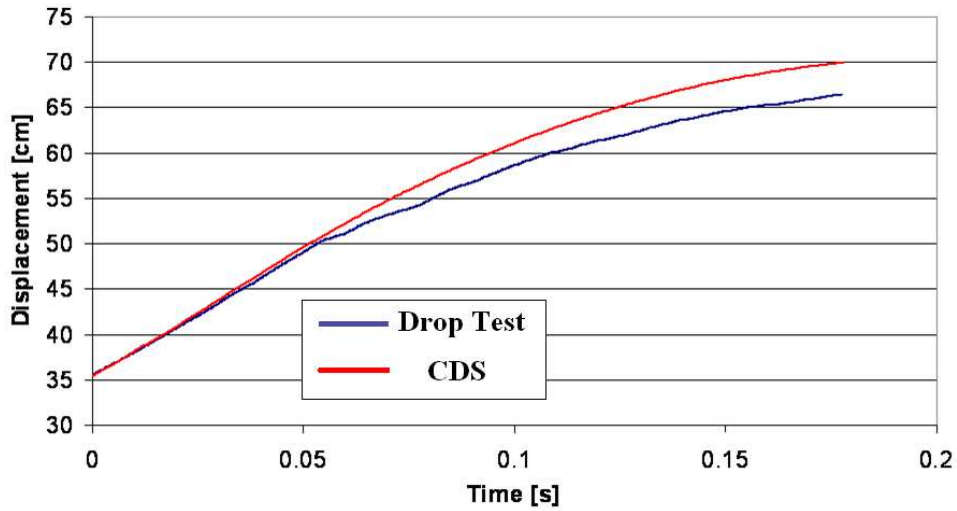


Figure 3-9. Comparison plot of CDS results and drop tests data for drop weight displacement.

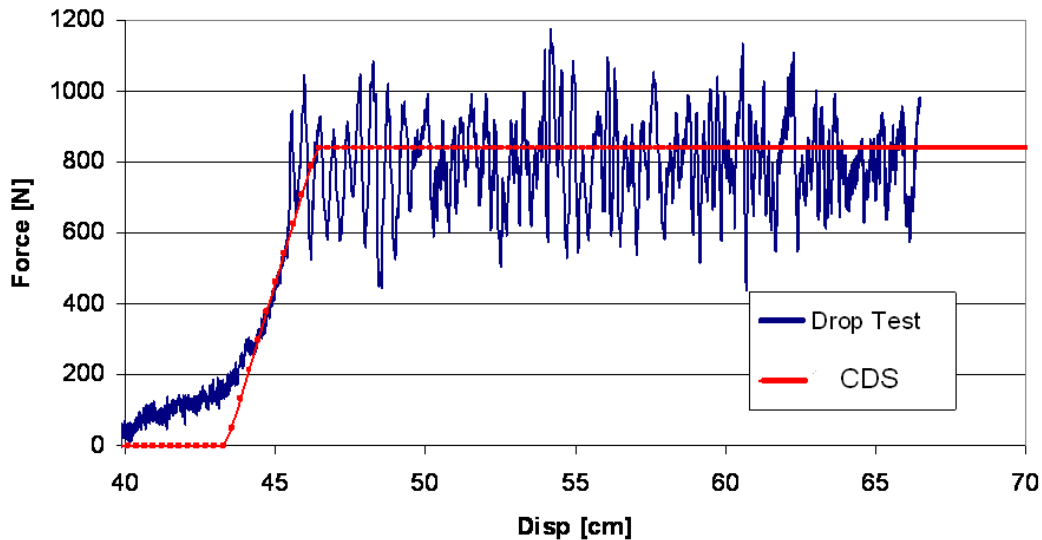


Figure 3-10. Comparison plot of CDS results and drop test data for transmitted forces.

### 3.2 Optimization Method

The greatest obstacles to optimizing cargo restraint systems are problem formulation and a complex design space with competing objectives. The optimization method developed is used to explore the design space to provide insight to a decision maker on how design variables, constraints, and objective functions influence restraint system design and their performance, prior to choosing a final design.

#### 3.2.1 Approach

The optimization method solves a multi-objective optimization problem, but does not provide a solution in the form of a single optimal configuration. Instead, a trade space is constructed spanning the space of possible solutions, in order to allow the user to identify and choose from Pareto optimal restraint configurations based on the user's preferences. The concept of Pareto optimality is typically found in multi-objective optimization problems. Miettinen defines Pareto optimal solutions as "a set of mathematically equally good solutions" when no unique solution exists [Branke et al. 2007]. Another way of viewing Pareto optimality is to consider a design to be Pareto optimal if there are no feasible designs that show an improvement in one objective without decreasing the performance in other objectives [Stump et al. 2002]. The Applied Research Laboratory Trade Space Visualizer (ATSV) is used in conjunction with the CDS to explore different restraint configurations and evaluate the performance in a crash event.

#### 3.2.2 Background on ATSV

ATSV utilizes a *design by shopping* paradigm, where the user first explores the design space and then chooses an optimal solution from a set of feasible designs [Stump et al. 2002]. To

accomplish this, ATSV samples and explores multi-dimensional trade spaces with an array of visual steering commands including random sampling and Pareto sampling.

The Exploration Engine feature acts as the mediator between ATSV and the simulation model to sample the input space and generate new design alternatives [Stump et al. 2009]. The system architecture for the Exploration Engine is shown in Figure 3-11 [Stump et al. 2009]. The basic sampler performs Monte Carlo simulations on the input variables (i.e., design variables) of the CDS. The Pareto sampler uses Differential Evolution (DE) to guide the sampling process [Price et al. 2005]. The selection strategy used within the DE algorithm for the Pareto sampler is DE/best/1/bin. The user can specify the population size, crossover probability, and mutation factor for the DE algorithm. Pareto sampling generates new solutions along a Pareto front that is defined by a user-specified direction of preference for each objective function [Stump et al. 2009].

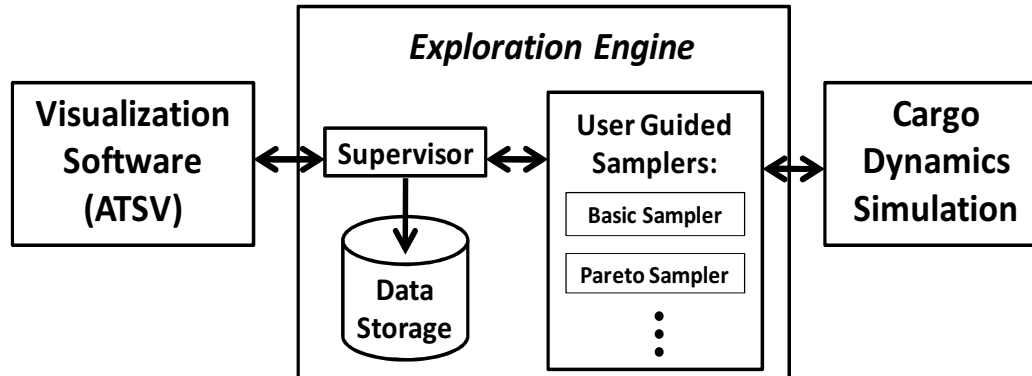


Figure 3-11. System architecture of ATSV’s Exploration Engine [Stump et al. 2009].

The optimal design is determined by analyzing the data using ATSV’s visualization and data analysis tools. A few examples of the visualization tools in ATSV are shown in Figure 3-12 [Stump et al. 2009]. The user can assign a relative weighting vector to a set of design variables and objective functions, and designs that perform well are highlighted to the user. Details on

ATSV's capabilities, implementation of DE, and visual steering commands can be found in [Stump et al. 2002] and [Stump et al. 2009].

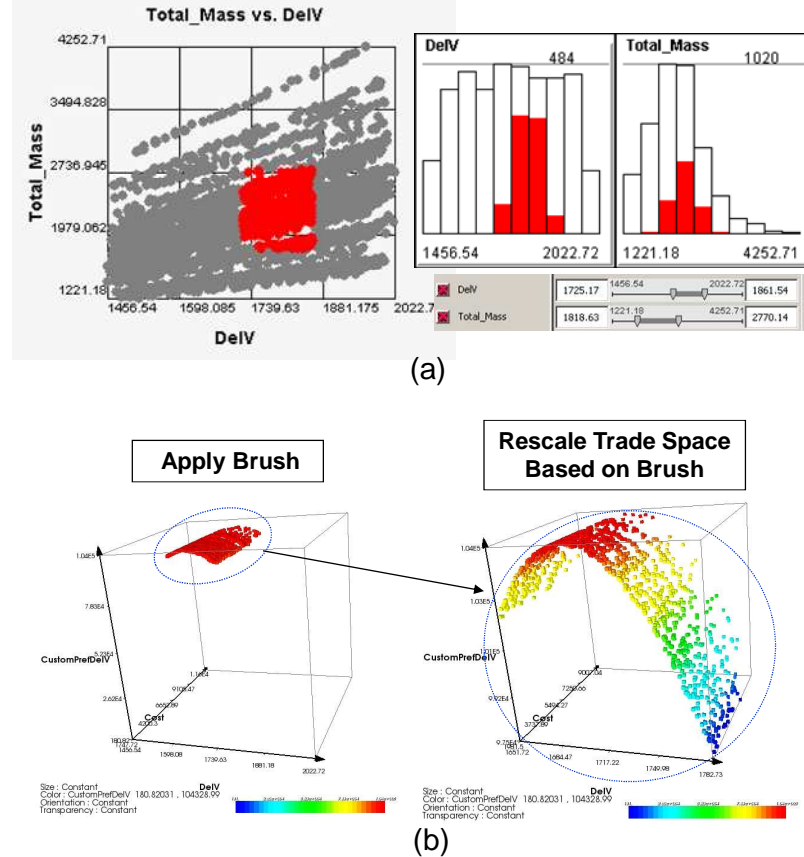


Figure 3-12. Examples of visualization tools in ATSV: (a) linked views that display the same brush settings; (b) using brushing to zoom in within the trade space [Stump et al. 2009].

### 3.2.3 Algorithm

As shown in Figure 3-13, the optimization method uses three different programs: ATSV, MATLAB (i.e., CDS), and MS Excel. Initially, the random sampler is used to explore the design space and identify trends. ATSV generates restraint configurations by defining pairs of mounting points for attachment, total number of restraints and load limiter device parameters (i.e. activation force, stroke). The input variables are sent to MS Excel to be converted into a

MATLAB compatible format for the CDS. The CDS then evaluates the given restraint system by simulating a crash event. The results from the simulation are recorded in ATSV as the objective function values. If applicable, an initial population for the Pareto sampler can be chosen from the restraint configurations generated by the random sampler and recorded in ATSV. The recorded data is subsequently analyzed within ATSV. The constraints are implemented in ATSV in the post-processing phase and a feasible region is plotted. ATSV is also capable of plotting the Pareto front based on user-defined preferences on the objective functions. The user is then able to analyze the Pareto optimal designs and decide which design is the most preferred restraint configuration.

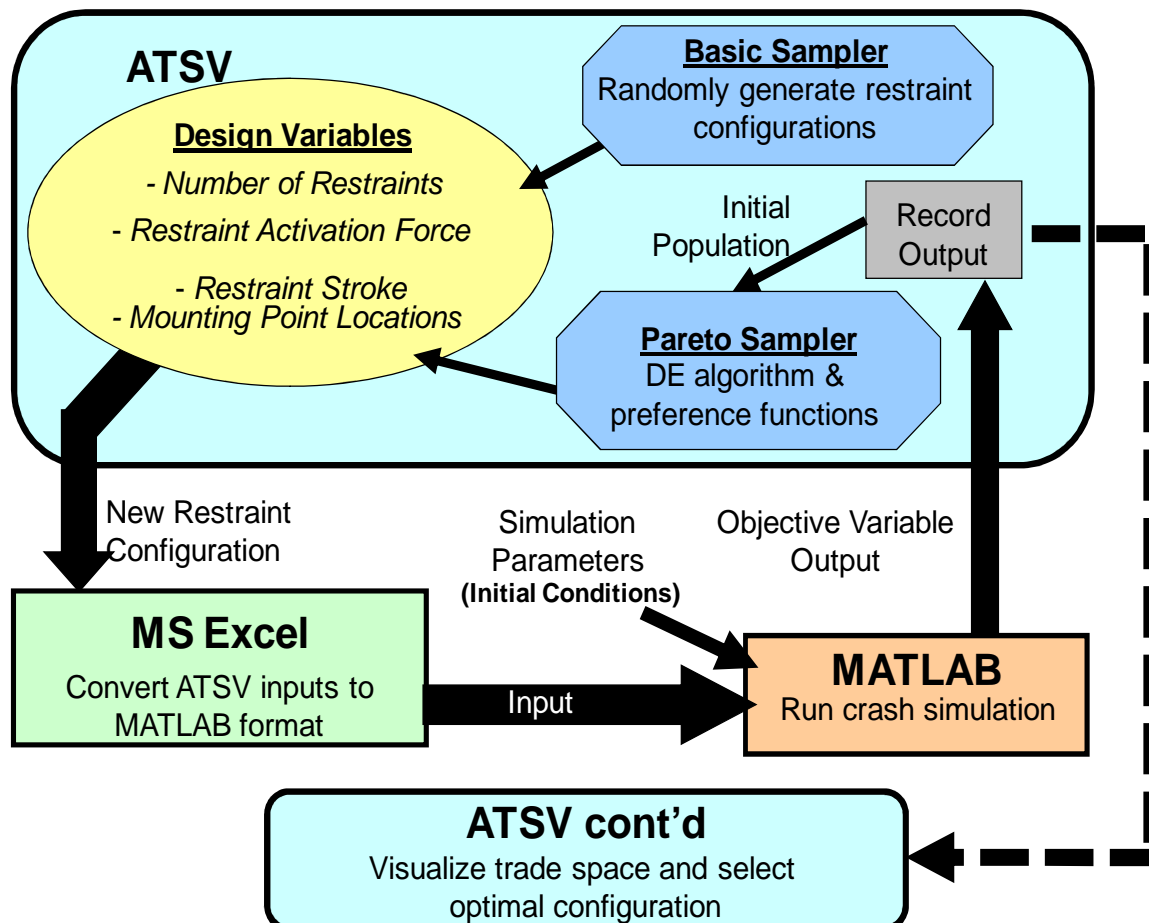


Figure 3-13. Flowchart of optimization method algorithm

### 3.2.1 Optimization Problem Formulation

The multi-objective optimization problem to be solved for energy absorbing cargo restraint systems can be written as

$$\begin{aligned}
 & \min_Q [N(Q), M_q(Q), D_x(Q, t_f), D_y(Q, t_f)] \\
 & s.t. \\
 & D_x(Q, t_f) = x_2(t_f) - x_1(t_f) \leq D_{x,\max} \\
 & D_y(Q, t_f) = y_2(t_f) - y_1(t_f) \leq D_{y,\max} \\
 & \dot{\vec{X}}_2(t_f) - \dot{\vec{X}}_1(t_f) = 0
 \end{aligned} \tag{3-8}$$

where  $Q$  is the vector which defines the restraint system and  $t_f$  is the time at the end of the simulation (i.e., crash event). The objective functions are to minimize the number of restraints of the restraint configuration,  $N$ , the total mass of the restraint configuration,  $M_q$ , the longitudinal cargo displacement,  $D_x$ , and lateral cargo displacement,  $D_y$ . The objective functions for the optimization studies presented in the following chapter were based on metrics used to evaluate cargo restraint systems. Constraints on the cargo displacement must be satisfied to achieve feasibility. The cargo displacement at the end of the simulation must be less than the maximum allowable displacement in both the longitudinal ( $D_{x,\max}$ ) and lateral ( $D_{y,\max}$ ) directions. Furthermore, the motion of the cargo relative to the cabin floor must be arrested by the end of the simulation as shown in the final equality constraint.

To provide a baseline for comparison, optimization studies were also conducted for chain restraints. The problem formulation for optimizing chain restraints, however, differs from the optimization of energy absorbing cargo restraint systems. For chain restraints, the optimization problem is shown below

$$\begin{aligned}
& \min_Q [N(Q), M_q(Q)] \\
& \max_Q [\sum_{i=1}^N F_{x,i}(Q), \sum_{i=1}^N F_{y,i}(Q)], \quad i = 0, 1, \dots, N \\
& \text{s.t.} \\
& \sum_{i=1}^N F_x(Q) - G_x * M_q \geq 0 \\
& \sum_{i=1}^N F_y(Q) - G_y * M_q \geq 0
\end{aligned} \tag{3-9}$$

where the objective functions are to minimize the number of restraints ( $N$ ) and total mass of the restraints ( $M$ ), while maximizing the total restraint force provided in the longitudinal and lateral directions. Displacement is not an objective variable for chain restraints as they are assumed to be rigid. A static analysis is used to evaluate chain restraint configurations, and thus the only constraints to be satisfied are that the total restraint force provided is equal to or greater than the static load factor multiplied by the cargo weight.

### ***Objective Functions***

The sole purpose of cargo restraints is to arrest the motion of the cargo. The ideal cargo restraint system would be lightweight, easy to use, require minimal preparation time, and capable of providing safety in a crash. For energy absorbing cargo restraint systems, the objective functions of the optimization problem are to minimize the number of restraints, total restraint system mass and cargo displacement. Although the objective functions indirectly address usability for cargo handlers, it is recommended that the results be reviewed by user and consider usability prior to choosing the optimal restraint configuration.

The objective functions for optimization studies conducted on currently used steel chain restraints differ from the ones used for energy absorbing restraints since steel chains are assumed to exhibit no elongation. Therefore, cargo displacement is not an applicable parameter. Instead,

the remaining objective functions are to maximize the amount of restraint the entire restraint system provides in the longitudinal and lateral direction.

### **3.2.2 Design Variables**

The restraint system vector ( $Q$ ) in Eqns. (3-8) and (3-9) contain the design variable information necessary to properly define a restraint system. The design variables of the restraint system vector are the type of restraint system components (e.g., load limiter, lanyard), number of restraints, load limiter parameters, and mounting point locations.

The number of restraints is an influential variable as it is also one of the objectives of the optimization method. The parameters of the load limiter (e.g., activation force, maximum load limiter stroke) are dependent on the number of restraints. To reduce the number of the restraints requires the load limiters to be more effective and able to dissipate more energy to arrest the cargo—which translates to increase load limiter weight and/or more allowable cargo displacement. Increasing the number of restraints can decrease the weight of each individual load limiters, but not necessarily the weight of the entire restraint system. There is, however, an upper limit to the number of restraints that can be used and it is defined by the amount of mounting points available. Furthermore, there is a trade-off between the number of restraints and usability for cargo handlers.

The load limiter parameters refer to the activation force and maximum stroke of the load limiter device. The load limiter parameters define the energy absorption capability of the restraint system and the weight of load limiters is directly proportional to the activation force and maximum load limiter stroke. It is assumed that doubling the activation force, or maximum stroke, of a load limiter results in twice the amount of energy it can dissipate and double the weight. The weight increases come from changing the dimensions of the load limiter — by

making it wider, thicker, or longer — to achieve different activation forces and maximum load limiter stroke values, but no changes to the actual material. The maximum load limiter stroke should be close to the amount of stroke needed to arrest cargo motion within the cargo displacement constraints in order to avoid added weight from excess material. Prescribing the activation force is dependent on the load capacity of the available mounting points. Results from previously conducted U.S. Army/NASA crash tests which found that metallic load limiters with activation forces that were too close to the mounting point load capacity resulted in failure of the mounting points. The test results were attributed to the variability in the force response of the load limiter and the strength of the mounting points [**Burrows et al. 1978**]. As a result of the test findings, the ACSDG recommends using higher load factors when designing mounting points [**Zimmermann et al. 1989**]. For the analytical studies conducted for this paper, the activation force of the load limiter is equal to the mounting point load capacity. Furthermore, it is assumed that the mounting points and restraint system can only fail at loads greater than the activation force.

The location of the mounting points chosen for restraint attachment defines the tie-down configuration which then defines the effective lanyard lengths for fabric lanyards and tie-down angles. Increasing the effective length of fabric lanyards decreases the stiffness of the overall restraint. The problem with decreasing lanyard stiffness is that more of the cargo displacement will be attributed to lanyard elongation—which does not dissipate energy—instead of load limiter stroke. This leads to an inefficient restraint system due to the cargo displacement constraints. Tie-down angles also influence the amount of effective restraint force that can be provided for any given direction. There is a trade-off when considering tie-down angles, as the restraint system must be able to satisfy requirements for impacts in multiple directions.

### 3.2.3 Additional Constraints

In addition to the constraints set in Eqns. (3-8) and (3-9), there are other general constraints which must be satisfied to achieve feasibility. The majority of the constraints of the optimization method are typically dependent on the specific cargo handling scenario. There are a few constraints, however, which hold for all optimization studies presented in this thesis:

- The distance between two mounting points cannot be greater than the maximum length of the restraint
- A mounting point can be used by only one restraint at a time
- Restraints cannot wrap around cargo. Although it is possible for restraints to wrap around cargo instead of using mounting points, the analysis does not consider this method of attachment
- All the restraints that compose a given restraint configuration have identical load limiter parameters (i.e., activation force, maximum load limiter stroke) and (i.e., material, load capacity, maximum length, stiffness)
- All mounting points having the same load capacity
- The load capacity of the mounting points is equal to the activation force of restraints and will fail at any load above the activation force
- Restraint system must satisfy the ACSDG requirements for impact in both the longitudinal and lateral directions

## 3.3 Static Analysis Method

For the analytical studies presented in the following chapter, the energy absorbing cargo restraint systems are compared to current restraint technology. The MB-I and MB-II restraints are

used for restraining heavy cargo and will provide a baseline for comparison. Nylon straps and nets are also used mostly for lightweight and loose cargo. The U.S. Army's field manual, FM 55-450-2, instructs cargo handlers to use a static analysis for chain restraint configurations. The key equation used for chain, and nylon strap, restraint analysis is given by [FM 55-450-2]

$$\frac{G \times W}{C \times P \div 100} = N. \quad (3-10)$$

The number of restraints required to restrain a load,  $N$ , is a function of the static load factor,  $G$ , the weight of the cargo,  $W$ , the load capacity of the restraint,  $C$ , and the percent of effective restraint,  $P$ . The percent of effective restraint is the amount of restraint that can be obtained in a specific direction and it is contingent upon the tie-down angle of the restraint. The value of  $P$  can be calculated using Eqn. (3-11), where  $\alpha$  is the vertical tie-down angle measured from the cabin

$$\begin{aligned} P &= \cos(\alpha) \cos(\theta) \text{ for longitudinal impact} \\ P &= \cos(\alpha) \sin(\theta) \text{ for lateral impact} \end{aligned} \quad (3-11)$$

floor and  $\theta$  is the side tie-down angle measured from the longitudinal axis. The solution to Eq. (3-10) provides the number of restraints required if all the restraints have the same tie-down angle and provide the same amount of restraint force.

The field manual recommends as a rule-of-thumb that all restraints be tied down as close to 30° sideways from the longitudinal axis and 30° from the lateral axis as possible. Furthermore, the number of restraints is always rounded up to the next even integer to maintain a symmetric tie-down configuration. This tie-down configuration is also referred to as "30/30". A cargo restraint with a 30/30 tie-down angle is shown in Figure 3-14. The static load factors used for analysis were taken from the field manual as discussed in Chapter 2. The field manual provides a "percentage restraint chart" with calculations on the amount of restraint that can be achieved for a given tie-down angle in any direction [FM 55-450-2 1992]. For example, a restraint that is tied down to 30/30 has a  $P$  value of 75% for longitudinal restraint. For the same tie-down angle, the  $P$

value for lateral restraint is 45%. The analysis does not explicitly account for elongation in the restraint. Additional details and examples of current methods used for restraint analysis can be found in FM 55-450-2.

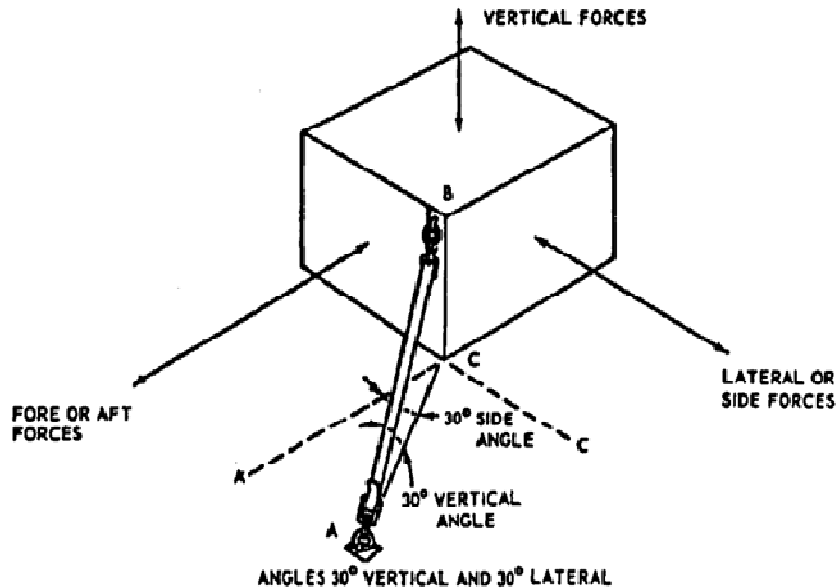


Figure 3-14. Restraint configuration with 30/30 tie-down angles [FM 55-450-2 1992].

### 3.4 Summary

A cargo dynamics simulation (CDS) was developed as a tool to evaluate cargo restraint systems in a crash event. An optimization method was developed by combining ATSV—a multi-dimensional data exploration and visualization software—with the CDS to create a trade space consisting of a wide spectrum of possible solutions. Cargo handlers currently use a static analysis to configure cargo restraint systems. The following chapter describes several analytical studies conducted as an exercise of the optimization method and to assess the benefits of using energy absorbing cargo restraint systems over current restraint technology.

## Chapter 4

### Results and Discussion

The objective of this chapter is to present and discuss the results obtained from comparative, parametric, and optimization studies. The studies were conducted using the analytical tools and methods described in the previous chapter. A comparative study on restraint system components was conducted using the cargo dynamics simulation (CDS) to compare energy absorbing restraint systems with different combinations of lanyards and load limiters. A parametric study was conducted to assess the influence of tie-down angles and find the optimum tie-down angle to be used as a rule-of-thumb for simplified tie-down configurations. Optimization studies were conducted as an exercise of the optimization method for a generic cargo handling scenario. The results of the optimization studies include a set of Pareto optimal restraint configurations from which the user may choose the final restraint system design. The influence of constraints, design variables, weighting of objective functions, and trade-offs that exist among the Pareto optimal designs are discussed in this chapter.

#### 4.1 Cargo Restraint Systems

The comparative, parametric, and optimization studies presented in this chapter were conducted for energy absorbing restraints and current restraint technology. The CGU-1/B, MB-I and MB-II restraints are used by cargo handlers today and their restraint specifications are provided in Table 4-1. More information on the current restraints can be found in MIL-PRF-27260C (CGU-1/B) and MIL-DTL-6458F (MB-I and MB-II).

Table 4-1. Specifications of current restraint technology featured in comparative study.

Restraint Type	Description	Load Capacity	Length	Mass	Elongation
CGU-1/B	Nylon strap	22.2 kN	6.1 m	1.7 kg	18%
MB-I	Steel Chain	44.5 kN	2.7 m	3.6 kg	3.6%
MB-II	Steel Chain	111 kN	2.7 m	11 kg	3.6%

Although the CGU-1/B restraint is a nylon strap restraint, and is typically used for lightweight cargo and loose cargo, the focus of this thesis is on cargo restraint systems for heavy cargo (e.g., vehicles, containers) on existing rotorcraft and future heavy lift rotorcraft. The nylon lanyard featured in the analytical studies was created by linearly scaling the mass, load capacity, and elongation properties of the CGU-1/B restraint. The Internal Cargo & Special Operations group at the Naval Air Systems Command (NAVAIR) conducted tension tests on CGU-1/B restraints to capture the force-elongation profile. The average elongation of the CGU-1/B restraint at its load capacity (22.2 kN) was found to be 18% of the effective strap length with 890 N of pretension [Anderson et al. 2010]. The effective strap length is the length of the restraint after pretension. If the restraint does not wrap around the cargo, the effective strap length is essentially the distance between the two mounting points used by the restraint.

The MB-I and MB-II restraints are steel chain restraints typically used for heavy cargo (e.g., vehicles, containers). NAVAIR also conducted tension tests on steel chain restraints and the tests results showed an elongation of 3.6% for MB-I restraints [Anderson et al. 2010]. In comparison to the elongation of nylon straps and load limiter stroke, the elongation of steel chains is negligible. Therefore, steel chain lanyards are assumed to be completely rigid. The MB-II restraint is not currently used on existing rotorcraft, as the mounting points are not strong enough to make use of the high strength restraint. The MB-II restraint is included in the comparative and optimization studies as it is possible for future heavy lift rotorcraft to incorporate stronger mounting points.

The energy absorbing cargo restraint system analyzed in this thesis features two main components: lanyard and load limiter. An example of an energy absorbing cargo restraint system is shown in Figure 4-1, where a nylon strap (lanyard) is combined with tear webbing. There are other components to the cargo restraint systems such as the tensioning mechanism and adjustable hook, but they were beyond the scope of the analysis. The purpose of the lanyard is to provide additional length to the restraint system. The characteristics of the ideal lanyard include high strength, high stiffness, low elongation, lightweight, and a length long enough to cover the distance between mounting points on the cabin floor and cargo. Depending on the type of lanyard used, it is possible to provide restraint by wrapping around the cargo in addition to using the mounting points.

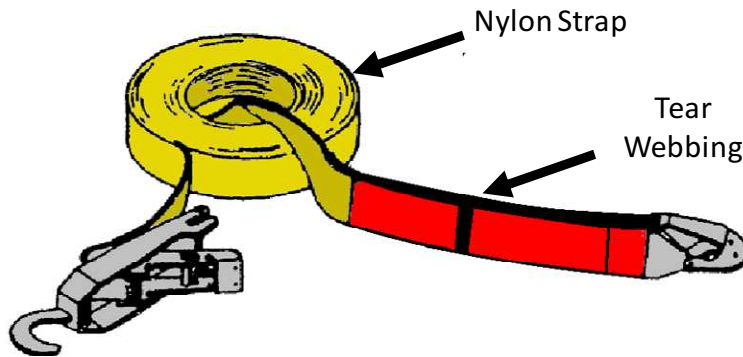


Figure 4-1. Energy absorbing cargo restraint system featuring nylon strap and tear webbing [Shefrin et al. 1969].

The analytical studies feature two types of energy absorbing restraint systems. One combines steel chain (e.g., MB-I, MB-II) with tear webbing and the other features a nylon strap also with tear webbing. A summary of the components of the energy absorbing restraints used in the comparative, parametric, and optimization studies is provided in Table 4-2. Each column in the table provides a range of values for the different types of lanyards and load limiters that participated in the analytical studies. The mass of the nylon strap lanyard is directly proportional to its load capacity. The properties of the nylon strap lanyards were obtained from linearly scaling

the CGU-1/B restraints to match the load capacity of the MB-I and MB-II for use on heavy cargo. For example, the CGU-1/B device has a load capacity of 22.2 kN and a mass of 1.7 kg. A nylon strap rated for 44.5 kN—which can be used as a lanyard or a restraint by itself—has a mass of 3.4 kg. The elongation of the nylon straps refers to the amount of stretch at the activation force and is equal to the elongation of the CGU-1/B restraint at its respective load capacity.

Table 4-2. Specifications of the energy absorbing restraints used in comparative study.

Component	Description	Load Capacity	Elongation at Load Capacity	Mass	Max. Length
Lanyard	MB-I	44.5 kN	n/a	3.6 kg	2.7 m
	MB-II	111 kN	n/a	11 kg	2.7 m
	Nylon Strap	44.5 kN – 111 kN	18%	3.4 kg – 8.5 kg	6.1 m
Load Limiter	Tear Webbing	44.5 kN – 111 kN	3.0 cm – 100 cm	0.07 kg – 6.0 kg	n/a

(1) For load limiters, the load capacity is equivalent to the activation force.

(2) For fabric lanyards, the stroke is equivalent to elongation at load capacity as a percentage of effective length.

The load limiter used in the analytical studies is an idealized version of tear webbing. Details on the load profile of both the steel chain/tear webbing and nylon strap/tear webbing restraints can be found in the previous chapter and in Figure 4-2. The restraint stroke at the activation force is dependent on lanyard stretch. Steel chain lanyards are assumed to be rigid and do not elongate. Nylon strap elongation is 18% of its effective length when loaded at the activation force. The post deployment stage is not taken into account in the analytical studies as the activation force is designed to be equal to the mounting point load capacity. Therefore, the restraint system will fail if loaded beyond the point of maximum load limiter stroke. The mass and elongation of the load limiter match the values obtained experimentally for tear webbing. The mass of the load limiter is proportional to the load capacity (i.e., activation force) and maximum load limiter stroke. For example, doubling the activation force, or maximum load limiter stroke, is assumed to double the mass of the load limiter. The upper/lower bounds of the activation force

for the load limiter equal the load capacities of the MB-I and MB-II restraints as the goal of the comparative study is to compare energy absorbing cargo restraints with the restraints currently used on heavy cargo. The elongation of the load limiter prior to activation is negligible [Miller 2010].

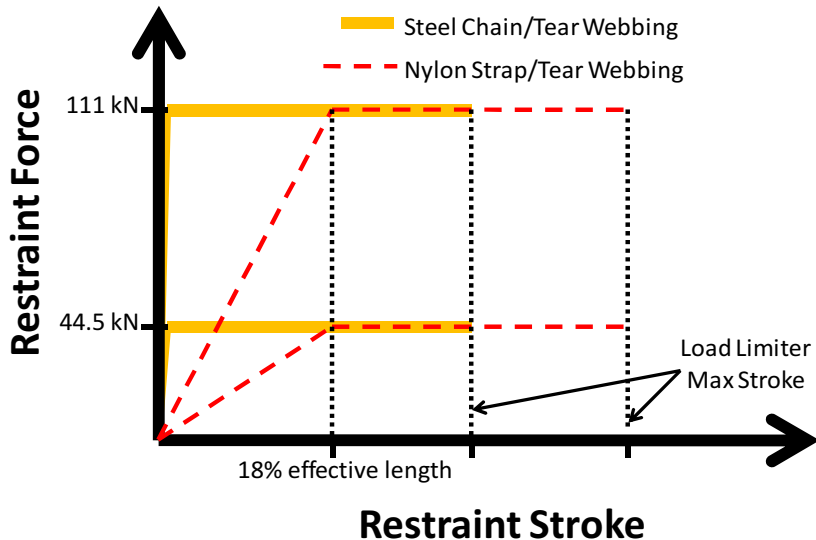


Figure 4-2. Load profile of steel chain/tear webbing and nylon strap/tear webbing restraints.

#### 4.2 Comparative Study of Steel Chain and Nylon Strap Lanyards With and Without Load Limiters in Simplified Tie-Down Configurations

A comparative study was conducted using the CDS and the static analysis method described in the previous chapter. The analysis focused on the components of energy absorbing restraint systems by concentrating on steel chains and nylon straps, both with and without tear webbing devices, in simplified tie-down configurations. Furthermore, the restraint systems were evaluated with both static and dynamic analyses. The comparative study results serve as a preliminary comparison of analytical methods in addition to cargo restraint components.

#### 4.2.1 Comparative Study Parameters

To focus on the restraint system components and the combinations of those components, the tie-down configuration and loading parameters were fixed for the comparative study. Restraint systems were evaluated using dynamic (CDS) and static analyses. The parameters for each restraint system in the comparative study include the number of restraints, restraint load capacity, load limiter activation force, and maximum load limiter stroke. The range of possible parameters values can be found in Table 4-1 and Table 4-2. There were no limits on the number of restraints, but there must be an even number of restraints used. All restraint systems were evaluated for forward longitudinal impacts. Furthermore, restraints were aligned with the longitudinal axis to provide restraint purely in the longitudinal direction as shown in Figure 4-3. The effective length of the nylon strap—featured both as a lanyard and restraint in the study—is 2.7 m. The cargo container has a mass of 4536 kg (10 kip).

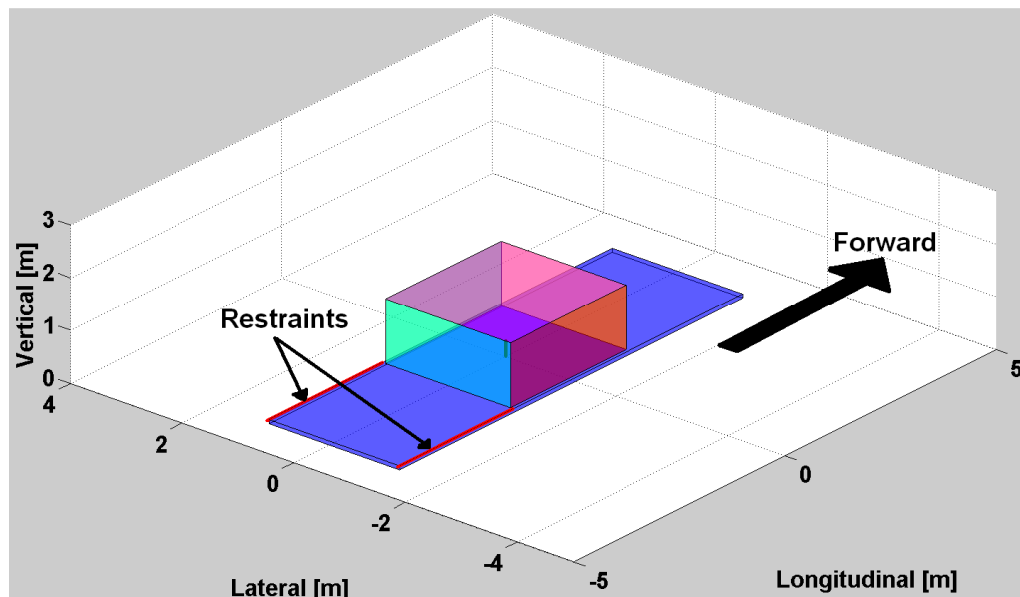


Figure 4-3. CDS screenshot of two restraints attached to the cargo using the tie-down configuration featured in the comparative study.

When configuring restraint systems with MB-I, MB-II, and CGU-1/B restraints; cargo handlers use a static analysis described in Chapter 3 with a static load factor of 4 G in the longitudinal direction [FM 55-450-2 1992]. For dynamic analysis, the crash parameters were set to follow the ACSDG forward longitudinal impact requirements provided in Chapter 2: 13 m/s impact velocity and a triangular crash pulse with a peak of 16 G. The energy absorbing restraints (steel chain/tear webbing, nylon strap/tear webbing) and CGU-1/B restraints were analyzed with the CDS. A simplified dynamic model was used for the MB-I and MB-II restraints. A sketch of the simplified model is shown in Figure 4-4. The cabin floor behavior is governed solely by the triangular crash pulse as detailed in Chapter 3. Although steel chain restraints are assumed to be rigid, it was treated as a linear spring with a 3.6% elongation [Anderson et al. 2010] in the section of the study that looked at steel chains alone. The elongation was incorporated to show the inadequacy of current restraint technologies is clear in both static and dynamic analysis.

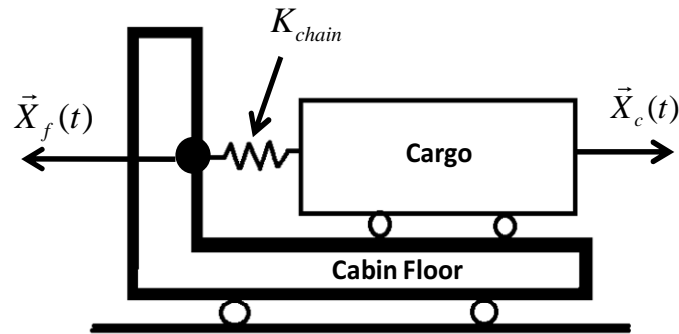


Figure 4-4. Sketch of the simple dynamic model for analyzing chain restraints (MB-I, MB-II).

#### 4.2.2 Comparative Study Results

The results of the comparative study are provided in Table 4-3. Current restraints (CGU-1/B, MB-I, and MB-II) and high strength nylon strap restraints (rated to 44.5 kN) were evaluated using the static analysis method. The rest of the results for the nylon strap, MB-I, MB-II, and energy absorbing restraints were obtained using a dynamic analysis.

Table 4-3. Comparative study results comparing energy absorbing restraints and current technology.

Row	Restraint System	Peak Accel.	Load Capacity	Total Mass	No. of Restraints	Max. Stroke	Cargo Disp.
1	CGU-1/B	4 G (Static)	22.2 kN	14 kg	8	n/a	n/a
2	MB-I		44.5 kN	15 kg	4		
3	MB-II		111 kN	22 kg	2		
4	CGU-1/B	16 G (Static)	22.2 kN	96 kg	32	n/a	n/a
5	Nylon Strap		44.5 kN	96 kg	16		
6	MB-I		44.5 kN	58 kg	16		
7	MB-II		111 kN	87 kg	8		
8	MB-I	16 G (Dynamic)	44.5 kN	86 kg	24	9 cm	9 cm
9	MB-I/ Tear Webbing			27 kg	4	126 cm	126 cm
10				34 kg	8	26 cm	26 cm
11	MB-II		111 kN	110 kg	10	9 cm	9 cm
12	MB-II/ Tear Webbing			49 kg	4	23 cm	23 cm
13				34 kg	2	104 cm	104 cm
14	Nylon strap		44.5 kN	82 kg	24	46 cm	46 cm
15				35 kg	6	105 cm	155 cm
16	Nylon strap/ Tear Webbing			49 kg	12	30 cm	80 cm
17		111 kN	111 kN	57 kg	6	16 cm	67 cm
18				33 kg	2	130 cm	181 cm

Cargo handlers are currently configuring restraint systems using a 4 G static load factor using CGU-1/B, MB-I, and MB-II restraints. Comparing rows 1–3 and rows 4–7, it is clear that the current method of restraining cargo is incapable of providing crash safety at 16 G. Concentrating only on the results from the static analysis (rows 1–3), the results show that cargo handlers need four times the number of restraints they are currently using to satisfy the static load factors for crash conditions (rows 4–7).

The comparative study also revealed a significant change that occurs when switching from a static (rows 4–7) to dynamic analysis (rows 8–18). For the same peak of 16 G, 50% more MB-I restraints are required when using a dynamic analysis (row 8) than the amount required from a simple static analysis (row 6). The same observations can be made when comparing nylon straps for static (row 5) and dynamic analysis (row 14). Furthermore, a static analysis does not explicitly account for the elongation of the lanyard/restraint. For the restraints with high

elongation (i.e., nylon strap), the static analysis (row 5) underestimated the number of restraints required and neglected to account for 46 cm of cargo displacement (row 14).

The number of steel chain restraints (MB-I, MB-II) required for 4 G static load factor (row 2–3) can also be considered the number of steel chain/tear webbing restraints required to restrain cargo up to a 4 G static load factor without activating the load limiter. The same is true for the number of nylon straps (row 5) required for a 4 G static load factor with respect to nylon strap/tear webbing restraints. A 4 G static load factor may be satisfactory for normal maneuvering flight conditions, but it certainly does not satisfy the ACSDG crash requirements.

The first line of results for each of the energy absorbing restraints show that the same restraint configurations which satisfy normal maneuvering flight conditions (4 G) can also satisfy the proper crash criteria (16 G), but with significant cargo displacement and a slight weight penalty. The static analysis at 4 G required four MB-I restraints (row 2). By incorporating a tear webbing device, four MB-I/tear webbing restraints can provide crash safety up to 16 G (row 9). The results also revealed that increasing load capacity (i.e., activation force) of the energy absorbing cargo restraints can decrease the number of restraints required, but also increase the total restraint system mass. This trend can be seen comparing rows 9 & 10, rows 12 & 13, rows 15 & 16, and rows 17 & 18.

There is, however, the additional parameter of maximum load limiter stroke that is unique to energy absorbing restraints. An upper limit on allowable cargo displacement is necessary to provide safety and is essentially defined by cabin space, but it is also necessary to utilize the full potential of energy absorbing restraints. For energy absorbing restraints, reducing allowable cargo displacement translates to increases in the number of restraints and total restraint mass. For example, comparing rows 17 and 18 can show the increases in number of restraints and weight for a decrease in cargo displacement, with all other parameters held equal.

The last line for energy absorbing restraints (rows 10, 13, 16 and 18) show that if both allowable cargo displacement and activation force were increased, energy absorbing restraints can reduce the number of restraints and total mass to less than what is required by currently used restraints.

The comparative study also revealed a distinct advantage of using steel chains as lanyards as opposed to nylon straps. In crash conditions, the number of MB-I/tear webbing restraints (row 10) required is 33% less than the number of nylon strap/tear webbing (row 16) at the same activation force. Furthermore, the MB-I/tear webbing restraints reduced the amount of cargo displacement required by up to 66%. The improvements in performance are attributed to the high stiffness to weight ratio of steel chain. The benefits of using lightweight nylon straps as lanyards are overshadowed by its high elongation with the presence of cargo displacement constraints.

### **4.3 Parametric Study**

A parametric study was conducted to assess the influence of tie-down angles on the energy absorbing cargo restraint system design. The design space features the same specifications for the cargo container and energy absorbing restraints used in the comparative study. The parameters of the study include side tie-down angle, vertical tie-down angle, and the number of restraints. As shown in Figure 4-5, the side tie-down angle ( $\theta$ ) is the angle of the restraint relative to the longitudinal axis of the aircraft and the vertical tie-down angle ( $\alpha$ ) is the angle of the restraint relative to the cabin floor.

The results of the parametric study are presented in terms of the number of restraints required for a tie-down configuration which has all the restraints tied down at the same angle. The allowable cargo displacement in both longitudinal and lateral directions was constrained to 100 cm. The results from the parametric study were used to find the optimum tie-down angle for a

simplified tie-down configuration. The optimum tie-down angle is one that requires the least amount of restraints, satisfies the crash requirements for both longitudinal and lateral directions, and does not violate the allowable cargo displacement constraints.

The cargo dynamics simulation was used to evaluate each cargo restraint system with the same crash conditions previously used in the comparative study for both longitudinal and lateral impacts. The tie-down configuration was constrained to be doubly symmetric to avoid rotation of the cargo container.

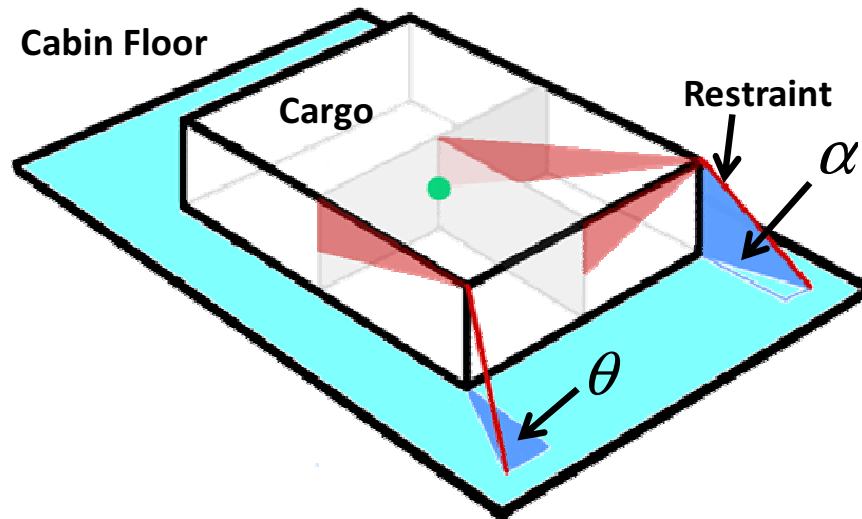


Figure 4-5. Diagram depicting the cargo, cabin floor, restraint, side tie-down angle ( $\theta$ ), and the vertical tie-down angle ( $\alpha$ ).

#### 4.3.1 Parametric Study Results

Plots of the parametric study results are shown for steel chain/tear webbing and nylon strap/tear webbing restraints in Figure 4-6 and Figure 4-7, respectively. The number of restraints refers to amount required to satisfy a maximum allowable cargo displacement constraint of 100 cm in both the longitudinal and lateral directions. A tie-down angle of 30/80, translates to a side tie-down angle ( $\theta$ ) of 30° and a vertical tie-down ( $\alpha$ ) angle of 80°.

The trends regarding tie-down angles stay consistent for both steel chain/tear webbing and nylon strap/tear webbing restraints. The plots show that the number of restraints required increases with increasing side tie-down angle and vertical tie-down angle. Increases in side tie-down angles results in restraints becoming less effective for longitudinal impacts — which happens to be the dominating scenario in this study.

For steel chain/tear webbing restraints, there were no significant changes in the number of restraints required for side angles between 10° and 30°. It can be seen that the amount of steel chain/tear webbing restraints steadily increases with increasing tie-down angle. As opposed to nylon strap/tear webbing restraints, where there is a dip in the number of restraints required for a 30° side tie-down angles. There were no significant changes in the number of restraints required for vertical tie-down angles between 10° and 40°. Increasing vertical tie-down angle reduces the amount of restraint in the longitudinal and lateral directions, but it is also important to have sufficient vertical restraint in the case of rebound. Since all restraints work in unison to provide restraining force in the vertical direction, the vertical tie-down angle should be prescribed to provide more restraint in the longitudinal and lateral directions. The U.S. Army FM 55-450-2 field manual provides a rule-of-thumb for cargo handlers to have restraints tied down as close to 30/30 as possible. The results from the parametric studies show that a 30/30 tie-down angle serves as a good rule-of-thumb for both currently used restraints and energy absorbing restraints.

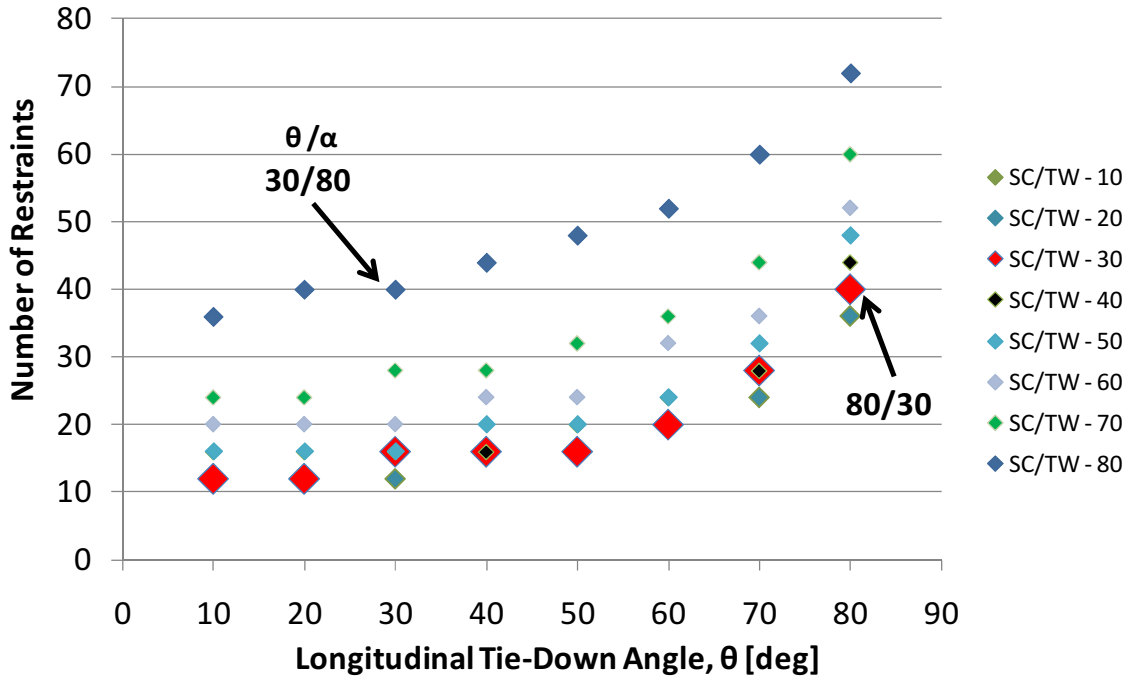


Figure 4-6. Plot of the number of restraints vs. side/vertical tie-down angle. Each series label provides the restraint type and the vertical tie-down angle. Series “SC/TW – 20” refers to steel chain/tear webbing restraint with vertical tie-down angle ( $\alpha$ ) of 20°.

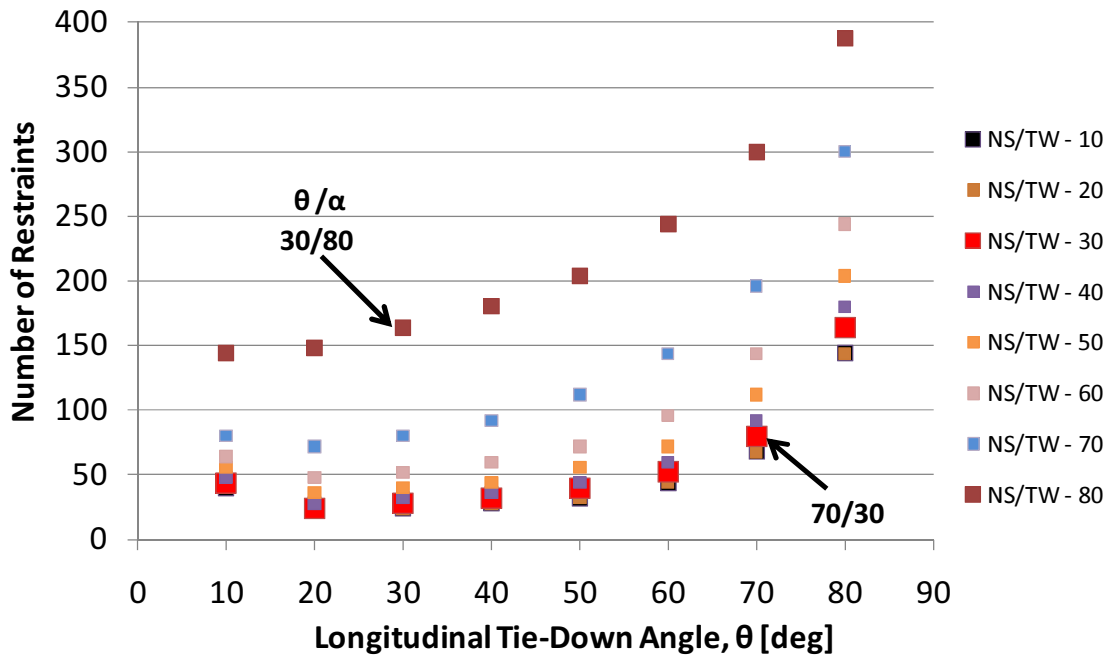


Figure 4-7. Plot of the number of restraints vs. side/vertical tie-down angle. Each series label provides the restraint type and the vertical tie-down angle. Series “NS/TW 2 – 20” refers to nylon strap/tear webbing restraint with vertical tie-down angle ( $\alpha$ ) of 20°.

## 4.4 Optimization Study

Optimization studies were conducted as an exercise of the optimization method described in the previous chapter. Three separate optimization studies were conducted for steel chain restraints and two different types of energy absorbing restraint systems. The design space created for the optimization studies is comparable to existing cargo and rotorcraft to serve as a generic cargo handling scenario. The focus of Optimization Study #1 is the MB-I and MB-II restraints. Optimization Study #2 was conducted for restraints featuring steel chain with tear webbing. The final optimization study was conducted for restraints featuring nylon strap with tear webbing. The objective functions mentioned in Chapter 3 were applied to all optimization studies. The constraints stated in Chapter 3 were also applied as well as some additional constraints specific to each study. The results of the optimization studies are presented in this section as well as a discussion on the influence of design variables, constraints, and weighting of objective functions.

### 4.4.1 ATSV Parameters

The Pareto sampler in ATSV allows the user to set parameters for the DE algorithm. The population size was set to 150; the crossover probability and mutation factor were both set to 0.9. A sufficiently large population size is recommended considering the large number of input variables. Increasing population size also helps to enhance diversity and provide reliable convergence, but at the cost of longer run times. The Differential Evolution Homepage recommends the population size be set to  $10*p$ , where  $p$  is the number of input variables [Ahlers 2010]. Mutation factors typically have an upper bound of 1.0 as premature convergence will occur if it is set too low. The role of crossover probability is “to provide extra diversity” to the population. It is recommended that the crossover probability be set close to 1.0 to minimize

performance losses [Price et al. 2005]. In ATSV, the Pareto sampler populates a Pareto frontier which is generated based on the preference weighting of the objective functions. For all optimization studies, the objective functions were equally weighted to generate the Pareto frontier and then specific designs were chosen based on preferences for different metrics and parameters.

#### 4.4.2 Design Space

The generic cargo handling scenario, which defines the design space for the optimization studies, features a single cargo container on top of a cabin floor as shown in Figure 4-8. Initially, the geometric center of the cargo container is located directly above the geometric center of the cabin floor. The cargo orientation is also aligned with the cabin floor, which is aligned with the  $x$  axis (i.e., longitudinal axis). The center of gravity for both the cargo and cabin floor is located at their respective geometric centers.

The cargo is a single rigid container that is 2.7 m long  $\times$  2.2 m wide  $\times$  1.2 m high. The cargo container mass is 4536 kg (10 kip). There are 26 evenly spaced mounting points located on the top edges of the container similar to existing cargo containers such as the Joint Modular Intermodal Container [MIL-STD-3028 2009]. The mounting point load capacities on the cargo match those of the cabin floor. The cargo is treated as a rigid body and assumed not to deform.

The cabin floor design is loosely based on existing cargo rotorcraft. The dimensions are 8.1 m long  $\times$  2.3 m wide with 17 evenly spaced mounting points on each side of the floor. Current rotorcraft can have mounting points rated up to 88.9 kN, but the ACSDG recommends greater load capacity even with the use of load limiters [Zimmermann et al. 1989]. The cabin floor used in this analysis features mounting points rated up to 111 kN — similar to fixed wing cargo aircraft [FM 55-9 1993]. To simplify the analysis, the effect of load degradation on mounting point load capacity due to shallow tie-down angles is neglected.

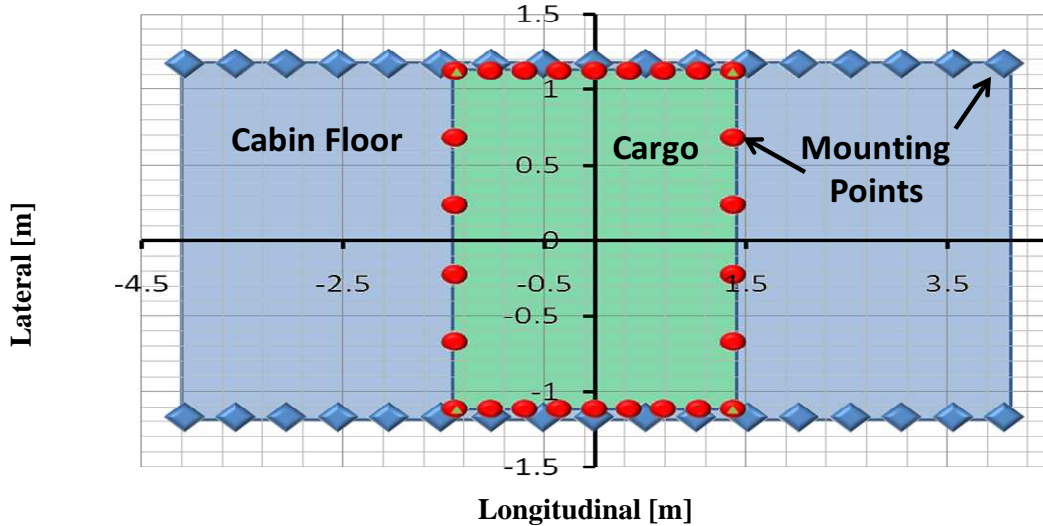


Figure 4-8. Top view of mounting points on cabin floor (blue) and cargo (red).

The energy absorbing restraints used in the optimization studies are the same as the ones used in the comparative and parametric studies. The design variables used in the optimization studies are all discrete, including the restraint parameters. Details on currently used restraint which were analyzed to provide a baseline for comparison are provided in Table 4-1. Details on the range of parameters for the energy absorbing restraints are provided in Table 4-2.

#### 4.4.3 Optimization Study #1: Steel Chain Restraints

The first optimization study was conducted for steel chain restraints without tear webbing. The optimal restraint configurations for the MB-I and MB-II restraints provide a baseline for comparison. The optimization method for the first study differs from the others as the CDS was not a part of the algorithm. Instead a static analysis was used that was similar to the static analysis method in Chapter 3, but without having all restraints tied down at the same angle. The static analysis was conducted using MS Excel and ATSV was used to guide the exploration of the design space and determine the Pareto optimal designs. The static load factors include 16 G

in the longitudinal direction and 10 G in the lateral direction matching the peak dynamic crash conditions recommended in the ACSDG. Cargo displacement is not a factor in this study as steel chain restraints are assumed to be rigid. A summary of the parameters of Optimization Study #1 is shown below:

#### Design Variables

- Number of restraints
- Location of mounting points used for attachment on cabin floor and cargo

#### Objective Functions

- Minimize number of restraints
- Minimize total mass of restraint system
- Maximize total restraint force in the longitudinal and lateral directions

#### Constraints

- Total restraint force in longitudinal direction  $\geq 16 \text{ G} * \text{Cargo Mass}$
- Total restraint force in lateral direction  $\geq 10 \text{ G} * \text{Cargo Mass}$
- Number of restraints  $\leq 26$
- Restraint force  $\leq$  Mounting point load capacity
- Tie-down configuration are symmetric along both longitudinal and lateral axes
- All restraints for a given restraint configuration are identical
- Restraints attach to mounting points in a straight line and do not wrap around cargo
- Mounting point can only support one restraint at a time
- Maximum distance between two mounting points used for restraint attachment is 2.7 m (i.e., max length of steel chain restraint)

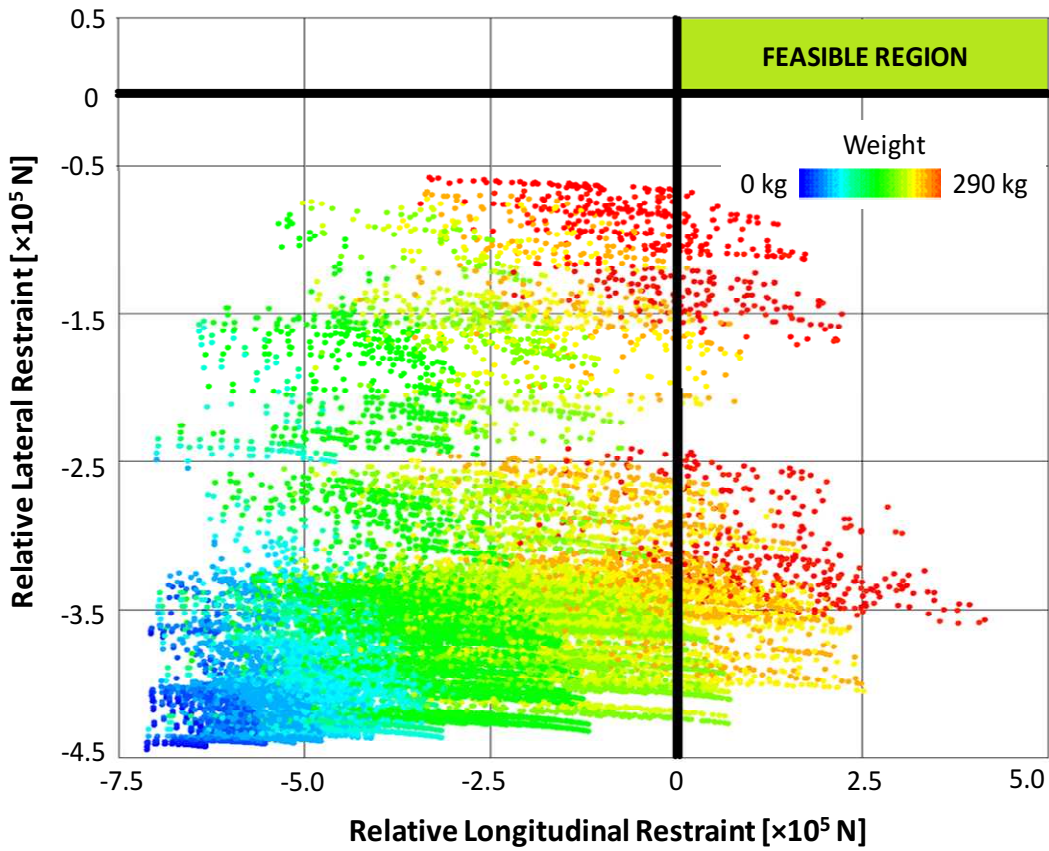


Figure 4-9. Plot of the results for Optimization Study #1 for MB-I and MB-II restraints.

A total of 41393 runs were conducted and none of the restraint configurations could satisfy the constraint to provide a sufficient amount of total restraint force in the lateral direction. A plot of the optimization study results are shown in Figure 4-9. The relative restraint force in each direction is calculated using Eq. (4-1). The "actual restraint force" is the total amount of

$$\text{Relative Restraint} = (\text{Actual Restraint}) - (\text{Required Restraint}) \quad (4-1)$$

restraining force the restraint system provides in a specific direction. The required restraint force is calculated by multiplying the cargo mass by the static load factor: 16 G in the longitudinal direction and 10 G in the lateral direction. Each and every restraint configuration in Figure 4-9 has a negative value for relative lateral restraint and has thus failed to satisfy the lateral impact requirements. The lack of feasible restraint configurations can be partially attributed to the short

length of the MB-I and MB-II restraints, and the width of the cargo container relative to the width of the cabin floor. The short length of the restraints reduced the amount of restraints that could be used as some mounting points on the cabin floor could not be reached from the cargo mounting points. Furthermore, the fact that the design space features a cargo container—which is nearly as wide as the width of cabin floor—limits the range of side tie-down angles that can be obtained to provide more lateral restraint.

The results clearly show that steel chains cannot provide crash safety in the design space specified for this study. The configurations featuring the MB-I restraint—which are currently used on cargo rotorcraft—were unable to provide enough restraint in either the longitudinal or lateral direction. There were, however, several restraint configurations for MB-II restraints which were at least able to satisfy the longitudinal restraint constraint. Among the set of restraint configuration that were feasible only in the longitudinal direction, the one that produced the most lateral restraint is shown in Figure 4-10. This particular restraint configuration features 26 MB-II restraints and has a total mass of 283 kg. The amount of restraint provided in the longitudinal direction had a surplus of 21 kN, but was deficient by 70 kN in the lateral direction.

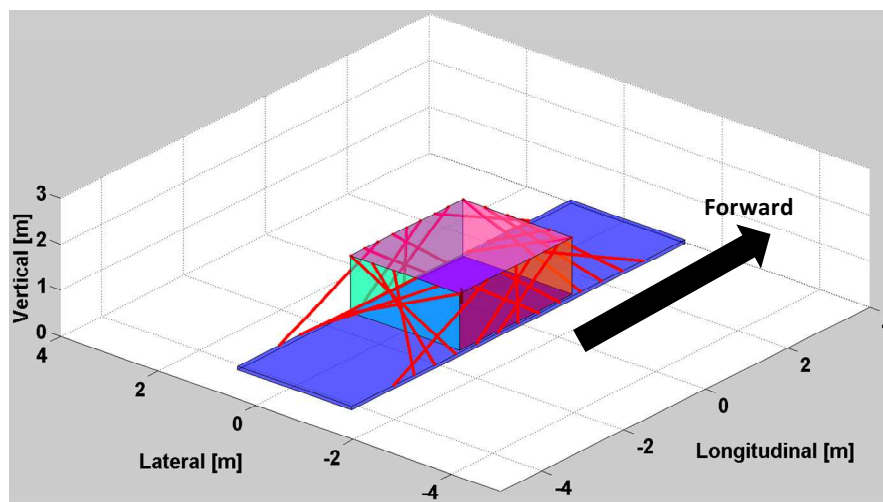


Figure 4-10. Visualization of restraint system closest to being feasible with steel chain restraints.

#### **4.4.4 Optimization Study #2: Steel Chain with Tear Webbing**

The focus of the second optimization study is the steel chain/tear webbing restraint. Details on the specifications and parameters of the steel chain lanyard and the load limiter are provided in Table 4-2. A summary of the parameters of the optimization study are provided in the list below:

##### Design Variables

- Number of restraints
- Location of mounting points used for restraint attached on cabin floor and cargo
- Tear webbing parameters (activation force, maximum load limiter stroke)

##### Objective Functions

- Minimize number of restraints
- Minimize total mass of restraint system
- Minimize cargo displacement in the longitudinal direction
- Minimize cargo displacement in the lateral direction

##### Constraints

- Cargo displacement in the longitudinal direction  $\geq 100$  cm
- Cargo displacement in the lateral direction  $\geq 5$  cm
- Number of restraints  $\leq 26$
- Restraint force  $\leq$  Mounting point load capacity
- Activation force = Mounting point load capacity
- Tie-down configuration are symmetric along both longitudinal and lateral axes
- All restraints for a given restraint configuration are identical in terms of components and their properties (e.g., activation force, maximum load limiter stroke, maximum lanyard length)

- Restraints attach to mounting points in a straight line and do not wrap around cargo
- Mounting point can only support one restraint at a time
- Maximum distance between two mounting points used for restraint attachment is 2.7 m (i.e., max length of steel chain lanyard)

Table 4-4. Summary of results for Optimization Study #2 on steel chain/tear webbing restraints.

Design	Transmitted Force	Total Mass	No. of Restraints	Max. Stroke	Longitudinal Displacement	Lateral Displacement
A	111 kN	152 kg	12	30 cm	53 cm	3 cm
B	111 kN	180 kg	16	6 cm	5 cm	5 cm
C	88.9 kN	197 kg	18	15 cm	66 cm	2 cm
D*	44.5 kN	113 kg	26	30 cm	88 cm	18 cm

\* Not a feasible design

A total of 21,075 runs were made using the optimization method and 267 of them were feasible designs. There were 61 Pareto optimal designs. Glyph and scatter plots of the feasible, and Pareto optimal, designs are shown in Figure 4-11 and Figure 4-12, respectively. Four restraint configurations are chosen for discussion: Design A, Design B, Design C, and Design D. Details and specifications for these three designs can be found in Table 4-4. Design A is the most preferred design with equally weighted objective functions. Design B is an example of a Pareto optimal design with more emphasis on low cargo displacement. Design C is the optimal restraint configuration with more emphasis on reducing the transmitted forces. Design D is the optimal restraint configuration which reduces transmitted forces enough to be used on current rotorcraft. Design D, however, could not satisfy the lateral cargo displacement constraint and is not shown in the plots of the feasible results.

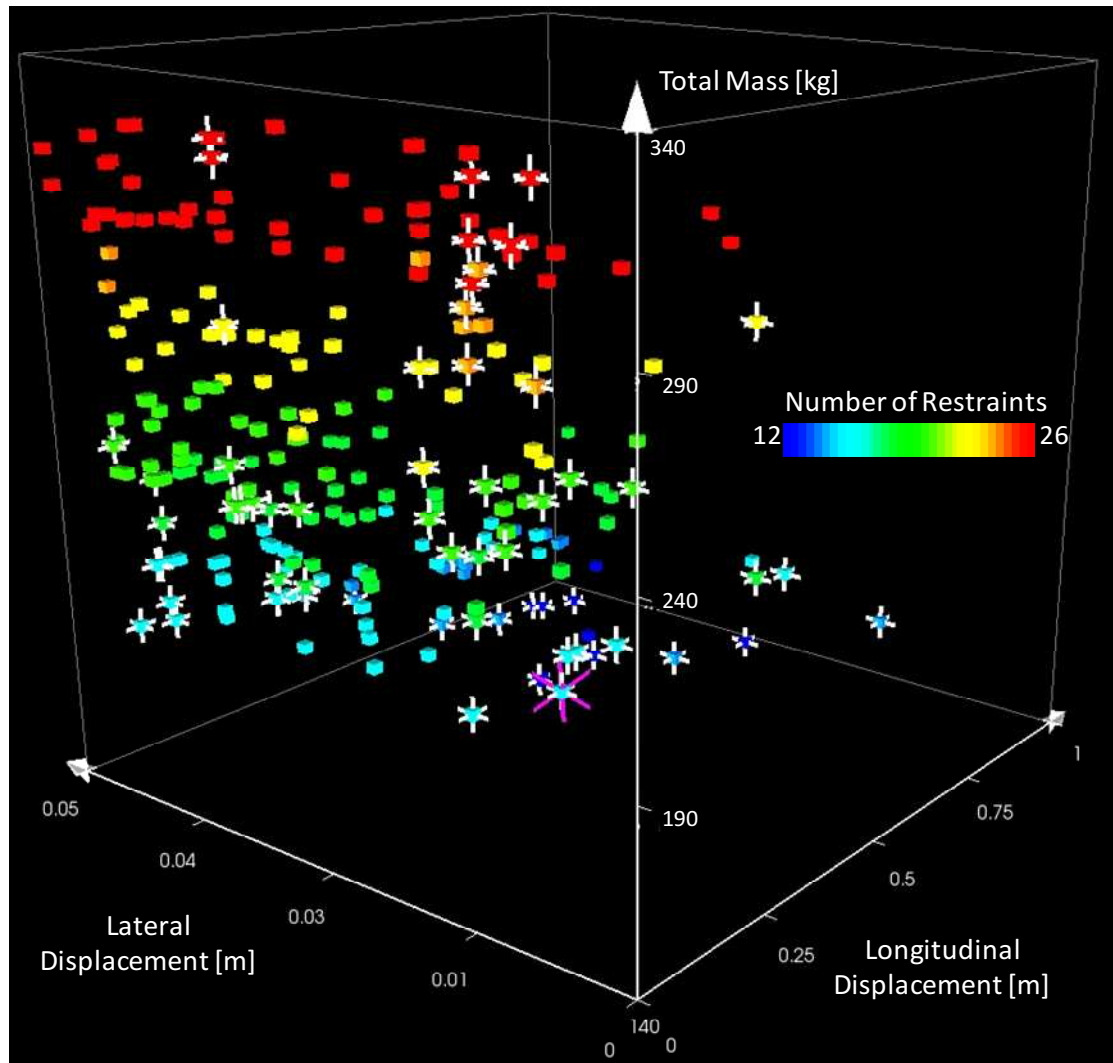


Figure 4-11. Glyph plot of the feasible results for Optimization Study #2. The Pareto optimal designs are marked by “+” in white.

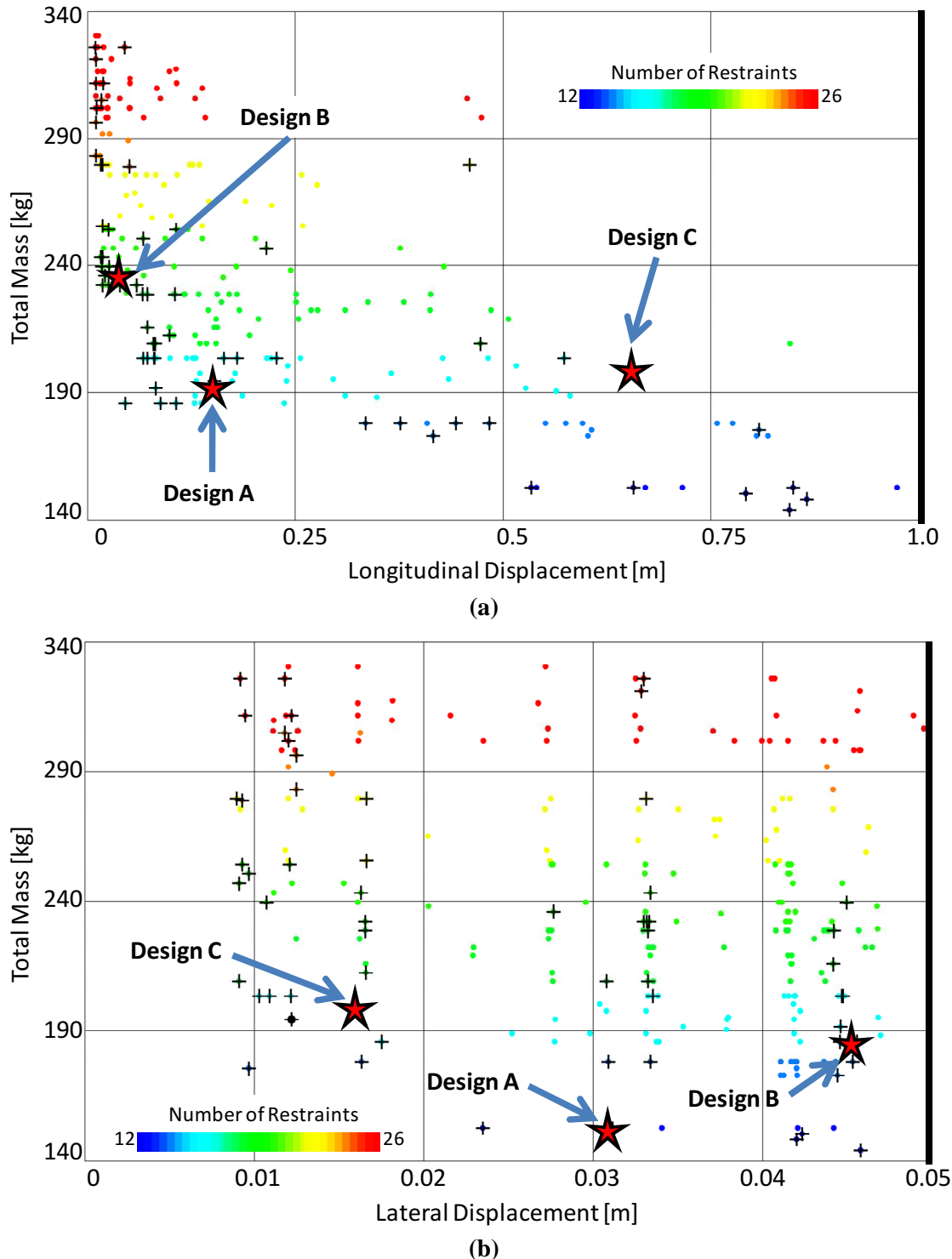


Figure 4-12. Scatter plot of the feasible results for Optimization Study #2. The Pareto optimal designs are marked by “+”.

### **Steel Chain/Tear Webbing – Design A**

The ATSV interface allows the user to view the Pareto frontier based on user defined weighting of preferences on the performance parameters. For the optimization study, the performance parameters are the objective variables: total mass, number of restraints, and cargo displacement in the longitudinal and lateral directions. The Pareto frontier is generated for this study by applying a preference to minimize each of the objectives.

The user can also individually weight each preference in order to emphasize the relative importance of each objective. Thus creating a linear weighting over the trade space and turning the problem into one of single objective optimization [Stump et al. 2002]. The most preferred design with equally weighting the objectives is Design A. A visual representation of the tie-down configurations of Design A can be found in Figure 4-13.

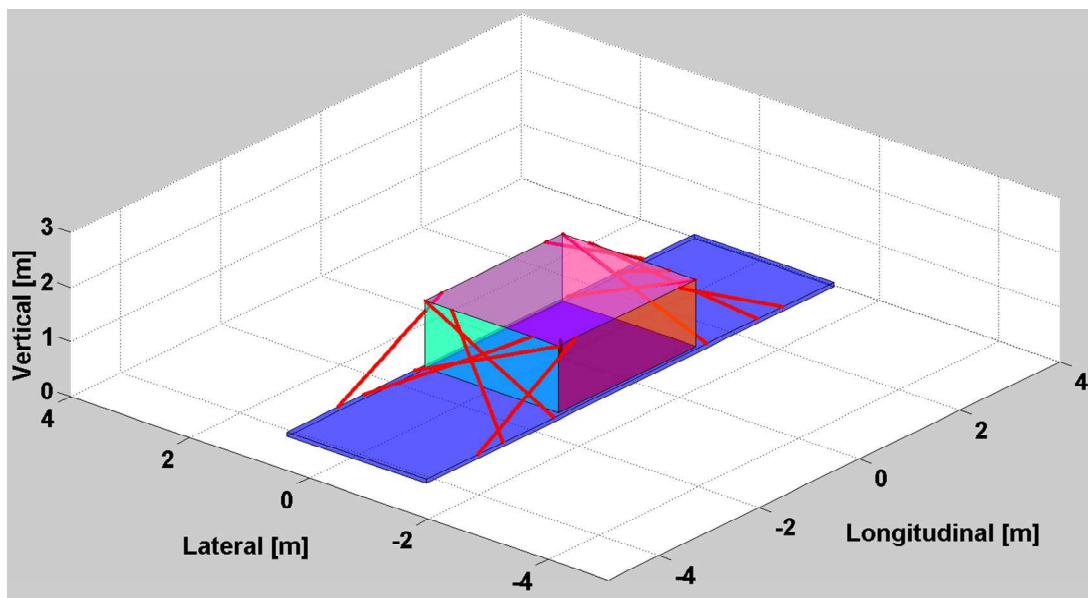


Figure 4-13. Visualization of Design A restraint configuration.

It is clear that the majority of the restraints feature a very wide side tie-down angle to satisfy the lateral impact criteria. Although the loads in the longitudinal direction are higher, the

low lateral displacement constraint proves to be the most stringent requirement. Design A will be used as the baseline for comparison for the other Pareto optimal designs. Details and specifications on Design A can be found in Table 4-4.

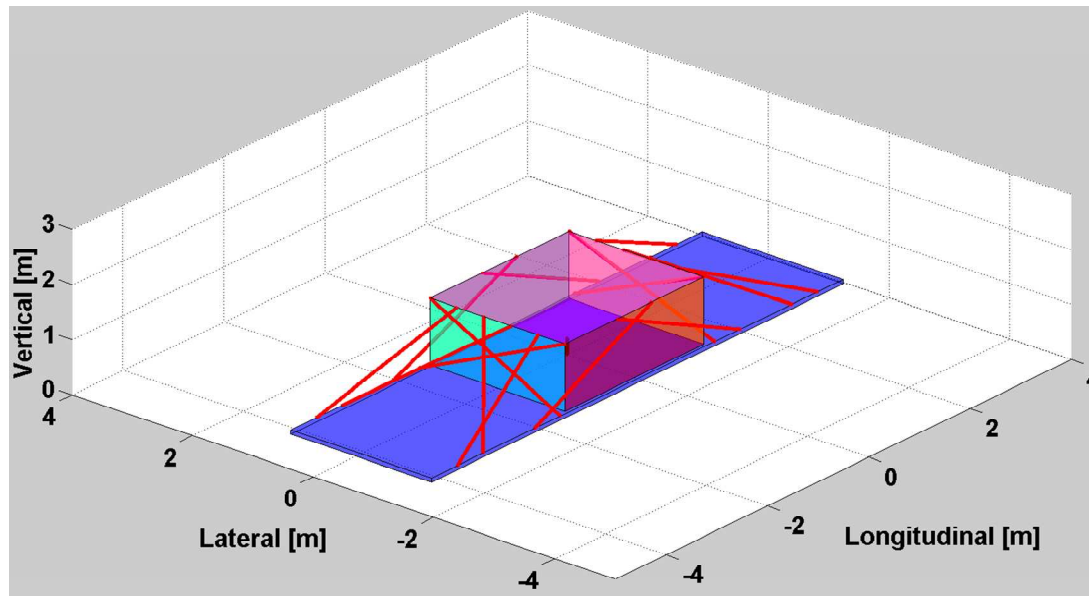


Figure 4-14. Visualization for Design B restraint configuration.

#### ***Steel Chain/Tear Webbing – Design B***

Although the Pareto frontier is generated by equally weighting the objectives, the user can choose a design with a stronger preference on reducing cargo displacement by moving up the Pareto frontier. Design B was chosen with a stronger preference to minimizing cargo displacement. A visual representation of the tie-down configuration for Design B is shown in Figure 4-14. The tie-down configuration is similar to Design A, but with a few more restraints featuring shallow side tie-down angles to provide additional longitudinal restraint. The trade-off for reducing cargo displacement is an increase in mass and more restraints. Compared to Design A, Design B reduces longitudinal displacement by 48 cm with a 2 cm increase in lateral displacement. The cost of reducing displacement is an 18% increase in total mass and 33% more

restraints. This trade-off is a direct consequence of implementing a low allowable displacement constraint. The load limiter requires stroke to dissipate energy: reducing allowable cargo displacement will diminish the advantages of using energy absorbing cargo restraint systems.

### ***Steel Chain/Tear Webbing – Design C***

One of the key benefits of using load limiters is being able reduce the loads transmitted to mounting points and the airframe structure. This allows designers of future rotorcraft to save on structural weight and simultaneously achieve crashworthiness. A visual representation of the Design C can be seen in Figure 4-15. Compared to Design A, Design C reduces the transmitted forces (i.e., activation force) by 20%. On the other hand, there are increases in all other objectives: 50% more restraints, 30% increase in total mass, and 13 cm more displacement in the longitudinal direction. There is only 1 cm less lateral displacement.

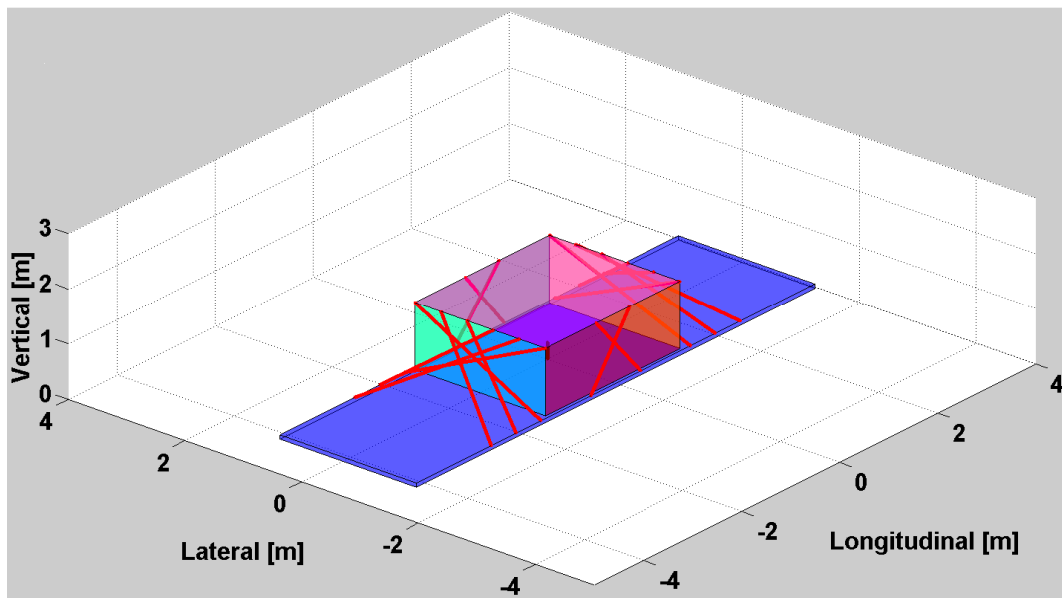


Figure 4-15. Visualization for Design C restraint configuration.

### ***Steel Chain/Tear Webbing – Design D***

Although Design C reduced transmitted forces, the restraint forces (i.e., activation force) exceed the mounting load capacities of current rotorcraft which are typically rated to 22.2 kN and 44.5 kN. Design D is a restraint configuration which reduces the transmitted forces (i.e., activation force), for use on current rotorcraft that feature mounting points with a load capacity of 44.5 kN, but is not a feasible design as it violated the lateral cargo displacement constraint. The optimization study was not able to produce a feasible restraint configuration for current rotorcraft. Again, the lateral displacement constraint was continually violated, but the restraint configuration closest to achieving feasibility is Design D. Design D is the restraint configuration with the lowest lateral cargo displacement while satisfying the longitudinal displacement constraint and adding a constraint on the activation force of all restraints to be 44.5 kN. A visual representation of Design D is shown in Figure 4-16. If 13 cm more displacement was allowed in the lateral direction, Design D would be feasible. Compared to Design A, Design D reduces the total mass by 26% and the transmitted force by 60%. These benefits come at a cost of more than double the amount of restraints and significant increases in cargo displacement.

Both Design C and Design D reduced transmitted forces, but only Design D had less mass than Design A. This is due to the strength of the lanyards for steel chain/tear webbing restraints. The lanyards for steel chain/tear webbing restraints were modeled after the MB-I and MB-II restraints. The MB-I restraint is rated up to 44.5 kN so higher activation forces would require the use of MB-II restraints which are rated to 111 kN. Therefore, Design C used MB-II restraints for lanyards and was thus overdesigned. Reductions in weight could have been achieved with Design C had there been a lanyard with lower strength and weight to just accommodate 88.9 kN.

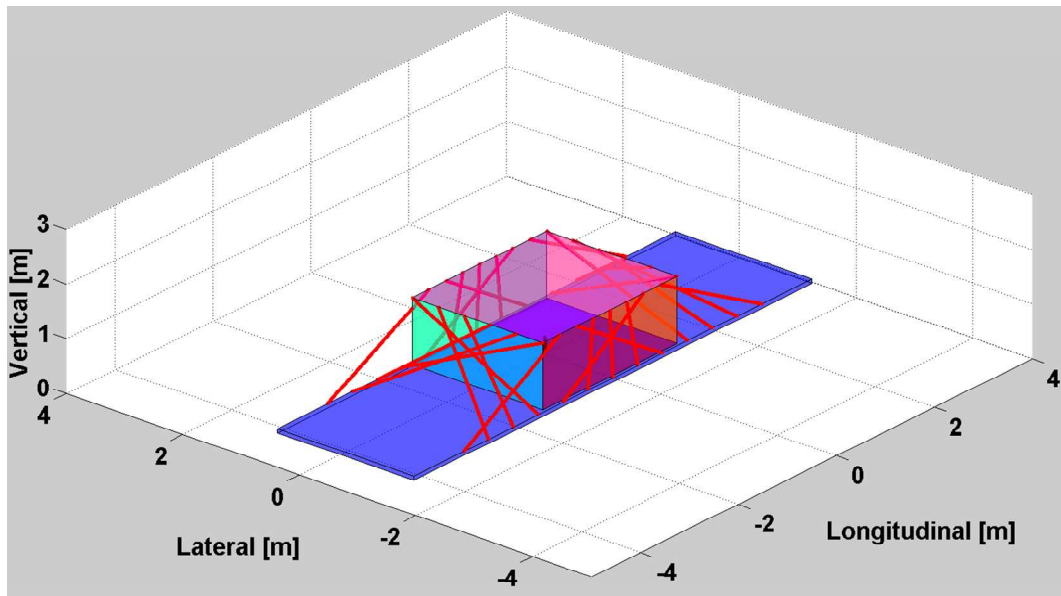


Figure 4-16. Visualization for Design D restraint configuration.

#### 4.4.5 Optimization Study #3: Nylon Straps with Tear Webbing

The focus of the third optimization study is on a nylon strap/tear webbing restraint system. The specifications of the restraints (Table 4-2), design variables, objective functions, and constraints for optimization #2 are shown below:

##### Design Variables

- Number of restraints
- Location of mounting points used for restraint attached on cabin floor and cargo
- Tear webbing parameters (activation force, maximum load limiter stroke)

##### Objective Functions

- Minimize number of restraints
- Minimize total mass of restraint system
- Minimize cargo displacement in the longitudinal direction
- Minimize cargo displacement in the lateral direction

### Constraints

- Cargo displacement in the longitudinal direction  $\geq 100$  cm
- Cargo displacement in the lateral direction  $\geq 5$  cm
- Number of restraints  $\leq 26$
- Restraint force  $\leq$  Mounting point load capacity
- Activation force = Mounting point load capacity
- Tie-down configuration are symmetric along both longitudinal and lateral axes
- All restraints for a given restraint configuration are identical in terms of components and their properties (e.g., activation force, maximum load limiter stroke, maximum lanyard length)
- Restraints attach to mounting points in a straight line and do not wrap around cargo
- Mounting point can only support one restraint at a time

A total of 14,868 runs were made using the optimization method, but all of the restraint configurations violated the lateral cargo displacement. Therefore, not a single one of the nylon strap/tear webbing restraint configurations can be considered feasible. A portion of the results are presented as glyph and scatter plots in Figure 4-17 and Figure 4-18. Similar to optimization studies #1 and #2, the criteria for lateral impact is the most difficult to satisfy. Several of the restraint configurations were able to satisfy the longitudinal displacement constraint, but every restraint configuration with nylon strap/tear webbing restraints violated the lateral displacement constraint.

Although nylon straps are also longer in length than the steel chain lanyard, and thus more mounting points are available for attachment, the narrow design space was a major constraint on the tie-down configurations. The inability to have wider side tie-down angles for

more restraint in the lateral direction was an important factor for this optimization study just as it was for Optimization Study #1 and #2.

The lack of feasible nylon strap/tear webbing restraint configurations, however, is mostly attributed to the elasticity of the lanyard. Nylon straps exhibit significantly more elongation at the activation force than steel chain. Before any energy is absorbed by the restraint, the lanyard exhibits an elongation of 18% of its effective length. Therefore, the high elongation of the lanyard, as opposed to the stroking of the load limiter, accounts for a majority of the allowable cargo displacement. In fact, the lateral displacement constraint is violated even before the activation force is reached.

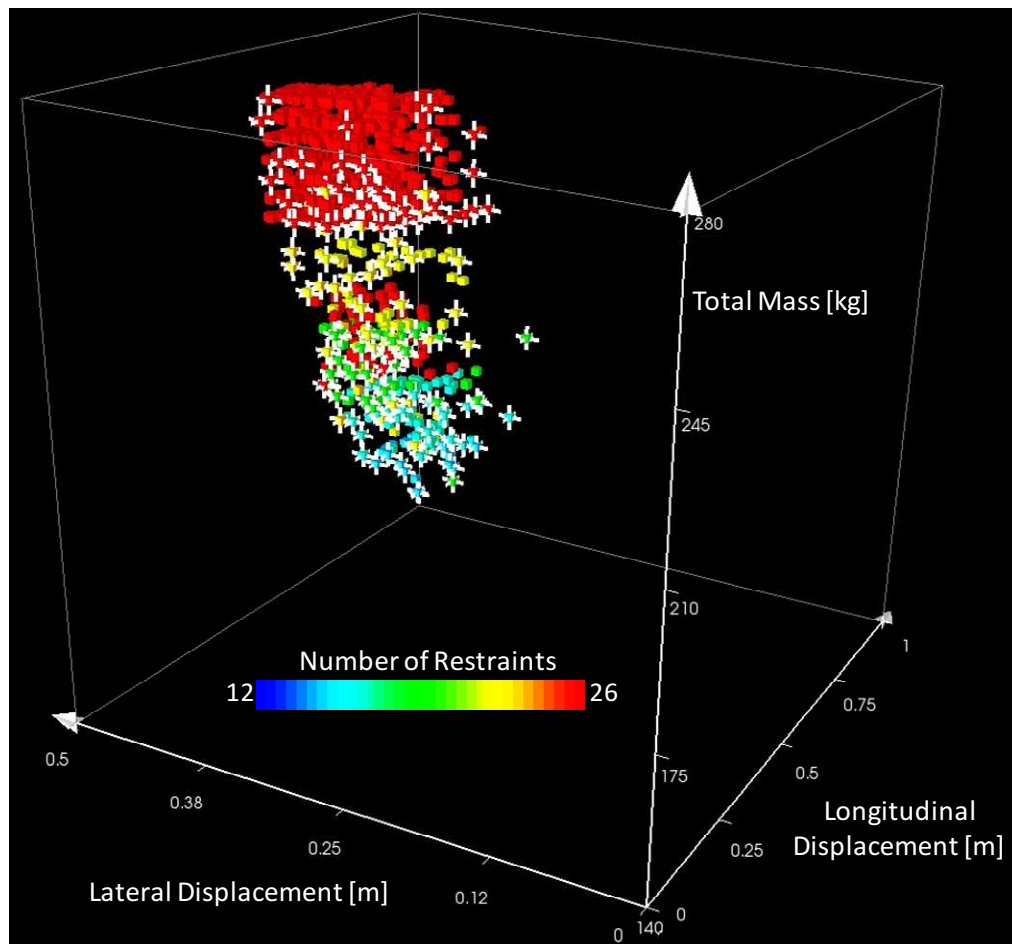


Figure 4-17. Glyph plot of sample set of Optimization Study #3 results. The Pareto optimal designs are marked by “+” in white. No feasible designs.

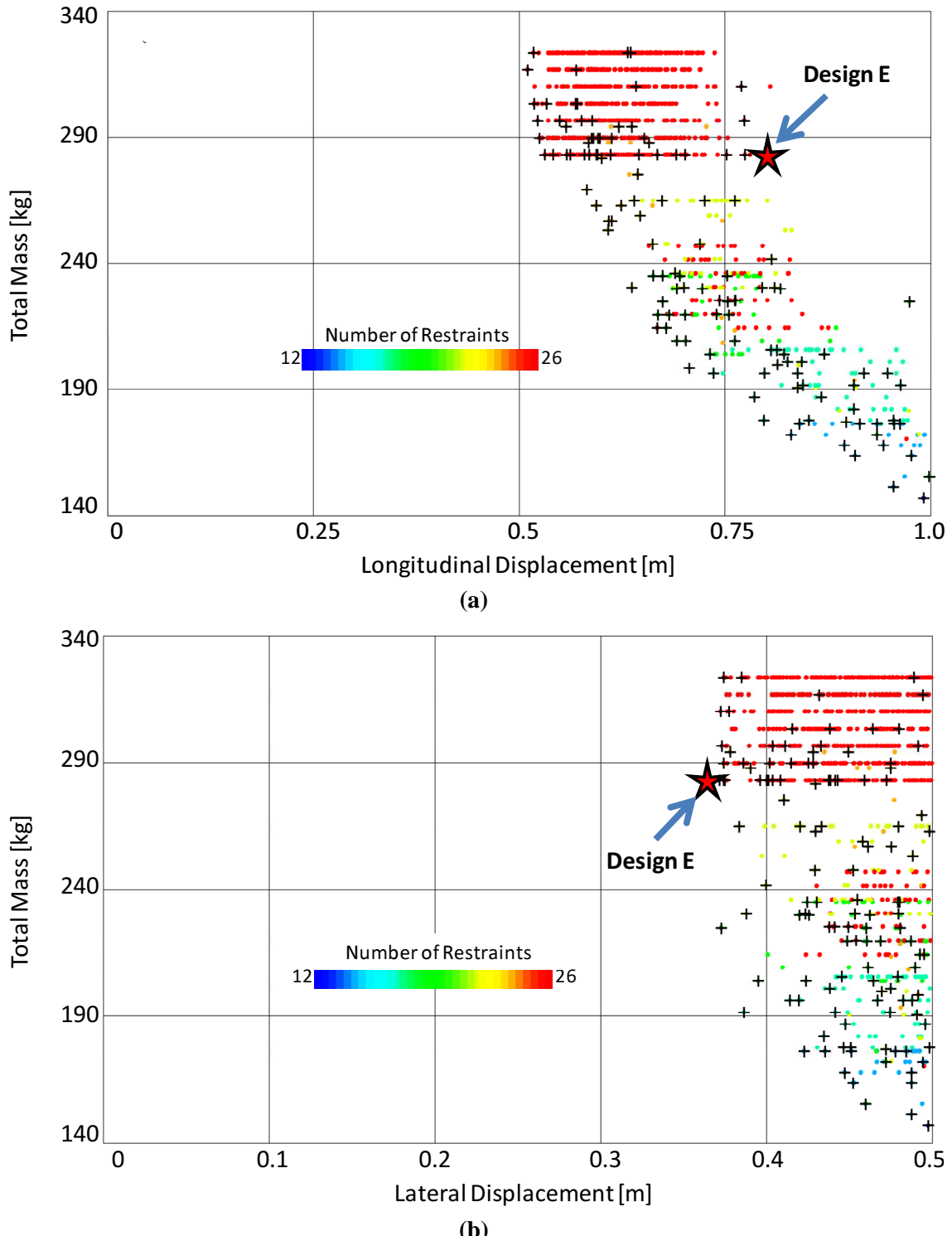


Figure 4-18. Scatter plot of Optimization Study #3 results. The Pareto optimal designs are marked by “+”. No feasible designs.

Table 4-5. Summary of results for Optimization Study #3 on nylon strap/tear webbing restraints.

Design	Transmitted Force	Total Mass	No. of Restraints	Max. Stroke	Longitudinal Displacement	Lateral Displacement
E*	111 kN	200 kg	20	24 cm	97 cm	37 cm
F*	44.5 kN	107 kg	26	30 cm	120 cm	65 cm

\* Infeasible designs

Two restraint configurations were chosen for discussion of the results from optimization #3. Design E is the restraint configurations which was closest to achieving feasibility for nylon strap/tear webbing energy absorbing cargo restraints. Design F is the restraint configuration closest to achieving feasibility while featuring a low activation force. A summary of the specifications of Design E and Design F are shown Table 4-5.

### **Nylon Strap/Tear Webbing – Design E**

The nylon strap/tear webbing restraint configuration closest to achieving feasibility is Design E. Minimizing preferences were implemented on all objectives, but reducing lateral displacement was the priority. A visual representation of the tie-down configurations of Design E can be found in Figure 4-19. It is clear that nylon strap/tear webbing restraints perform poorly compared to steel chain/tear webbing restraints. Design E requires more restraints, total mass, and cargo displacement when compared to Design A and Design B from Optimization Study #2. It would seem that the nylon strap lanyards of nylon strap/tear webbing restraints should have an advantage with a higher strength-to-weight ratio than steel chain. Furthermore, the long length of the nylon straps also allows for a lower vertical tie-down angle for more effective restraint in the longitudinal and lateral directions. The shortcoming of nylon straps is the high elongation, coupled with the low cargo displacement constraint, which prevents the nylon strap/tear webbing restraint from providing adequate safety.

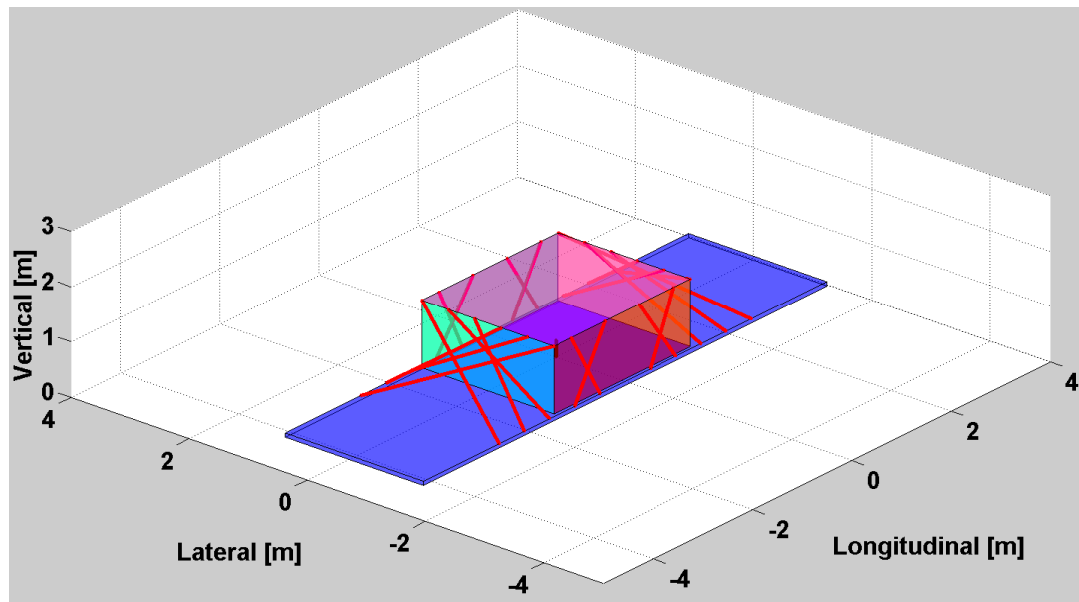


Figure 4-19. Visualization for Design E restraint configuration.

#### **Nylon Strap/Tear Webbing – Design F**

Similar to Design E, Design F is the nylon strap/tear webbing restraint configuration closest to achieving feasibility with a low activation force. A visual representation of Design F is shown in Figure 4-20. Design F is different from the other sample restraint configurations as it violates both longitudinal and lateral displacement constraints by a significant margin. It is clear that nylon strap/tear webbing restraints are incapable of reducing transmitted forces and providing crash safety. The key factor again is allowable cargo displacement. Design F features the lowest mass out of all the other sample restraint configurations, but also requires the most amount of displacement. If the displacement constraints were increased, then it would be possible to find a steel chain/tear webbing restraint configuration which requires less displacement and less restraints for the same amount of total mass as a nylon strap/tear webbing restraint configuration.

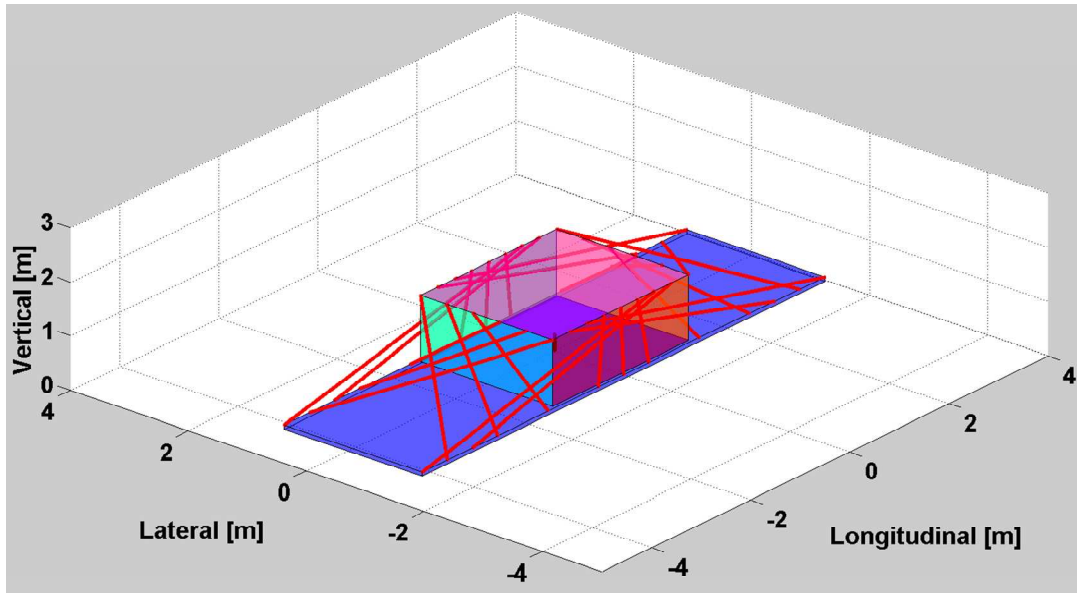


Figure 4-20. Visualization for Design F restraint configuration.

#### 4.4.6 Discussion of Results

Three optimization studies were conducted for three different types of cargo restraint systems. The first optimization study on the MB-I and MB-II restraints was conducted to provide a baseline for comparison. The results of the study did not find any feasible restraint configurations for currently used cargo restraints (e.g., MB-I, MB-II) within the prescribed design space due to the inability to provide a sufficient amount of lateral restraint. On the other hand, there are several feasible designs for energy absorbing cargo restraint systems. A summary of the sample designs from Optimization Study #2 and #3 are shown in Table 4-6.

Table 4-6. Summary of sample designs from Optimization Study #2 and #3.

Restraint Type	Design	Total Mass	No. of Restraints	Long / Lat Displacement	Feasible?	Application
Steel Chain/ Tear Webbing	A	152 kg	12	53 cm / 3 cm	Yes	Best overall performance
	B	180 kg	16	5 cm / 5 cm	Yes	Low cargo displacement
	C	197 kg	18	66 cm / 2 cm	Yes	Low transmitted forces
	D	113 kg	26	88 cm / 18 cm	No	For use on current rotorcraft
Nylon Strap/ Tear Webbing	E	200 kg	20	97 cm / 37 cm	No	Best overall performance
	F	107 kg	26	120 cm / 65 cm	No	For use on cargo rotorcraft

Two different types of energy absorbing cargo restraint systems were analyzed. Both restraint systems featured a load limiter combined with either steel chain or nylon strap as the lanyard component. A comparison plot of the feasible designs for both restraint systems is shown in Figure 4-21, Figure 4-22, and Figure 4-23. The results from optimization study #1 (steel chain/tear webbing) and optimization study #2 (nylon strap/tear webbing) have a convex shape and curve upwards near the origin — where the objective values would be zero — but the nylon strap/tear webbing results are shifted further back. This essentially shows that the energy absorbing cargo restraints with steel chain as the lanyard requires less cargo displacement for the same number of restraints and total mass. The high elongation of nylon strap lanyards is the deciding factor as satisfying cargo displacement constraints was critical to achieving feasibility. The benefits (e.g., strength-to-weight ratio, cost) of using nylon straps, however, does not outweigh the shortcomings in terms of elongation and stiffness.

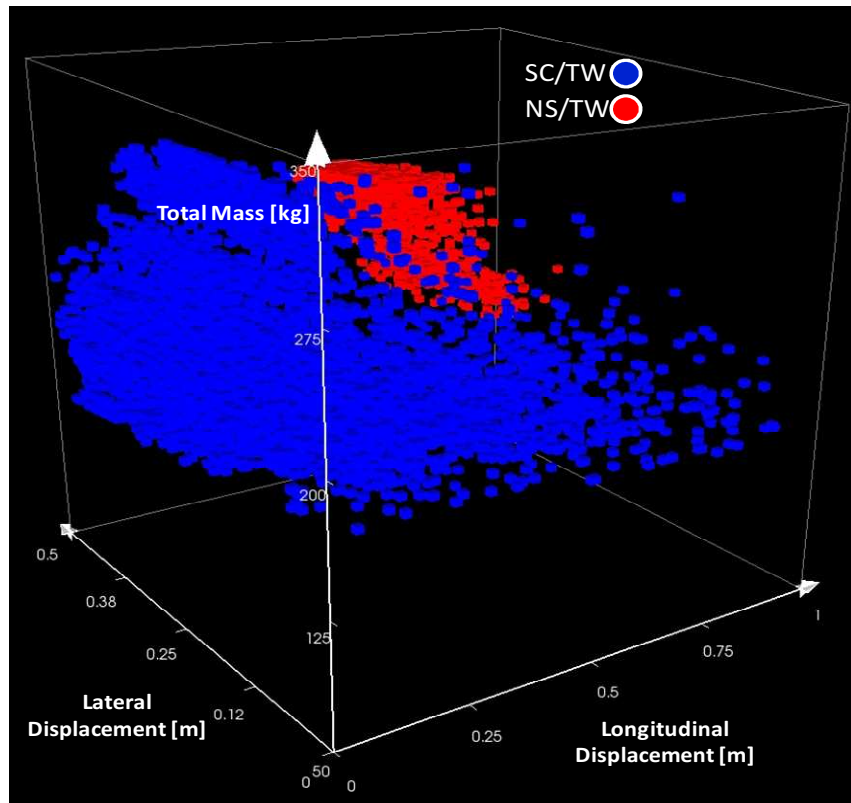


Figure 4-21. Glyph plot results from optimization studies on steel chain/tear webbing (SC/TW) and nylon strap/tear webbing (NS/TW) restraints.

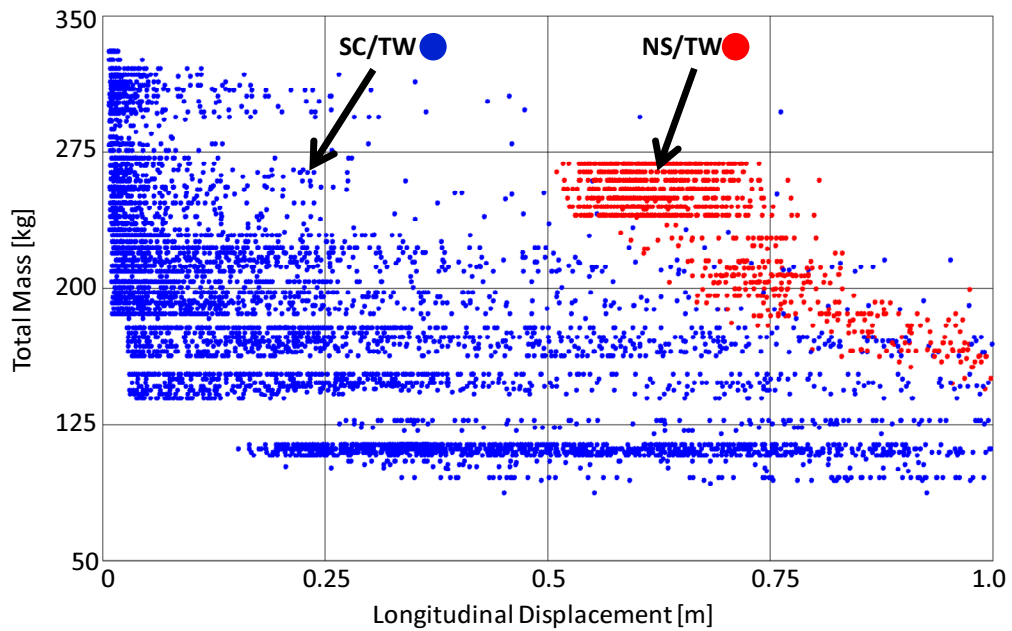


Figure 4-22. Scatter plots of longitudinal cargo displacement results from optimization studies on steel chain/tear webbing (SC/TW) and nylon strap/tear webbing (NS/TW) restraints.

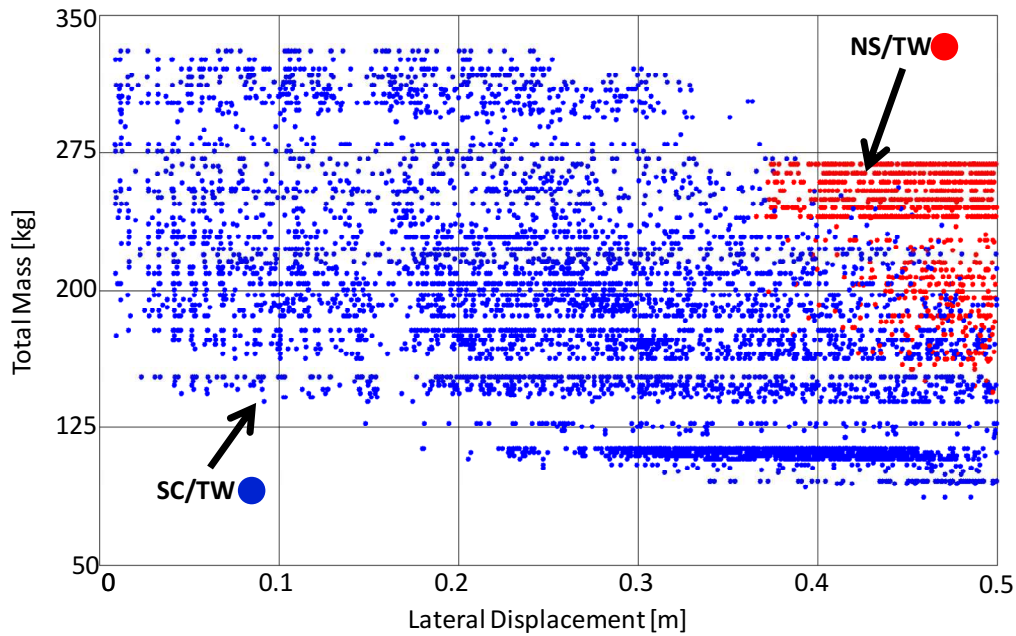


Figure 4-23. Scatter plots of lateral cargo displacement results from optimization studies on steel chain/tear webbing (SC/TW) and nylon strap/tear webbing (NS/TW) restraints.

In addition the influence of the lanyard component, several trends were observed regarding the design variables. The comparative study provided insight into the influence of the activation force on the objectives. For both steel chain/tear webbing and nylon strap/tear webbing restraints, majority of the Pareto optimal designs featured the highest activation force when equally weighting the objective functions. The result of reducing the activation force (e.g., Design C, Design D, and Design F) was an increase in the number of restraints required and allowable cargo displacement. The total mass of the restraint system, however, was reduced. Furthermore, the restraint configurations with the least amount of restraints, and lowest total mass, resulted in the most cargo displacement. In general, a reduction in one objective requires an increase in the other objectives.

The allowable cargo displacement constraint had the most influence on restraint system design, with the number of restraints, activation force, maximum load limiter stroke, and tie-

down configurations all being dependent on the displacement constraints. The particularly low lateral displacement constraint proved to be too difficult to satisfy for nylon strap/tear webbing restraints and significantly limited the number of feasible designs for steel chain/tear webbing restraints. For all optimization studies, the lateral impact criteria proved to be the most stringent requirement to satisfy. The design space allowed for a maximum of 26 restraints, but that was not enough to provide sufficient lateral restraint due to the inability to use tie-down angles which could provide more restraint in the lateral direction.

## Chapter 5

### Requirements and Design Criteria for Cargo Restraint Systems

The objective of this chapter is to recommend requirements, design criteria, and provide guidance to cargo handlers for using energy absorbing cargo restraints. The requirements that energy absorbing cargo restraints must satisfy are presented as two distinct categories: normal maneuvering flight conditions and crash conditions. Recommended design criteria are provided based on observations made in the optimization and comparative studies presented in Chapter 4. Guidelines for cargo handlers for load preparation are provided through restraint tables that can be used for several different cargo handling scenarios. Regression models were created from the restraint table data to provide cargo handlers with a single equation to use to configure a crashworthy energy absorbing cargo restraint system. In addition to requirements based on operating conditions, design criteria are provided to address usability. Considerations must be made regarding ease-of-use when introducing new technology.

#### 5.1 Design Conditions and Requirements

A crash is a singular event and is considered the worst-case scenario which drives cargo restraint system design. Cargo restraint systems, however, must also be designed to provide safety in situations which may produce lower acceleratory loads, but occur on a regular basis. Therefore, the requirements for cargo restraint systems are twofold: 1) Restraine cargo to a fixed position in normal maneuvering flight conditions; 2) Arrest cargo motion within an allowable displacement in a crash.

### 5.1.1 Normal Maneuvering Flight Conditions

For the requirements proposed in this chapter, the normal maneuvering flight conditions are defined as the conditions experienced in recurring flight operations; where the loads on the cargo are induced by the acceleration from takeoff, maneuvers, gusts, and landing. The conditions do not include the high G loads from hard landings and crash events. The key requirement under normal maneuvering flight conditions is that the cargo restraint system must be able to restrain the cargo to a fixed position within some tolerance due to elongation of the lanyards and while keeping the restraint forces below the activation force of the load limiter. The amount the cargo is allowed to displace due to lanyard elongation will be dependent on the mission and cargo handling scenario. Prohibiting cargo movement in normal maneuvering flight operations will prevent injuries and avoid interference with crew operations which may require personnel to move around inside the cargo cabin area.

The analysis used to evaluate energy absorbing cargo restraint system in normal maneuvering flight conditions focus solely on the lanyard component without any contribution from the load limiter. A static analysis can be used to evaluate energy absorbing cargo restraint systems that feature lanyards with high stiffness (e.g., steel chain) and low elongation. It is recommended that stiff lanyards with low elongation are used as the results from the analytical studies in Chapter 4 show that they can also improve the performance of the cargo restraint system in crash conditions. The load factors to be used in the static analysis can be obtained from existing load preparation documents. The FM 55-450-2 field manual in particular provides load factors of 4 G and 1.5 G in the longitudinal and lateral directions, respectively. These load factors are based upon the operating conditions experienced on U.S. Army rotorcraft.

As a sample exercise, a few restraint configurations from the optimization studies presented in the previous chapter are evaluated for normal maneuvering flight conditions. The

first cargo restraint configuration is Design A, which was obtained from Optimization Study #2 on steel chain/tear webbing restraints. The lanyard component of Design A is a steel chain; therefore a static analysis can be used. The analytical results show that for Design A can provide a surplus of 130 kN of restraint in the longitudinal direction and 216 kN in the lateral direction. Therefore, Design A is a restraint configuration which can satisfy both the normal maneuvering flight conditions and the crashworthiness conditions. Also from Optimization Study #2 is Design D, which featured low activation force with for use on current rotorcraft. Design D was not feasible as it violated the lateral displacement constraints. Although, Design D is capable of satisfying the normal maneuvering flight conditions by providing surplus of 59 kN of restraint in the longitudinal direction and 86 kN in the lateral direction. Design D is an example of a restraint configuration which satisfies normal maneuvering flight conditions, but cannot provide crash safety. All feasible restraint configurations from the optimization studies were able to satisfy both normal maneuvering flight and crash conditions.

### **5.1.2 Crash Conditions**

The crash conditions refer to an event which results in catastrophic damage to the aircraft such as a crash or hard landing. The velocity change at impact is 13 m/s and 6.5 m/s in the longitudinal and lateral directions, respectively. The acceleration at the cabin floor is approximated as a triangular pulse with a peak of 16 G and 10 G in the longitudinal and lateral directions, respectively.

The peak of the crash pulse is clearly larger in magnitude than the static load factors normal maneuvering flight conditions. For energy absorbing cargo restraint systems, the key requirement in crash conditions is to be able to arrest the motion of the cargo without violating an allowable displacement constraint. Unlike the normal maneuvering flight conditions, the goal is

to take advantage of the load limiter and utilize its full energy absorbing potential. The allowable displacement can be unique to each cargo handling scenario and is dependent on several factors including aircraft type, location of the cargo, and location of occupants. At the very least, the cargo displacement must be constrained to prevent the cargo from moving into occupied space and injuring crew members. Additionally, the cargo should not be allowed to impinge on areas of the airframe structure which hold up high mass items (e.g., engine, gearbox, rotor) and are essential to providing a protective occupant envelope.

The cargo dynamics simulation and optimization method described in Chapter 3 are recommended to be used as tools to design and evaluate crashworthy cargo restraint systems. The ACSDG and MIL-STD-1290 should be used as a reference for the crash conditions and loads to be used in the design and evaluation of cargo restraint systems.

## **5.2 Cargo Restraint System Design Criteria**

From the results of the optimization and comparative studies in the previous chapter, several trends were observed regarding the design parameters of energy absorbing cargo restraint systems. Recommendations to achieve optimal restraint system design are provided from the trends observed. Simply minimizing objective functions, however, is not sufficient to design an optimal restraint system. It is also crucial to consider usability for cargo handlers and facilitate load preparation procedures.

### **5.2.1 Lanyard**

The lanyard component of the restraint system should exhibit high stiffness, high strength-to-weight ratio, and low elongation at the activation force to have an efficient energy

absorbing cargo restraint system. Lanyards with low elongation can reduce cargo movement in both normal maneuvering flight and crash conditions. A stiff fabric (e.g., Kevlar) has an advantage over metals with the capability of wrapping around the cargo as another form of attachment in the case where no mounting points are available. Furthermore, in an emergency situation where the cargo must be released immediately, it is possible to cut through a fabric restraint with a blade. Conversely, the disadvantages of using high strength, low elongation fabric materials can include susceptibility to environmental effects and high cost [Shefrin et al. 1986].

### 5.2.2 Load Limiter

The results from the comparative and optimization studies provide insight on the influence of the load limiter parameters on the performance of energy absorbing cargo restraint systems. Improvements in terms of minimizing number of restraints and resultant cargo displacement can be achieved by increasing the activation force. A reduction in restraint system weight can be achieved by decreasing the activation force, but with an increase in the number of restraints. From a usability standpoint, the weight and number of restraints should be kept to a minimum to prevent increases in load preparation time.

Prescribing the activation force of the load limiter will depend on the mission and the preference on reducing weight or reducing the number of restraints. It is recommended that the activation force of the load limiter be designed close to the mounting point load capacity to dissipate as much energy as possible with variability in mounting point strength and in the transmitted forces taken into consideration. Furthermore, the maximum load limiter stroke of the load limiter should be just over the minimum required to arrest the cargo in a crash event to avoid excess weight. A factor of safety should be incorporated in load limiter design by adding more stroke than the minimum required.

In addition to tailoring load limiter parameters, the hardware design of the load limiter should be simple and ergonomic. The use of fabric materials over metals is beneficial as one of the major issues with the wire bender concepts included a bulky design and the abundance of moving metal parts that lead to injuries for cargo handlers [Anderson et al. 2010].

### 5.2.3 Tie-Down Configuration

The tie-down configuration should be symmetric about the longitudinal and lateral axes to prevent rotation from an impact in either direction. The ACSDG and FM 55-450-2 recommend that the restraint system be symmetric only about the longitudinal axis, but symmetry about the lateral axis is also important considering the little space existing between the cargo and the side walls of the cabin. Although the loads in the lateral direction may be less in magnitude, cargo rotation could allow a corner of the cargo container to impinge on a side wall, weaken the airframe, and allow high mass items (e.g., gear box, rotor) to breach into the occupied cabin space. It is also recommended that energy absorbing cargo restraints are tied down to an angle as close to 30/30 as possible as a general rule-of-thumb. From the results of the parametric study presented in the previous chapter, a 30/30 tie-down angle was found to be the optimum angle by providing sufficient restraint in the longitudinal, lateral, and vertical directions with the least number of restraints.

The tie-down configuration can also affect usability and load preparation. It is recommended that the footprint of the tie-down configuration be kept to a minimum to provide clear walkways for personnel inside the aircraft. Furthermore, the restraints should attach to mounting points that are easiest to access while preserving the required tie-down angles. As discussed in the previous chapter, there are situations where the cargo is nearly as wide as the

cabin. Therefore, mounting points on the sides of the cargo may be difficult to reach and increase load preparation time.

### 5.3 Restraint Tables

It is unlikely that cargo handlers will have the time or resources to conduct optimization studies prior to load preparation. Nonetheless, they must still be able to select and configure a restraint system that satisfies the requirements for both normal maneuvering flight and crash conditions. An example of restraint tables was created to demonstrate a method of providing guidance on configuring restraint systems for a variety of cargo handling scenarios. The analysis for the restraint tables utilized the cargo dynamics simulation and features both nylon strap/tear webbing and steel chain/tear webbing restraints. The tear webbing device has an activation force of 44.5 kN and a maximum load limiter stroke of 1.2 m. Furthermore, the tie-down configurations were simplified to be doubly symmetric, and all restraints were tied down at an angle of 30/30. The input parameters, and their corresponding range of values, which defined the cargo handling scenarios are shown in Table 5-1. A sample of the restraint table data is shown in Table 5-2.

Table 5-1. Restraint table parameters and values.

Parameter	Range of Values
Activation Force	44.5 kN
Max. Stroke	1.2 m
Restraint Type	Steel Chain/Tear Webbing, Nylon Strap/Tear Webbing
Direction	Longitudinal, Lateral
Cargo Weight	22.2 kN → 88.9 kN
Crash Pulse Peak	4 G → 16 G (Longitudinal), 1.5 G → 10 G (Lateral)
Impact Velocity	10 m/s → 13 m/s (Longitudinal), 4.4 m/s → 6.4 m/s (Lateral)
Cargo Displacement	10 cm → 150 cm (Steel Chain/Tear Webbing) 50 cm → 200 cm (Nylon Strap/Tear Webbing)

The output of the restraint table is the number of restraints required and the maximum load limiter stroke required by each restraint. The number of restraints is rounded up to the nearest multiple of four to satisfy the doubly symmetric tie-down configuration.

Table 5-2. Sample restraint table for longitudinal impacts.

Restraint Type	Steel Chain/Tear Webbing (Impact Velocity = 13 m/s)											
Longitudinal Pulse Peak	4 G			8 G			10 G			16 G		
Allowable Displacement [m]	< 0.1	< 1.0	< 1.5	< 0.1	< 1.0	< 1.5	< 0.1	< 1.0	< 1.5	< 0.1	< 1.0	< 1.5
Cargo Weight	Number of Restraints Required											
22.2 kN	8	4	4	8	8	4	12	8	4	16	8	8
44.5 kN	12	8	8	16	12	8	24	12	8	28	12	12
66.7 kN	16	8	8	24	16	12	32	16	12	44	16	16
88.9 kN	20	12	12	32	20	16	44	20	16	56	28	20

Although the restraint tables eliminate the need to conduct an optimization study, cargo handlers will still have to sort through a large archive of restraint tables for one that corresponds to the desired scenario. To make things simpler, a regression analysis was conducted for the restraint table data to create a set of equations which the cargo handlers can use to quickly select and configure the energy absorbing cargo restraint systems. ATSV has a built-in feature to conduct a multivariate least-squares regression analysis on the restraint table data. The analysis does not, however, include a procedure to search and remove outliers against the dataset regression to enhance the quality of the fit. A quadratic function with four input variables is used to model the dataset with four different equations corresponding to the two types of energy absorbing cargo restraints (steel chain/tear webbing, nylon strap/tear webbing) and two impact directions (longitudinal, lateral). The input variables of each equation include cargo weight, crash pulse peak, impact velocity, and allowable cargo displacement. The number of restraints required

is the dependent variable of the regression model. The general form of the regression model is provided by the following equation:

$$\begin{aligned} N = & b_1 + b_2 \cdot W + b_3 \cdot P_G + b_4 \cdot D + b_5 \cdot V + b_6 \cdot W^2 + \\ & b_7 \cdot P_G^2 + b_8 \cdot D^2 + b_9 \cdot V^2 + b_{10} \cdot W \cdot P_G + b_{11} \cdot W \cdot D + \\ & b_{12} \cdot W \cdot V + b_{13} \cdot P_G \cdot D + b_{14} \cdot P_G \cdot V + b_{15} \cdot D \cdot V \end{aligned} \quad (5-1)$$

where  $N$  is the number of restraints required,  $W$  is the cargo weight,  $P_G$  is the crash pulse peak,  $D$  is the allowable cargo displacement, and  $V$  is the impact velocity. The range of values for the allowable cargo displacement and impact velocity are dependent upon on the direction of impact. The coefficients ( $b_i$ ) of Eq. (5-1) for all four models can be found in the Appendix A.

To use the regression models, the user (e.g., cargo handler) must first choose a restraint type. The regression model will then calculate the number of restraints required for longitudinal and lateral impacts. For example, if the user chooses steel chain/tear webbing restraints (SC/TW), then the "SC/TW – Longitudinal" and "SC/TW – Lateral" regression models will be used to determine the number of restraints required. The nylon strap/tear webbing regression models are labeled "NS/TW – Longitudinal" and "NS/TW – Lateral". However, the output of each regression model is the number of restraints required to satisfy the conditions for a single direction. Therefore, the larger of the two regression model solutions will determine the final number of restraints required to ensure that the restraint system is able to provide adequate safety in both directions.

Details on the regression model are presented in Table 5-3. The sample sizes were tailored to increase the quality of fit of the regression model, based on observations made regarding the relationship between the input and output variables. First, a lower limit exists for impact velocity where at some minimum value the impact does not create enough change in energy to require more than the minimum number of restraints. Second, specifically for

nylon strap/tear webbing restraints the allowable cargo displacement must be high enough to allow the load limiters to activate. The reason for changing the range of allowable displacement for nylon strap/tear webbing restraints is that the number of restraints required is highly dependent on whether or not the load limiters are involved. This observation supports the results from the analytical studies and is discussed in detail in Chapter 4.

Table 5-3. Summary of the details from regression analysis.

Model	Mean	Standard Deviation	Number of samples	R <sup>2</sup>	Standard Error
SC/TW – Longitudinal	1.20E-6	1.78	960	0.95	0.057
SC/TW – Lateral	2.52E-6	2.43	720	0.89	0.091
NS/TW – Longitudinal	-1.91E-4	5.11	1024	0.92	0.160
NS/TW – Lateral	-6.63E-6	5.74	768	0.86	0.207

The error of the regression model is calculated using Eq. (5-2), where *Predicted N* is the output from the regression model and *Actual N* is the data from the restraint tables.

$$\text{Error} = (\text{Predicted } N) - (\text{Actual } N) \quad (5-2)$$

A negative error value corresponds to the model under-predicting the number of restraints required. The mean, standard deviation, and standard error are calculated using the error values of each of the four regression models. The mean (i.e., average error) for all four models is approximately zero. The standard error is fairly low for the steel chain/tear webbing models and is higher for nylon strap/tear webbing models. The low values for standard error also show that the sample size is adequate to describe and analyze with the regression model and that there is less uncertainty in the mean value estimate. The high values of the correlation coefficient, R<sup>2</sup>, values correspond to the goodness of fit over the dataset. It is clear that the “SC/TW – Longitudinal model” has the best fit based on the mean, standard deviation, standard error, and R<sup>2</sup> value. A sample histogram is shown in Figure 5-1 for “SC/TW – Longitudinal” regression model. The histogram shows a Gaussian distribution in the error as do the histograms for the

remaining three models. Histogram plots for the other regression model results can be found in the Appendix A. It is noted that from the Gaussian nature of the distribution, a low standard deviation would assist to decrease the severity of under-predicting the number of restraints required to provide adequate safety. The issues that arise with over-predicting include excess weight and increases in load preparation time. Overall, the regression analysis using the least-squares method with a quadratic function works well to predict the restraint table data. Future efforts should be made to develop a method of applying a factor of safety to be to the regression model predictions. A single load factor simply applied to all model predictions may prevent safety issues from under-predicting the number of restraints required, but there will be a higher probability of over-predicting the number of restraints required and creating issues regarding load preparation time and restraint system weight.

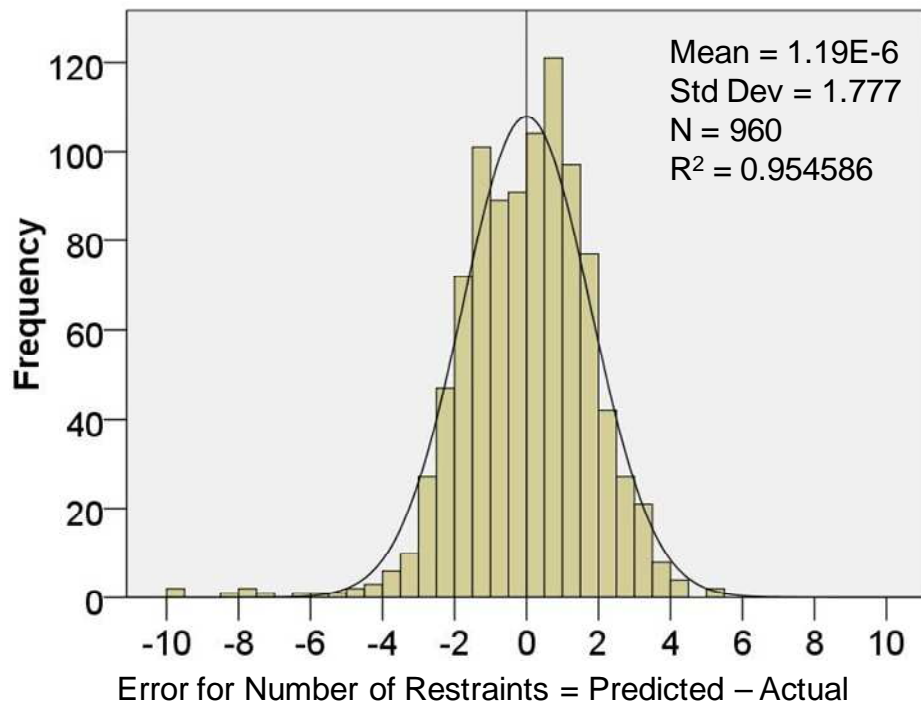


Figure 5-1. Histogram plot of the error from “SC/TW – Longitudinal” regression model.

## Chapter 6

### Conclusions and Recommendations for Future Work

#### 6.1 Summary

A method and tools have been developed to select and configure energy absorbing cargo restraint systems that are optimized for crew safety. A cargo dynamics simulation was created to evaluate energy absorbing cargo restraint systems in a complex design space during a crash event. An optimization method was developed to explore the design space and optimize the parameters of the cargo restraint system to enhance crew safety. Sample studies were conducted as an exercise of the optimization method. A set of requirements and restraint tables were created to provide guidance to cargo handlers to properly use energy absorbing cargo restraints. Finally, a regression model was developed to simplify the process of configuring the cargo restraint system for cargo handlers.

Energy absorbing cargo restraints were found to be able to provide safety in a crash event when current restraint technology could not. Properly designing the components of the energy absorbing cargo restraint system, specifically the lanyard component, is crucial to achieving crashworthiness. Results from the analytical studies showed that lanyards of low stiffness and high elongation were detrimental to performance of the cargo restraint system. Furthermore, the constraint on allowable cargo displacement was found to be the most influential factor in restraint system design. A few centimeters of displacement can be the difference between a survivable and fatal event within the confined spaces of cargo aircraft. In addition to the design of the restraint system components, the tie-down configuration is the final step in designing the optimal crashworthy energy absorbing restraint configuration. The tie-down configuration determines the

tie-down angles and the amount of restraint provided in any given direction. A compromise must be made between the amount of effective restraint in the longitudinal and lateral direction. Although the loads are much greater for longitudinal impacts, the low lateral cargo displacement constraints make the lateral impact criteria the most difficult to satisfy. The optimal cargo restraint system, however, requires more than improvements in performance parameters or minimizing objective functions. It is just as important, if not more, to always take usability into account in each step of the design process of cargo restraint systems. The final step before fielding new technology is obtaining user approval.

## **6.2 Analytical Studies**

Comparative, parametric, and optimization studies were conducted for energy absorbing cargo restraints and currently used chain restraints. The cargo handling scenario featured a cargo container with a mass of 4536 kg (10 kip) subject to a crash event. The design space defined the constraints on cargo displacement: maximum of 100 cm in the longitudinal direction and 5 cm in the lateral direction. The comparative study results provided some preliminary insight into the benefits of incorporating load limiters as well as the influence of restraint stiffness—specifically lanyard stiffness. The results of the parametric study confirmed that a 30/30 tie-down angle can be continue to be used as rule-of-thumb by cargo handlers for energy absorbing cargo restraint systems. The results of the optimization study show that only steel chain/tear webbing restraint systems can provide crash safety with high activation force. A feasible steel chain/tear webbing restraint configuration with an activation force low enough for current aircraft could not be found. There were also no feasible restraint configurations using steel chain or nylon strap/tear webbing restraints. The steel chain restraint configurations could not provide a sufficient amount of

restraint in the lateral direction. The high elongation of the nylon straps led to violations of the lateral cargo displacement constraints for nylon strap/tear webbing restraints.

Sample Pareto optimal restraint configurations from the optimization study were investigated in detail. In Optimization Study #2 for steel chain/tear webbing restraints, Design A and Design B were compared to provide insight on the influence of displacement constraints on restraint system design. Compared to Design A, Design B reduced longitudinal cargo displacement by 48 cm and an increase in lateral displacement of 2 cm. The reduction in displacement required 33% more restraints and an 18% increase in total mass. One of the benefits of using energy absorbing cargo restraint systems is reducing transmitted forces (i.e., activation force). Design C was the optimal restraint configuration for a 20% reduction in transmitted forces compared to Design A. The trade-off included increases in total mass (30%), number of restraints (50%), and 13 cm more displacement in the longitudinal direction. A weight reduction could not be achieved with Design C as it had to use an overdesigned lanyard component. For future steel chain/tear webbing restraint system design, the chain lanyards should be designed to accommodate the activation force of the load limiter in order to keep the weight to a minimum. Further reductions in transmitted forces are required for current rotorcraft as they typically contain mounting points rated up to 44.5 kN. There were no feasible restraint configurations for such a low activation force, but Design D was the closest to achieving feasibility. Compared to Design A, Design D could reduce the forces transmitted to the airframe by 60% and decrease total mass by 26%. However, Design D also required more than double the number of restraints of Design A and was 13 cm over the limit for lateral displacement.

There were several trends observed regarding the influence of the design variables and constraints. The number of restraints, total restraint system mass, and activation force can be reduced by increasing allowable cargo displacement. An improvement in the objectives can also be achieved by increasing load limiter stroke, but only with an increase in displacement

constraints. To avoid excess weight, it is recommended that load limiter stroke is designed to be the minimum required to arrest the cargo. On the other hand, designing a load limiter with more stroke than is required would be similar to increasing the factor of safety. An alternative avenue for improvement is increasing activation force and the mounting point load capacity. A majority of the Pareto optimal configurations featured the highest activation force possible — especially in the regions of low cargo displacement. Therefore, higher activation forces can further minimize cargo displacement, number of restraints and total restraint system mass. On the other hand, a reduction in activation force can reduce transmitted forces and total mass, if provided with enough allowable cargo displacement and a significant increase in the number of restraints is acceptable. Lanyard stiffness is especially important considering the fact that none of the nylon strap/tear webbing restraints were feasible. Lanyards with high stiffness and low elongation can reduce cargo displacement and increase efficiency of energy absorption. The lanyard must be designed with materials of high stiffness, high strength, and low elongation. Stacking several elastic lanyards (e.g., nylon straps) in parallel to decrease the elongation at the activation force is an inefficient method of decreasing lanyard elongation and will result in a significant increase in restraint system weight. Cargo displacement should be a result of load limiter stroke as it dissipates energy as opposed to lanyard elongation.

It is recommended that a comparative study be conducted on the weight savings achieved from increasing or decreasing mounting point load capacity on future heavy lift rotorcraft. Increasing mounting point load capacity will result in a more efficient restraint system and reduce the number of restraints and cargo displacement. Decreasing mounting point load capacity can lead to weight savings in the airframe structure and restraint system, but with significant increases in cargo displacement and number of restraints. Any cargo restraint system suggested as feasible by the proposed optimization method requires a final step of review by the user to assess its practicality and usability. The objective functions indirectly address usability, but additional

metrics could be used such as the overall footprint of the cargo restraint system and how much of the cabin space it occupies. It is also possible to change the tie-down configuration to use mounting points located more forward or aft on the cargo and cabin floor. As long as the tie-down angle, mounting point load capacity, and effective strap length are conserved; switching between mounting points will not affect the characteristics of the restraint configuration.

### **6.3 Design Requirements and Guidance**

To provide guidance for cargo handlers a set of requirements, design criteria, and a template for restraint tables are provided. The design criteria for restraint system components were based on trends observed from the analytical studies. The existing load preparation documents used by cargo handlers do not require restraint systems to be designed for crash loads or specifically address the use of energy absorbing cargo restraint systems. Furthermore, documents for designing crashworthy aircraft (e.g., MIL-STD-1290, Aircraft Crash Survival Design Guide) do not provide requirements in regards to the performance of energy absorbing cargo restraints in normal maneuvering flight conditions. A new set of requirements is proposed in which the cargo restraint system must satisfy criteria for two conditions: 1) normal maneuvering flight conditions, 2) crash conditions. In normal maneuvering flight conditions, the restraint system must hold the cargo to a fixed position. This situation requires that the restraint forces stay below the activation force and prevent activation of the load limiters. In a crash event, the restraint system must arrest the cargo within a specified amount of cargo displacement. Existing documentation on load preparation (e.g., FM 55-450-2) and crashworthy design (e.g., Aircraft Crash Survival Design Guide, MIL-STD-1290) can serve as references for the loads the restraint system must withstand.

Cargo handlers abandoned earlier energy absorbing cargo restraint concepts in part due to the unfamiliarity with the characteristics of the restraint system. A set of restraint tables were compiled which provided crashworthy energy absorbing cargo restraint system design for an array of possible cargo handling scenarios. The restraint tables were not included in the thesis due to the large amount of data. The following parameters were varied to generate the cargo handling scenarios: restraint type, impact direction, cargo weight, crash pulse peak, allowable cargo displacement, and impact velocity. All restraint configurations were doubly symmetric, tied down at an angle of 30/30, and featured an activation force of 44.5 kN. The restraint tables provided the number of restraints required based on the cargo handling scenario. A regression analysis was conducted to simplify the design process for cargo handlers so they would only have to calculate two equations prior to each mission. The regression model predictions correlated well with the restraint table data, but more work is required to increase the goodness of fit or improve the margin of safety. The situations where the regression models underpredicted the number of restraints required results in a restraint system unable to provide adequate crash safety.

#### **6.4 Recommendations for Future Work**

The research presented in this thesis led to the development of a cargo dynamics simulation and optimization method for energy absorbing cargo restraint systems. Furthermore, several studies were conducted including parametric, comparative, and sample design studies. Nevertheless, further investigations should be performed to enhance the tools and methodology to design the optimal energy absorbing cargo restraint system and provide the most crash safety.

### **6.4.1 Cargo Dynamics Simulation**

To design crashworthy cargo restraint systems, a tool to evaluate cargo restraint systems in crash conditions is necessary. The cargo dynamics simulation (CDS) was developed for this purpose, but improvements can be made to obtain higher accuracy. Several assumptions and approximations were made to simplify the CDS and make it less computationally expensive.

#### ***Cargo/Cabin Floor Friction***

The decision to neglect cargo/cabin floor friction provided more conservative results. Furthermore, friction is not considered a reliable factor in arresting cargo. The extent of conservatism, however, from this simplifying assumption is not fully understood and there is a risk of overdesigning the restraint system. Therefore, it is recommended that research is conducted on the influence of cargo/cabin floor friction and the methods to model it in the cargo dynamics simulation.

#### ***Restraint Modeling***

The energy absorbing cargo restraints featured in the analysis were idealized to simplify the calculations. The experimental data from drop tests of tear webbing, show a very complex load response of the load limiter. Furthermore, the nylon strap lanyard was assumed to be linearly elastic while the steel chain lanyards were considered to be completely rigid. It is recommended that future research consider using a more accurate model of the cargo restraint and its components. It is not yet clear the manner in which using ideal restraints may have affected the results. It is possible that a highly detailed model of the restraints may not affect the overall results.

### ***Beyond Unidirectional Impacts***

The CDS was developed to analyze a six degree-of-freedom system. The studies that were conducted in this thesis, however, focused on unidirectional impacts and symmetric tie-down configurations. Helicopter crashes in real life, however, can be subject to situations beyond unidirectional impacts. Incorporating rotational effects and combined impact loadings would bring the analysis much closer to reality. The critical condition may be the one in which the cargo rotates to allow a corner to impinge upon the cabin walls. In this scenario, it is possible that the wall structure may be damaged to the extent where it may no longer able to provide a safe occupant volume.

### ***Structural Analysis***

Currently the focus of the CDS is cargo movement. It is crucial to also consider the effect of transmitted forces on the structure in addition to cargo movement. Structural analysis of the cabin floor, side walls, and airframe is needed to properly assess the overall effects a cargo restraint system may have during a crash event. The peak force transmitted to the airframe is dependent on the activation force of the load limiter. Structural analysis can determine floor deflections produced from transmitted forces that can potentially significantly alter the characteristics of the restraint system. A detailed analysis can also help determine restraint parameters (e.g., activation force). It is recommended that a trade study be conducted to assess the benefits of lowering activation force to reducing structural weight. The trade-off, however, is an increase in the number of restraints and possibly total restraint system weight.

### ***Experimental Validation***

The CDS was validated by comparing model predictions with previously conducted drop test experiments. Further validation is recommended by conducting tests which are similar to what the CDS is simulating. It is difficult to match the exact parameters (e.g., cargo weight, dimensions), but scaled tests could be conducted of cargo tied down by restraints to a platform.

### ***Design Space***

The design space created for the studies conducted was based off existing cargo rotorcraft. The focus, however, should expand to include future rotorcraft. A topology optimization study on the location of mounting can contribute to the design of future heavy lift rotorcraft. This study can also be coupled with the trade study previously mentioned on mounting point load capacity.

#### **6.4.2 Optimization Method**

The optimization study was conducted through ATSV and MATLAB. This method, however, required long run times to obtain a detailed view of the trade space. Furthermore, ATSV is very useful in the preliminary stages to exploring the design space and to gain insight on the influence of design variables. Now that there is more information on the design problem, a specialized approach may be preferred. An investigation should be made into methods of reducing run times as well as different optimization algorithms which may be better suited for this application.

### **6.4.3 Guidance for Cargo Handlers**

The importance of usability has been discussed in this thesis, but additional efforts must be made to assess and improve the ease-of-use of energy absorbing cargo restraint systems. A dialogue must be established with the cargo handlers to ensure their approval of this new technology. Energy absorbing cargo restraints can provide crash safety with minimal weight penalty, but it must not increase load preparation time or complicate the process.

In addition to usability, further investigation should be conducted into the simplifying the process of configuring crashworthy energy absorbing cargo restraint systems. A regression model was developed in this thesis for this very purpose. Model predictions, however, were not consistent and can use improvement. Cargo handlers cannot be expected to have ample amount of time to run simulations and optimization studies for each and every mission.

## References

- Ahlers, F. J., Carlo, W. D., Fleiner, C., Godwin, L., Keenan, M., Nath, R. D., Neumaier, A., Philips, J. R., Price, K., Storn, R., Turney, P., Wang, F., Van Zandt, J., Geldon, H., Gauden, P. A., "Differential Evolution Homepage," International Computer Science Institute, accessed 8 June 2010, <<http://www.icsi.berkeley.edu/~storn/code.html>>.
- Anderson, T. and Myers, D. Private Conversation. Patuxent River. 22 April 2010.
- Avery, J. P., "Cargo Restraint Concepts for Crash Resistance," USAAML Technical Report 65-30, Phoenix, AZ: Aviation Safety Engineering and Research; June 1965.
- Baker, M. J., "Physics – Dynamics – Collision Response," 2010, accessed 8 June 2010, <<http://www.euclideanspace.com/physics/dynamics/collision/index.htm>>.
- Beer, P. B., Johnston, Jr., E. R., Clausen, W. E., "Vector Mechanics for Engineers: Dynamics," 7<sup>th</sup> ed., New York, NY, McGraw-Hill; 2004, p. 820 – 826.
- Burrows, L., Lane, R., and McElhenny, J., "CH-47 Crash Test (T-40) Structural, Cargo Restraint, and Air Crew Inflatable Restraint Experiments", USARL Technical Report 78-22, AD-AD05584, U.S. Army Research and Technology Laboratories, Fort Eustis, April 1978.
- Branke, J., Deb, K., Miettinen, K., Slowinski, R., "Multiobjective Optimization: Interactive and Evolutionary Approaches," Berlin, Germany, Springer-Verlag; 2008, p. 1 – 26.
- FM 55-450-2 "Army Helicopter Internal Load Operations," Department of the Army, June 1992.
- FM 55-9, "Unit Air Movement Planning," Department of the Army, April 1993.
- Hagon, M. J., 2009, "Characterization and Design of Lightweight Energy Absorbing Cargo Restraints," MS Thesis, The Pennsylvania State University, University Park, PA.
- Hagon, M. J., Kong, W., Bakis, C. E., Yukish, M. A., and Smith, E. C., 2008, "Energy-Absorbing Textile Devices for Heavy Cargo Restraints," Proc. American Helicopter Society 64th Annual Forum, Montréal, Canada.
- MIL-DTL-27443F, "Detail Specification Pallets, Cargo, Aircraft, Type HCU-6/E and HCU-12/E," July 2003.
- MIL-DTL-6458F, "Detail Specification Chain Assemblies, Single Leg, Aircraft Cargo Tie Down," April 2008.
- MIL-PRF-27260C, "Performance Specification Tie Down, Cargo, Aircraft, CGU-1/B," November 1998.

MIL-STD-1290A (AV), "Light Fixed- and Rotary- Wing Aircraft Crash Resistance," September 1988.

MIL-STD-3028, "Joint Modular Intermodal Container," June 2009.

Price, K., Storn, R. & Lampinen, "J. Differential evolution – A Practical Approach to Global Optimization," Berlin, Germany; Springer-Verlag; 2005.

Romero, J.A., "Restrained Cargo Dynamics in Road Transportation: Direct Tiedowns," Heavy Vehicle Systems, vol. 11, no. 2, pp. 115 – 132, 2004.

Russo, A., "Aircraft Cargo Restraint System," USAAVLabs Technical Report 66-50. Fort Eustis, VA. September 1966.

Schaub, H., Junkins, J. L., "Analytical Mechanics of Space Systems," 2<sup>nd</sup> Edition, Reston, VA, American Institute of Aeronautics and Astronautics, Inc.; 2009.

Shefrin, J., Russo, A., and Reichardt, W. T., "Integral Helicopter Cargo Restraint System," USAAVLabs Technical Report 69-68, Boeing Vertol Co, Philadelphia, PA, 1969.

Shefrin, J. , Campbell, R. F., Hate, R. L., and George, H. L., "State-of-the-Art Crashworthy Mounting Systems for Military Aircraft," National Specialist's Meeting on Crashworthy Design of Rotorcraft, Atlanta, GA, April 1986.

Miller, S. W. Private Conversations. Penn State University. January – August 2010.

Stump, G., Lego, S., Yukish, Simpson, T. M., and Donndelinger, J. A., "Visual Steering Commands for Trade Space Exploration: User-Guided Sampling With Example," Journal of Computing and Information Science in Engineering, vol. 9, no. 4, pp. 044501-1 – 044501-10, 2009.

Stump, G., Simpson, T. M., Yukish, M., and Bennett, L., "Multidimensional Visualization and Its Application to a Design By Shopping Paradigm," 9<sup>th</sup> AIAA/ISSMO Symposium on Multidisciplinary Analysis and Optimization, Atlanta, GA, September 2002.

Tenney, B. S., 2008, "Joint Heavy Lift -- Full Steam Ahead," Vertiflite, vol. 54, no. 2 , pp. 18 – 20.

Wess, D. B., "Aircraft Restraint Mechanism," Technical Memorandum 04-094, Applied Research Laboratory, State College, PA, October 2004.

Zimmermann, R. E., Warrick, J. C., Lane, A. D., Merritt, N. A., Desjardins, S. P., and Bolukbasi, A. O., "Aircraft Crash Survival Design Guide," vol. I & III, USAAVSCOM TR-89-D-22A,C , December 1989.

## Appendix A

### Restraint Table Regression Models

A regression analysis was conducted on the data compiled from a series of restraint tables. The results of the analysis were four equations to model four different sets of data:

1. SC/TW – Longitudinal
2. SC/TW – Lateral
3. NS/TW – Longitudinal
4. NS/TW – Lateral

The “SC/TW – Longitudinal” equation is a regression model for restraint table data specifically for steel chain/tear webbing restraints and longitudinal impacts. The “steel chain/tear webbing – Lateral” equation is a regression model for restraint table data specifically for steel chain/tear webbing restraints and lateral impacts. The same goes approach applies for two nylon strap/tear webbing (NS/TW) equations. The general form of the regression model equation is shown below:

$$\begin{aligned}
 N = & b_1 + b_2 \cdot W + b_3 \cdot P_G + b_4 \cdot D + b_5 \cdot V + b_6 \cdot W^2 + \\
 & b_7 \cdot P_G^2 + b_8 \cdot D^2 + b_9 \cdot V^2 + b_{10} \cdot W \cdot P_G + b_{11} \cdot W \cdot D + \\
 & b_{12} \cdot W \cdot V + b_{13} \cdot P_G \cdot D + b_{14} \cdot P_G \cdot V + b_{15} \cdot D \cdot V
 \end{aligned} \tag{A-1}$$

where  $N$  is the number of restraints required,  $W$  is the cargo weight,  $P_G$  is the crash pulse peak,  $D$  is the allowable cargo displacement, and  $V$  is the impact velocity. The coefficients ( $b_i$ ) for all four models can be found in Table A-1. Histogram plots of the error calculated from the regression model and restraint table data can be found in Figures B-1 through B-4.

Table A-1. Coefficients for regression model equations.

Coefficients [units]	SC/TW - Longitudinal	SC/TW - Lateral	NS/TW - Longitudinal	NS/TW - Lateral
$b_1$	1.956E+00	2.072E+00	3.294E+00	6.265E+00
$b_2 [N^{-1}]$	2.986E-04	8.857E-06	1.269E-03	1.153E-03
$b_3 [m^{-1} s^2]$	2.690E-01	5.815E-01	1.285E+00	1.389E+00
$b_4 [m^{-1}]$	1.481E+00	-4.272E+00	-3.523E+01	-3.247E+01
$b_5 [m^{-1} s]$	-4.359E-01	-1.447E-01	1.792E+00	2.636E+00
$b_6 [N^{-2}]$	2.500E-09	5.333E-09	1.563E-10	1.042E-09
$b_7 [m^{-2} s^4]$	-1.944E-02	-5.493E-02	-8.281E-02	-1.432E-01
$b_8 [m^{-2}]$	6.915E+00	1.078E+01	2.501E+01	2.944E+01
$b_9 [m^{-2} s^2]$	-1.250E-02	-6.667E-02	-1.445E-01	1.641E-01
$b_{10} [m^{-2} N^{-1} s^2]$	6.108E-05	6.567E-05	9.513E-05	5.914E-05
$b_{11} [N^{-1} m^{-1}]$	-6.680E-04	-7.650E-04	-1.811E-03	-1.688E-03
$b_{12} [N^{-1} m^{-1} s]$	5.987E-05	1.267E-04	1.509E-04	2.919E-04
$b_{13} [m^{-3} s^2]$	-9.508E-01	-1.478E+00	-2.030E+00	-1.741E+00
$b_{14} [m^{-2} s^3]$	8.289E-02	2.195E-01	2.565E-01	4.513E-01
$b_{15} [m^{-2} s]$	6.339E-02	-7.188E-01	-7.033E-01	-5.660E+00

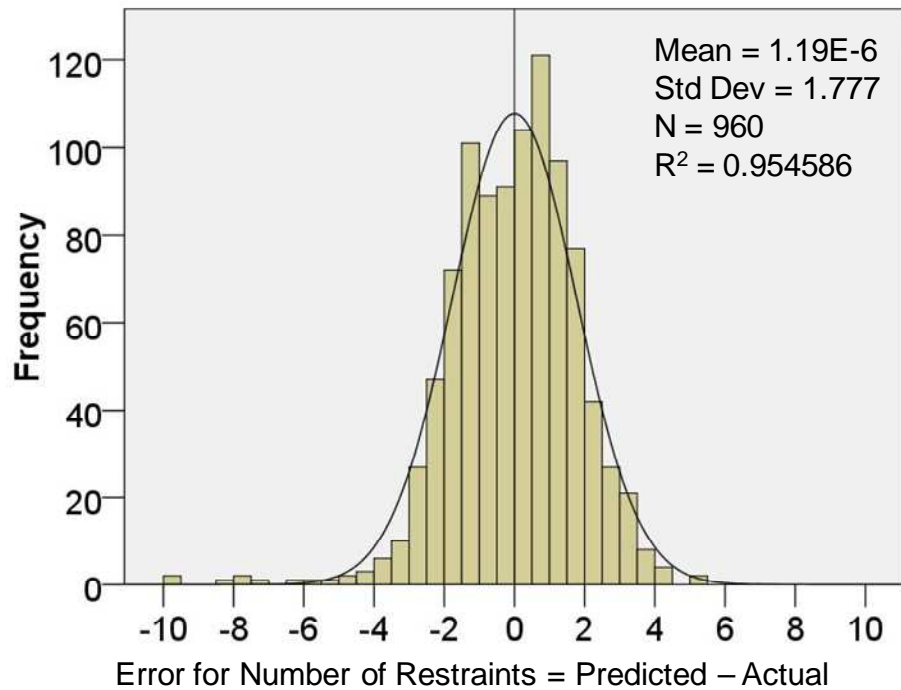


Figure A-1. Histogram plot for SC/TW – Longitudinal error.

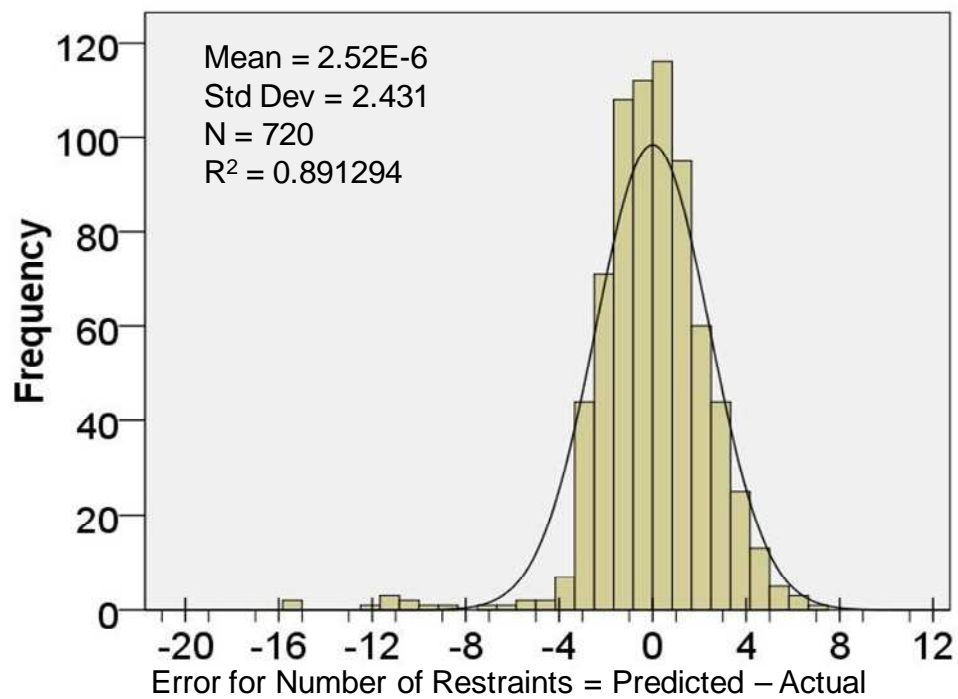


Figure A-2. Histogram plot for SC/TW – Lateral error.

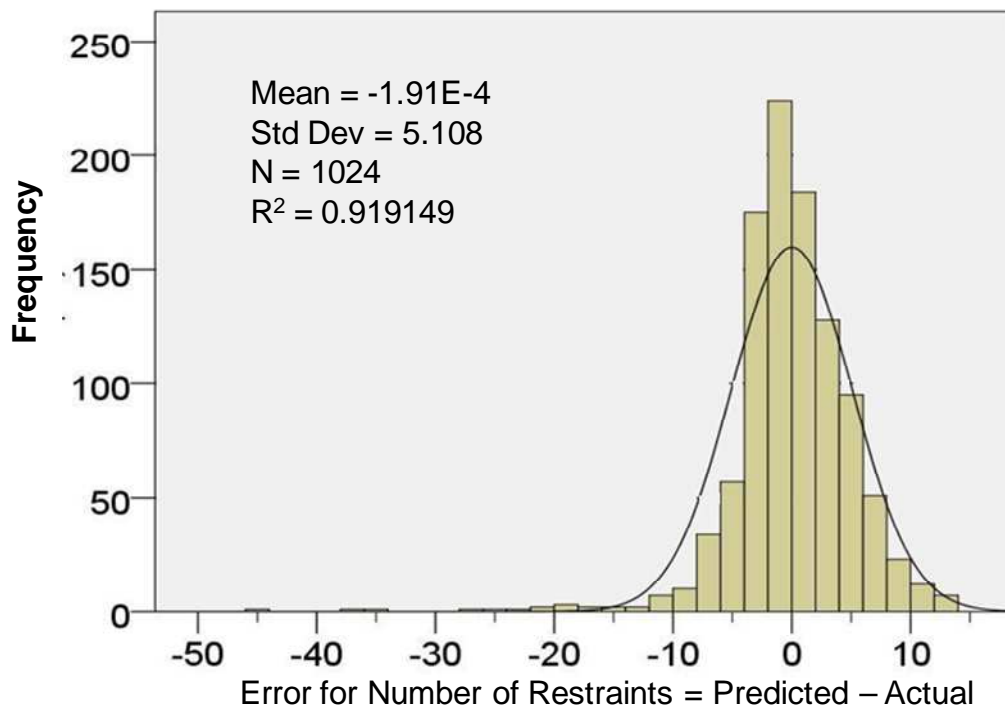


Figure A-3. Histogram plot for NS/TW – Longitudinal error.

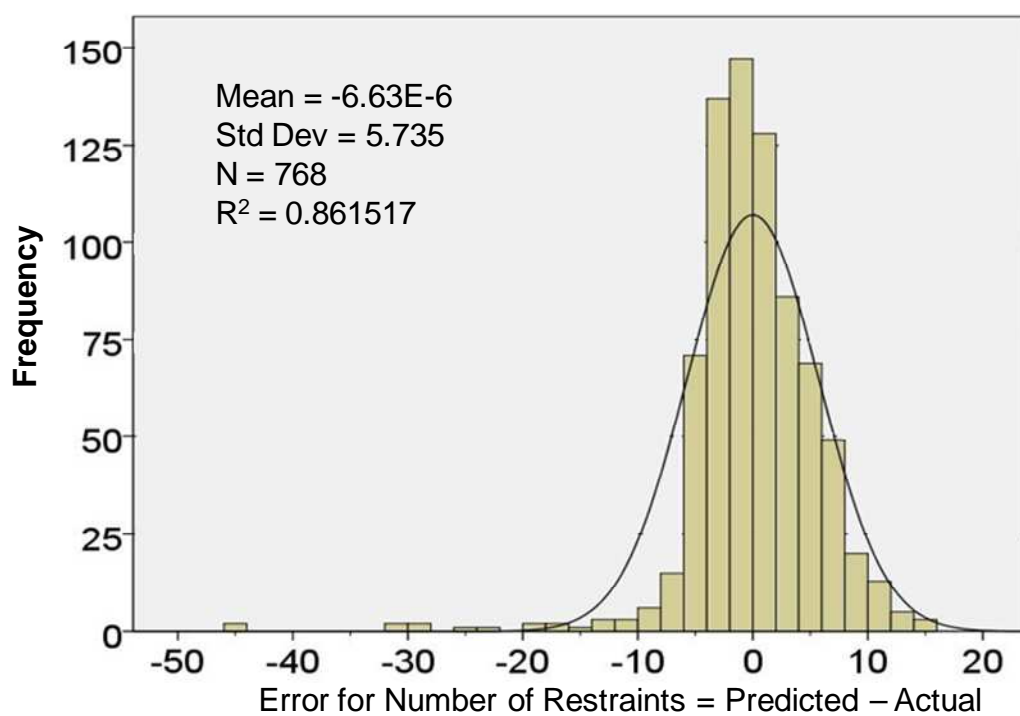


Figure A-4. Histogram plot for NS/TW – Lateral error.